PENINSULA TECHNIKON

DEVELOPMENT OF A NON-MONOCHROMATIC LIGHTWAVE SENSOR FOR APPLICATIONS IN SMART STRUCTURES RESEARCH

by

Mohammed Tariq Ekeramodien KAHN

A thesis submitted in fulfilment of the requirements for the degree of

Master of Technology (M.Tech)

Supervisor: B.Sun Ph.D

Supervisor: R.Tzoneva, Ph.D

Cape Town (1998)

PENINSULA TECHNIKON

Abstract

DEVELOPMENT OF A NON-MONOCHROMATIC LIGHTWAVE SENSOR FOR APPLICATIONS IN SMART STRUCTURES RESEARCH

by MTE KAHN

The purpose of this study was to perform an investigation into advances in the field of opto-electronics and to develop a suitable lightwave sensor, for application in smart structures research. Included in the scope of this research was the theoretical development and analysis of an appropriate technology to lead to an implementation of such sensors. This project forms part of an overall plan to gain experience in opto-electronic (photonic) sensor design.

In research done previously in smart structure monitoring, piezo-electric techniques with the usual electrical interconnections was used. In a highly distributed sensor system the problems of electromagnetic interference, the tribo-electric effect and noise could be problematic. In this research, opto electronic techniques were thoroughly researched and an improvement on laser based fibre-optic interferometers was made. A non monochromatic lightwave interferometer was developed from theory and a prototype tested. The results suggests that an interferometric sensor can be operated with a non monochromatic source by using a second interferometer to modulate the frequency spectrum of the light before it is detected by a photodetector. Various test and measurement circuits for improved photodetector performance were evaluated, as well as a study of signal processing techniques that would be of use for an upgrade of the project where specific feature detection and analysis using the

sensor is envisaged. A specification for a computer based data acquisition system was developed to do initial tests. The project should continue, with the sensor head being improved and all the necessary signal processing routines programmed into a Labview based data acquisition system.

ACKNOWLEDGMENTS

The author wishes to thank Dr Bohua Sun of CRATECH, at Peninsula Tecnikon for his inspirational suggestions that initiated this research, and for his initial guidance and supervision that has contributed to me completing this research with great excitement. Thanks in this regard is also deserving to Dr Raynitchka Tzoneva, for limited supervision and for encouraging me to deliver a paper at an international conference, dealing with part of my work. I also thank the staff in the Department of Electrical Engineering, in particular Mr Tom van Breda, who provided the necessary staff release so that I could write up this thesis. In this regard, the Vice Rector Academic, Dr Johan Tromp is also gratefully acknowledged. Particular thanks also to the FRD, whose funding of this project, provided value added inspiration as well as making possible the delivery of a paper dealing with concepts of this research at the International Conference on Systems, Signals, Control and Computers '98.

TABLE OF CONTENTS

Contents

LIST OF FIGURES

LIST OF SYMBOLS

W_g	Continuous wavelet transform
*	complex conjugation
b	translation parameter
a	dilation or scale parameter
$\psi(t)$	Morlet wavelet
i	imaginary
e	exponential
g(t)	time varying signal
x(t)	time varying signal
E	Energy
λ	wavelength
Eg	Energy (electron volts)
h	Plank's constant
c	speed of light
$[J_{ij}]$ (*j* and *i* any integer)	Jones matrix
E_r	Optical intensity or energy reflected
E_i	Optical intensity or incident energy
$[H_r]$	reflected amplitude transfer matrix
t_i	amplitude transmission coefficient
r_i	amplitude reflection coefficient

θ	phase or phase angle
θ_p	phase perturbation
V	cavity specific visibility
n_r	refractive index
L	Length or length of cavity
f	frequency
[K]	coupling matrix
k	cross power coupling ratio
[I]	identity matrix
$*^T$	conjugate transpose of matrix
T_{AA} or T_{AB}	Transmittance or reflectance
ω	frequency
$S(\omega)$	normalised optical power spectrum
k_p	constant of proportionality
R	Reflectivity
α	optical loss constant of proportionality
Em	ratio of frequency of vibration to undampded frequency
A_m, A_s	vibration amplitudes
M	Mass
l_o	critical length
a_c	core radius
N_a	Numerical aperture

$p(x)$	probability density function
Σ	summation
$\int$	integration
$P(x)$	distribution function
$\bar{x}$	mean value
σ	variance
R_{xy}	cross-correlation
R_{xx}	auto correlation
$\longleftrightarrow$	transformation
$\lvert\ \rvert$	absolute value
n	index
N	integer value
τ	increment in time
T	period of time
t	time
q	membrane displacement
M_r	membrane radius
φ	tilt angle
R_f	feedback resistance
R_i	input resistance
i_o	output current
i_p	photo current

M	FIR filter length
H(z)	discrete transfer function
H(s)	frequency domain transfer function

GLOSSARY

Absorption. The process whereby light is lost. It is caused by the presence of residual impurities, including OH^-(hydroxyl) ions.

Actuator A device, in this case electromechanical, to correct or otherwise influence the outcome of a process or event.

Analogue signal. A signal in which variations in intensity are used to transmit information. An analogue signal varies continuously with time.

Bandwidth. This is typically 100 000MHz km for singlemode and 500 MHz km for multimode fibre at 1300nm.

Composite cables Cables which contain both optical fibre and copper pairs. The latter often being used to transmit electrical power.

Cut-off wavelength. The wavelength of light at which single mode fibre starts to propagate one mode only. This is typically at greater than 1150nm.

Connector A device which couples the fibre to the source or detector

Coupler A device which splits or joins lightwaves in two or more optical fibres

Coupling loss Occurs at the point where the fibre and receiver or detector connects

Crosstalk It occurs due to the presence of one channel's signal in an adjacent channel

Directional coupler Routes the optical power to a specific port depending on the direction of propagation

Dispersion is a measure of the spreading of an injected light pulse

Distributed Reference to sensors, controllers and actuators widely dispersed through a system.

Distributed-feedback laser A type of laser diode with spectral width of <0.01 nm

DSP digital signal processing

Fabry-Perot Interferometric method used to detect phase and convert the signal into an amplitude variation

Fabry-perot laser Laser based on a the optical resonance in a cavity, the centre wavelength which has a typical tolerance of +/-3 nm

Fabry-perot resonator This is a bandpass optical filter that transmits a narrow band of wavelengths and reflects others

FIR Finite impulse response filter

FOG Fibre-optic gyroscope. A technique used to detect rotation, i.e. Sagnac interferometer method.

Frequency division multiplexing Data in channels of bandwidth(BW) are upconverted in a mixer/modulator by carrier frequencies(f) to form a single transmission channel. The combined channels and the resultant composite waveform is transmitted over the fibre link

ILED Infrared light emitting diode

Intelligent structure A structure that have both sensory elements, actuators and controllers highly distributed throughout it that can enable it to respond to changes in conditions automatically.

Interferometry Technique used to determine the refractive index profiles of optical fibres, i.e. phase detection

IIR Infinte impulse response filter

Jitter This is defined as short-term timing or phase variations in a received regenerated signal pulse from that of the ideal

Laminate Reference to layered construction method envisioned in the manufacture of IS.

LD Laser diode

LED light emitting diode

Mach-Zender interferometer A method based on transmitted light interferometry

Macrobending .Light lost from the optical core due to macroscopic effects such as tight bends being induces in the fibre itself

MDP Minimum detected power. This is the received power less any coupling losses between detector and any coupling device

Michelson method Reflected light based interferometer

Microbending Light lost from the optical core due to microscopic effects resulting from deformation and damage to the core-cladding interface.

Modal noise Noise caused due to different time delays which in turn is caused by dispersion

Monolithic Uniform throughout. The antithesis of laminated.

Multimode fibre Fabricated from either multicomponent glass compounds

Multiplexing This function combines multiple channels into a composite signal for transmission.

Numerical aperture Refers to the relationship between the core, air, cladding and the acceptance angle of an optical fibre interface.

Operating wavelength It is the wavelength at which the optical source transmits light.

Optical aperture Area onto which light falls

Optical receiver It contains a photodetector, amplification section, and signal-recovery circuitry. It converts the received optical power signal to a voltage signal

Optical transmitter This contains the drive electronics and optical source. It converts the transmitted signal voltage to optical power

Photocurrent It is the current generated when optical power is absorbed by the detector

Piezoceramic Refers to ceramic materials that have piezoelectric properties, typically lead zirconate titanate (PZT)

Polarimetric sensor Used to detect changes in the polarization state of the light caused by an external disturbance, i.e. used for pressure measurement

PVDF Polyvinaldene fluoride is a polymer piezoelectric film.

Receiver dynamic range It is the range of wavelengths that the receiver can detect

Responsivity It is the ratio of the photocurrent generated for a unit of optical power

Rx Receiver

Singlemode fibre Fabricated from a single narrow strand of doped silica in order to reduce attenuation. It allows only one lightwave mode to propagate with no multiple reflections within the fibre.

SLD Superluminescent diode

SOT Selective observability transducer

Splice A point where two fibres are permanently joined

Star-coupler It couples power from one of N fibre input ports to all N output ports

T-coupler It splits power in one direction from one fibre to two

TDM Time division multiplexing. Interleaves multiple lower-speed digital data channels for transmission over one higher speed channel

Transducer A device that transform energy from one type to another, usually with reference to sensory elements. Typically the transformation of kinetic energy to electrical energy.

Tx Transmitter

Waveguide It refer here to is a fibre optic cable

Wavelength coupler Couples power from multiple sources, operating at different wavelengths, onto a single fibre

WDM Wavelength division multiplexing. Individual transmission channels are carried on separate optical wavelengths and combined in a single fibre at the optical link

Chapter 1

INTRODUCTION

"...hence we must believe that all sciences are so interconnected that it is much easier to study them all together than to isolate one from the others. If therefore anyone wishes to search out the truth of things in serious earnest, he ought not to select one special science, for all the sciences are so co-joined with each other and interdependent."

Rene Descartes (1596-1650) in his 1629 text, "Rules for the Direction of the Mind." A mathematician and philosopher, Descartes systematised analytical geometry and is sometimes called the father of modern philosophy.

Ever since human beings began to think, we have exchanged information and have given measures to quantities in an attempt to understand our surroundings. In a continual process towards perfection, we are still developing and refining our tools to improve our understanding of all kinds of mechanisms. The field of engineering and scientific instrumentation encompasses activities in many engineering sciences. Among these are the branches of electronic engineering, optical engineering, mechanical measurement, data processing and computation. Each of these functions may take place by manual, semi-automatic, or automatic means. The element responsible for the quantifying of any measurement being of course,

the sensor or measurement instrument. The following quotation demonstrate this concept vividly:

" Instrumentation in general has been considered as being the art and science of designing , constructing and applying physical devices and systems for extending , refining, or supplementing the sensory , perceptual or communicative facilities of man."

W. Wildhack, Proceedings Nationial
Conference on Instrumentation, 1953

This thesis sets out the results of an investigation into the use of optical techniques to measure physical parameters, such as vibration, with the aid of high precision measurement techniques and by proposing the use of a PC based data acquisition system in the design.

The overall concept of the work was to develop parameters for a micro-interferometer for use in smart structures research. The project forms part of an overall plan to gain experience and expertise in photonic sensor design to produce a cost effective computer based fibre optic analysis system that could initially be applied in smart structures but which could also be applicable to other fibre-optic sensor design research at Peninsula Technikon.

The thesis is arranged in to several chapters, each dealing with specific aspects of the development. Chapter 2 presents an overview of fibre optic sensors, signal processing techniques and control methodologies that would be applicable to smart structures. For instance, the choice of sensors for large structures, such as an oil platform, bridge or building can be challenging. Point sensing can be performed adequately with current technology, but large arrays or sensor networks tend to be impractical and hampered by electromagnetic interference and other noise sources. Opto-electronic sensing with fibre-optics as either transmission lines or sensing elements can offer significant advantages over classical instrumentation using say

strain gauges, piezo-resistive elements, accelerometers or thermo-couples. The development of effective control techniques however would also be able to enhance the development of complex structures that are intended to be classified as "intelligent." This chapter concludes with an assessment of the applicability of lightwave sensors in smart structures.

Chapter 3 presents the results of a theoretical development of a non-monochromatic based sensor design to achieve an optical interferometric effect without the use of a laser in optical fibres. The results in this chapter suggests that an interferometric sensor can be operated with a non monochromatic source by using a second interferometer to modulate the frequency spectrum of the light before it is detected by a photodetector. This findings, was prepared for publication in the "IEEE Aerospace and Systems Engineering Journal.", and represent a substantially original approach to apply to the optical processing part of the problem.

Chapter 4 deals with the development and integration of the technique discussed in chapter 3 into an actual vibration sensor design. An overview of traditional vibration sensor heads, as well as signal processing considerations were taken into account and reported as essential to the sensor head design. A Pro-Engineer model was suggested to be used to develop the sensor head for a more refined implementation than the proposed prototype.

In Chapter 5 the measurement system is discussed and the opto-electronic interface subassemblies and signal conditioning modules designed. The results of tests and recommendations are made.

In the appendices attached, the following may be noted. Appendix 1 is a copy of the paper submitted to the ICSSCC 98 conference as a direct result of the research for this thesis. Appendices 2, 3, 4, and 5 are reports presented by myself to the SAIMC, and industry, the FRD, seminars at CRATECH and was compiled also as

a direct result of this thesis research. I intend to make these reports available in teaching activities at the Peninsula Technikon as well. Appendix 7 consists of component data sheets , and appendix 8 consists of the circuit diagrams of the prototype units.

Equations in the thesis development have been numbered in each respective chapter starting with the chapter number as prefix and (1) for the first equation reported. This was generally the easiest and more readable format that I could adopt. Appendix 9 contains all equations in order of usage in the main thesis.

Chapter 2

SMART STRUCTURE TECHNOLOGY WITH FIBRE OPTIC SENSORS

2.1 INTRODUCTION

In this chapter an overview of fibre-optic sensors, signal processing techniques and control methodologies applicable to smart structures are introduced. It presents essentially a technology-overview and provided the background for the thesis development theme.

The idea of using light to send information began to be developed scientifically in the 1800's when John Tyndall, an English physicist, demonstrated that he could direct light down a stream of water. This could well be described as the ancestor of modern fibre-optic communications technology. The development of the laser during the 1960's, and the ever increasing trend to innovate and develop new opto-electronic products, created an exciting avenue of research and applications in electrical engineering, as well as other disciplines. In the Telecommunications industry, opto-electronics have found wide application prospects in the form of

fibre-optic communication networks. In South Africa, fibre-optic linked PABX's have been developed for commercial applications by several key R&D concerns. The United States Department of Defence indicated a willingness to fund research into an ALL OPTICAL communications network. They are envisioning users such as medical personnel of the future, who would be able to perform remote archive searches and telesurgery, as well as the Aerospace interest in the development of Intelligent Structures with opto-electronic sensing and control. The benefits of using opto-electronics for sensing applications are becoming more apparent as research into novel measurement and instrumentation techniques are beginning to bear fruit.

The area of smart structures, both at the micro and macro level is a research activity of the Centre for Research in Applied Technology (CRATECH) at Peninsula Technikon. In this regard sensor technology for both dynamic as well as static structures, such as civil engineering structures are envisaged. Civil engineering projects and the construction of buildings and plants contribute a fair percentage of Southern African GNP. International trends to hold contractors or owners responsible for structural guarantees over prolonged periods of time, so called Design Build and Operate contracts, are changing the nature in which structures will be built in the next century. Artificial Intelligence (AI) techniques in structural / construction engineering have already found potential applications. AI has the potential to help design engineers develop vital structural design infrastructure. Less obvious, however, is the need for the development of acceptable sensor technology for applications in structural health monitoring, or even truly Intelligent Structures (IS) that can adapt to changing conditions, such as seismic activity. The development of sensor systems suitable for civil engineering projects or plant construction, as well as control mechanisms capable of great flexibility or adaptation is discussed in this chapter. The sensor developed for this thesis is intended to be useful in such structural applications.

Smart structures are required to have very high performance characteristics and are expected to operate over a wide range of environmental conditions. Space and terrestrial smart structures of the 21st century are expected to employ embedded fibre-optic sensors in various configurations [1].Recently, continuos fibre composite materials , either polymer matrix or advanced metal matrix, have been developed. These composites are also referred to as engineered or structured materials. Researchers and design engineers attempting to incorporate sensors into such new designs are faced with numerous additional signal processing variables. It is at this juncture that wavelet analysis, a very recent and powerful signal processing tool, can make a difference. This overview will also demonstrate the theory and implementation of wavelets as a powerful signal analysis tool, applicable to optimised smart structure sensors, as well as more general applications.

2.2 OPTICAL SENSING FOR SMART STRUCTURES TECHNOLOGY REVIEW

2.2.1 Intelligent or Smart structures : a definition

Intelligent structures can be classified as being a subset of active structures that have highly distributed or multiplexed actuator, sensor and control systems embedded within it. The age of the Intelligent or Smart Structure is the natural successor to modern man's progression from the Stone Age through to the present Synthetic Materials Age [1]. The nineteen nineties has seen the intelligent or smart structure development emerge as a truly multidisciplinary field. A Smart structure is defined [2] as **"a nonbiological structure that has definite designed in purpose and will, and some means to achieve that purpose."** It is in the achievement of these objectives that electronics and information technology will find an increasing role to play in the development of adequate sensor, control and actuation mechanisms

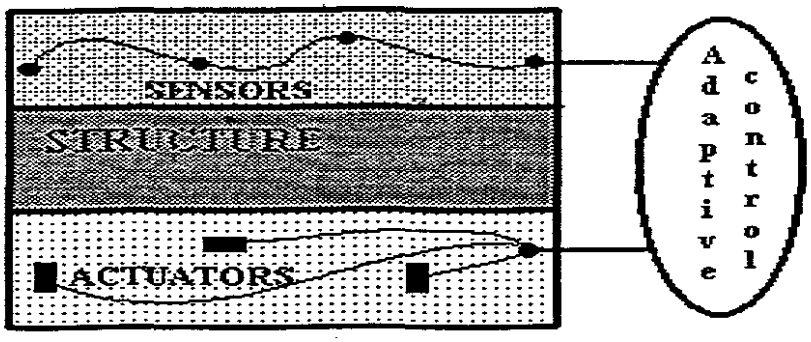

Figure 1 Embedded sensors and actuators in composite structures with adaptive control

One approach to the development of intelligent structures is to use fibre-optic sensors embedded within a composite material. Intelligent structures is also the ultimate goal of much research in the fields of mechanical and aerospace

engineering. Advances in the field of laminated materials, especially research into the controllability of piezoceramic laminates as viable replacements for monolithic materials , have made it necessary to consider the **research into electronics technology** to enable optimal sensing, actuation and control of such material. [1] [2] [3]

Laminated materials, configured as plates, having built in sensing, actuation and control elements can more properly be classified as the basic building blocks of intelligent skins or hulls. Such hulls could be used to damp audible noise in vibrating structures. Audible noise can be psychologically annoying as well as being a cause of irreparable damage to human ears. The damping of radiated sound, often necessary in an aircraft cabin, can be listed as at least one viable application of material with such properties.

Further examples include the reduction of jitter in aiming systems and robotics control, seismic control of buildings and so on. These can all be classified as structures, in the proper sense of the word, that could benefit from self sensing, actuation , and even learning, to compensate for changing environmental or structural conditions. The proper control of elements of structures is in itself an avenue of much present research [4][5]

2.2.2 Sensing: A key factor in IS realisation

The choice of sensors for large structures, such as an oil platform, bridge or building can be challenging. Point sensing can be performed adequately with current technology, but large arrays or sensor networks tend to be impractical and hampered by electromagnetic interference and other noise sources. Opto-electronic sensing with fibre-optics as either transmission lines or sensing elements can offer significant advantages over classical instrumentation using say strain gauges, piezo-resistive elements , accelerometers or thermo-couples.

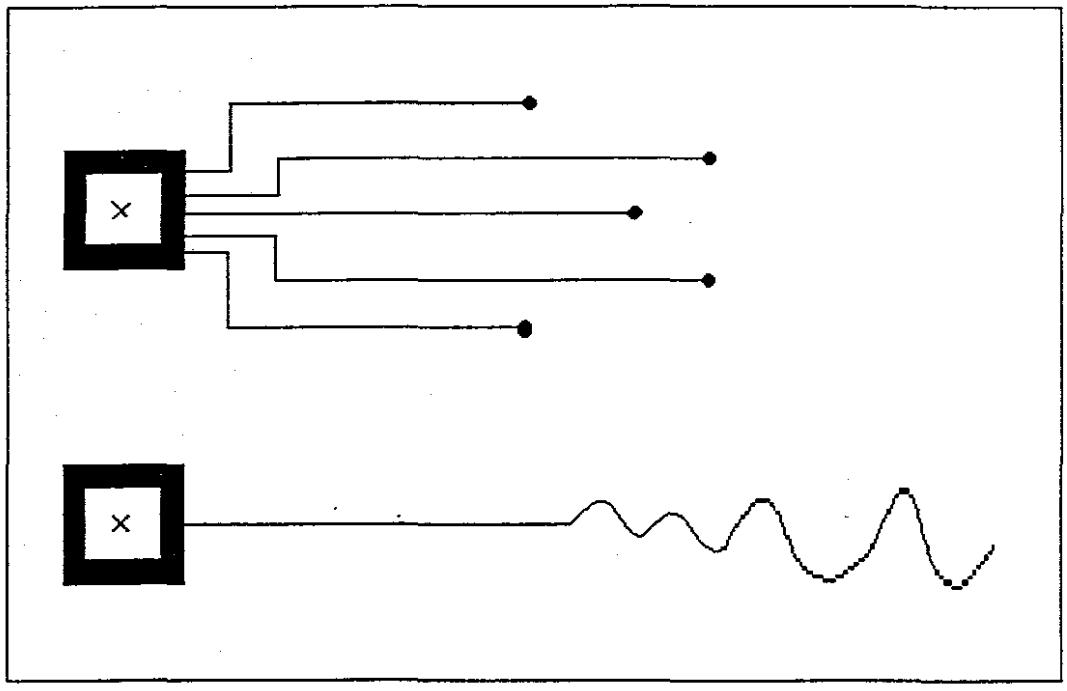

Figure 2 Fibre-optic cables simplify sensor distribution and arrangements : point sensing as well as distributed.

The critical component technologies necessary for the viable application of intelligent structures are : selective observability transducers (optimised sensors), controller architecture and methodology, and effective actuators. Sensor technology therefore becomes a key factor. In the selection of an optical fibre and optical system for measuring the response of smart structures, it is important to be familiar with the basic types of fibre and their waveguide characteristics. Lightwaves in optical fibre can be considered and analysed as guided waves much like that of the corresponding microwave technology. Optical waves are guided when they are constrained to lie within a channel between two other media, the refractive index of the channel material being slightly higher than those of the other media, so that the light can bounce along the channel by means of total internal reflection(TIR) at the boundaries between the media

2.2.2.1 Fibre optic waveguides

The three basic types of fibre-optic cable available for generalised are step-index single mode, step index multimode, and graded-index multimode The light transmission and refractive index profile of two of these types of fibres are shown in figure 3. A more complete discussion and assessment of fibre-optic waveguide theory can be found in appendices 3 and 4.

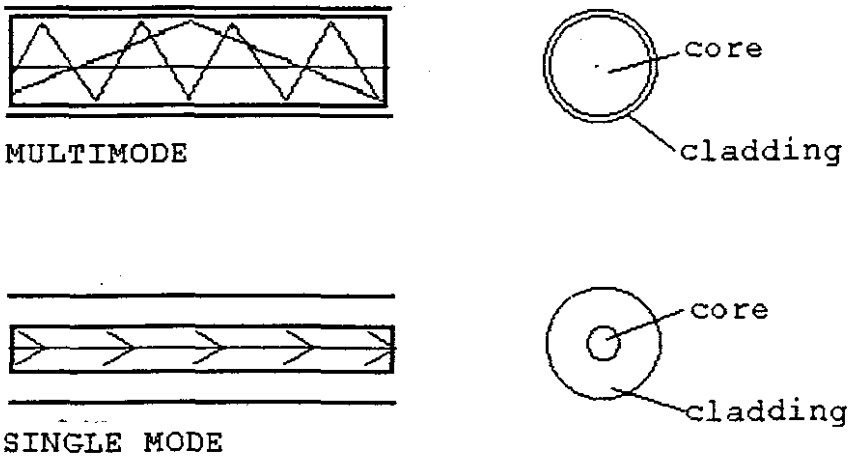

Figure 3: Basic optical fibres and resulting waveguide

The behaviour of light transmitting through each of these types of fibres is produced by the difference in cladding and core glasses and their relative refractive indices. The cladding has a lower refractive index and therefore the lightwave transmitted in the fibre refracts from the interface between the core and cladding producing different waveguide characteristics, due to total internal reflection of the incident lightwaves.

2.2.2.2 Types of sensor configurations

There is three types of opto-electronics based sensor systems that have a potential application in smart structures. These are intensity, polarization and micro-interferometry. In addition to the above sensor configurations, fibre-optic sensors may be either intrinsic or extrinsic. This is further discussed in the chapter that follows.

2.2.3 Extrinsic Sensors:

2.2.3.1 Micro-machined sensors

Traditional vibration sensing was based on using accelerometers. Developments in micromechanical accelerometry have been well advanced and have indicated a trend to develop greater compatibility of transducers that can interface directly with microprocessor based electronics. [6]

Such sensors can be readily mass produced and can be robust and compact. Batch fabrication of silicon based vibration accelerometers have been developed for the biomedical field to measure heart wall motion. Sensitivities of 0.001g to 50g over a 100Hz bandwidth have been reported. [7] Vibration and stress measurement using micro-machining techniques with the piezo-junction effect in bipolar transistors, have been reported with size less than 4 x 4 mm. Piezo-junction silicon devices can typically be configured as uni-axial devices, with no cross sensitivity, and by simultaneous integration of signal processing circuitry on the same die, signal to noise ratios have been significantly improved. [8]

However, all these methods depend on the usual electrical interconnections in circuit arrangements and highly distributed sensors may suffer from electromagnetic and tribo-electric interference and noise. This may be significant in large or complex structures. These problems may be overcome by using opto-electronic techniques. [3] [9]

Recently, micromachined pressure sensors have been developed that surpasses piezo-resistive sensors in terms of robustness, temperature effects and drift. It is reported that these sensors can be directly **optically addressed**, without the need for electronics (in the classical sense!). [10]

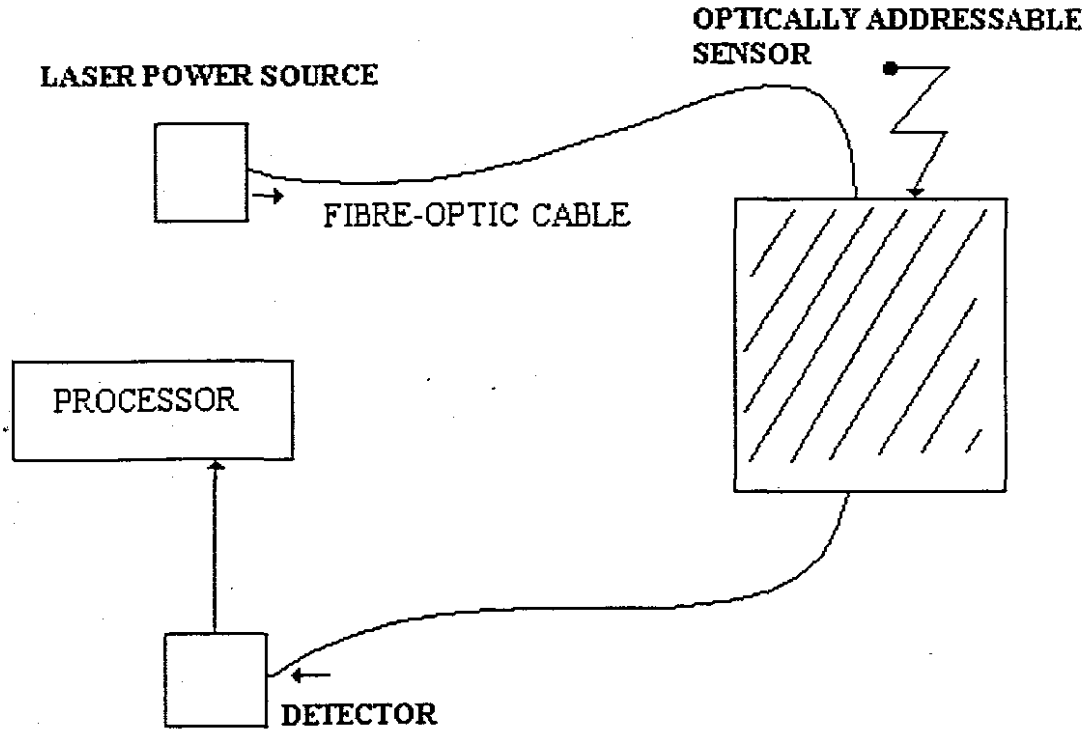

Figure 4 Micromachined sensors that are optically powered and addressable

2.2.3.2 Spectroscopic sensors:

These are essentially sensors based on spectral absorption or emission, and lends itself ideally to opto-electronics based technology. [9] This is basically extrinsic sensing. Blackbody radiation detectors have been commercially developed to measure temperatures between 500 and 2000^0 C. Photoluminescence detectors are also commercially available to measure between 0 and 200^0 C with 0.1^0C resolution. These sensors are ideally suited for remote measurements away from hazardous environments. The development of suitable infrared transmitting fibre will enhance this technology even further.

2.2.4 Intrinsic Sensors

The term intrinsic covers those types of fibre-optic sensors that employ some change in the waveguide medium as a means of modulating the light guide.

2.2.4.1 Microbend techniques

One of the oldest fibre-optic strain sensors is the microbend sensor. The opto-electronics and signal processing circuitry for microbend sensors are generally inexpensive and make it ideal for low cost applications. Macrobending, or controlled buckling, optical fibre sensors have been developed for strain and displacement measurements that can complement or surpass traditional microbend techniques [11].

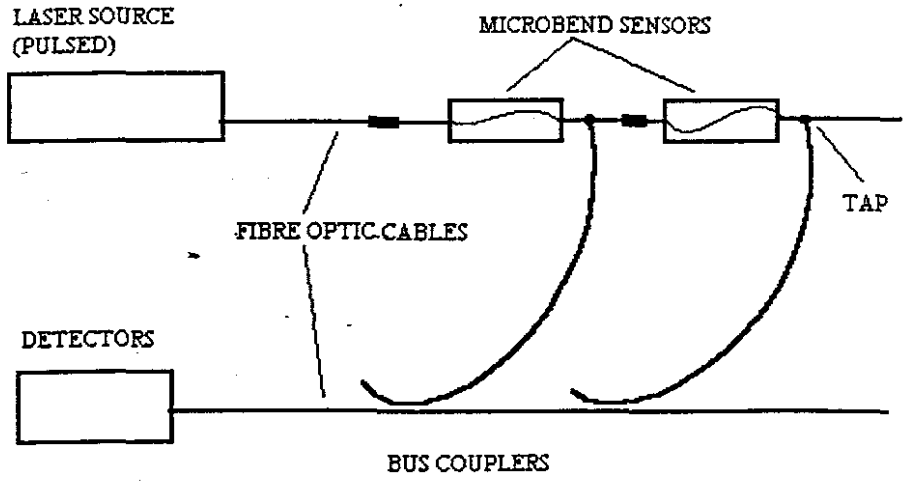

Figure 5 Microbend sensors arrays can be optically addressed

2.2.4.2 OTDR (optical time-domain reflectometry)

Fibre-optic based OTDR techniques is another well established opto-electronic sensor solution. Rayleigh backscatter methods can be used in distributed sensors for large structures, and is essentially a measure of backscatter signature as a function of time, from the launch of an interrogating laser pulse. Coupled with microbend sensors, OTDR have been used in a wide range of applications in Europe, including monitoring of the Berlin-Mansfield bridge, to establish crack growth and dynamic loading. [3]

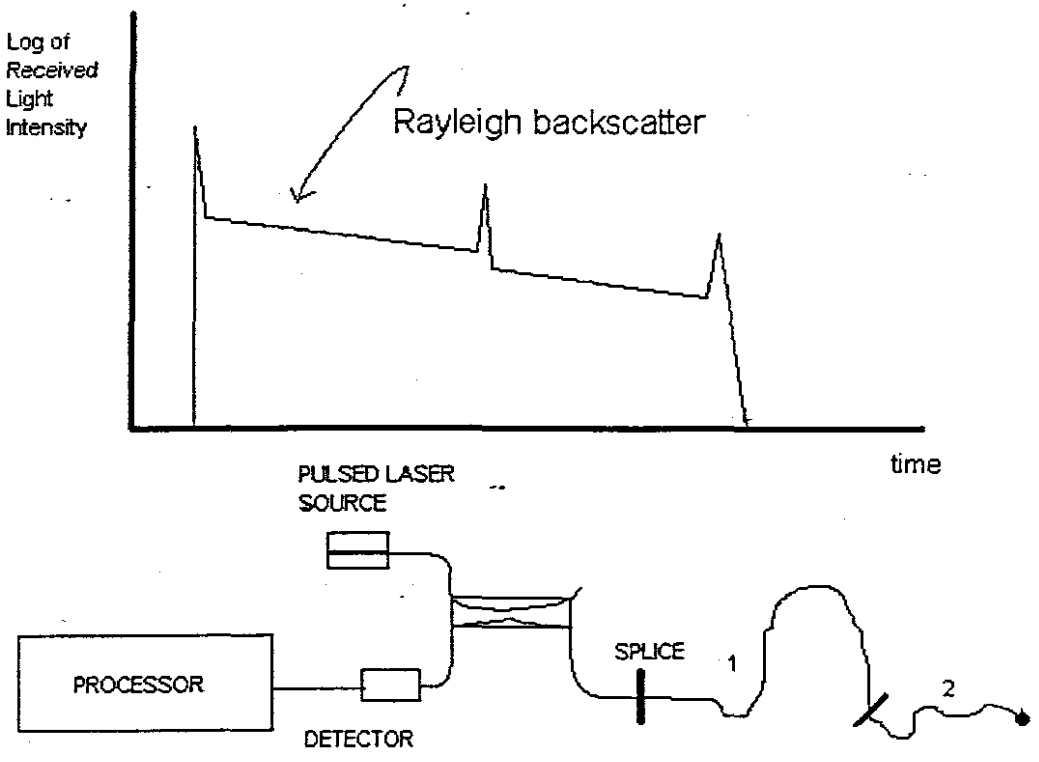

Figure 6 Typical OTDR backscatter signature and sensor configuration.

2.2.4.3 Interferometric sensors

Interferometry originally had a purely optical origin and displacement measurements of minute degrees is possible with it. Classical Michealson and Mach-Zehnder interferometers usually required bulk optical components, beam splitters and stable measurement benches. With the advent of lasers and improved optical fibre technology, the bulk optical components was replaced by opto-electronic components. This lead to much more feasible inteferometric sensor applications. Multiplexed Mach-Zehnder sensors have been reported to date. [12]

Yet another technique, that of using internal reflections in a Fabry-Perot cavity, have proved to be of great value in sensor technology. Fabry-Perot interferometers have been configured as temperature sensors for point measurement applications [13] and requires in general much simpler signal processing electronics. Distributed interferometric sensors have been used to measure strain and movement on high tension wires [9]. Perhaps the most famous application of an intererometric sensor technique is that of the Sagnac based fibre-optic gyroscope [14], used in guidance systems.

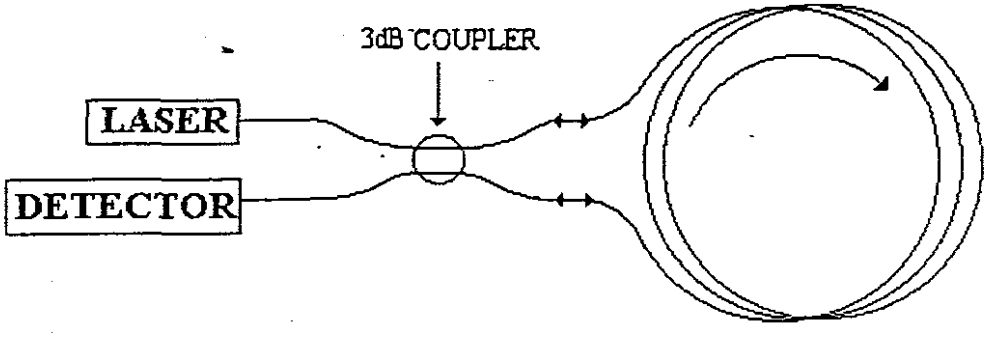

Figure 7 The Sagnac optical fibre gyroscope

2.2.5 Signal transmission

Having demonstrated the possibilities as well as the extent of development and research in opto-electronic sensors, one can visualise the next chapter in the development of intelligent structures that make use of such sensors. How, for instance would measurement and control signals be coupled, transmitted and processed over long distances? The concept of optical-fibre amplifiers have been advanced [15] [16] and have already found applications in the telecommunications industry. Ebrium doped fibre amplifiers (EDFA) could be used for long distance signal transmission or all optical processor information transfer.

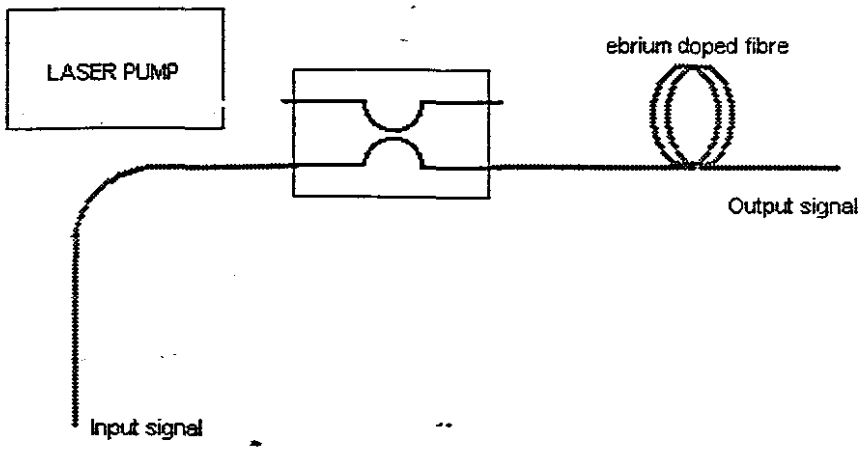

Figure 8 Ebrium doped fibre amplifier

2.2.6 Optical processing

Silicon based opto-electronic integrated circuits (OEIC's) [17], hold promise for the development of a completely integrated solution for signal processing of sensor signals. OEIC's is envisioned to outperform electrical circuits and is essentially the outcome of integrating optics and electronics on the same substrate. Another development of vital importance is signal analysis tools.

2.3 SIGNAL PROCESSING AND ANALYSIS FOR SMART STRUCTURES - TECHNOLOGY REVIEW

The high levels of monitoring and complex objectives with embedded sensors in smart structures, require accurate calibration of the sensors and an efficient , rapid data analysis method.

2.3.1 Signal analysis : Basics

With signal analysis tools we attempt to decompose a signal into its elementary building blocks. Any signal can be represented in terms of its constituents and the way we view these representations will give us different information about the signal. For instance the Shannon or amplitude/time representation is the most common or familiar representation. This is typically the way a signal will be displayed on an oscilloscope, as illustrated below.

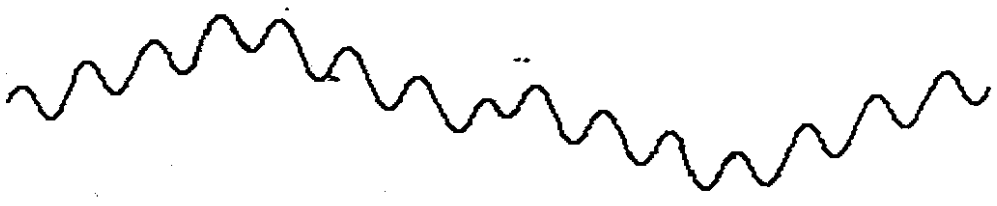

Figure 9 : Shannon Amplitude - Time representation

Another representation of a signal is by means of its frequency content. Classical Fourier analysis will typically represent the signal in Figure 9 by the representation in Figure 10.

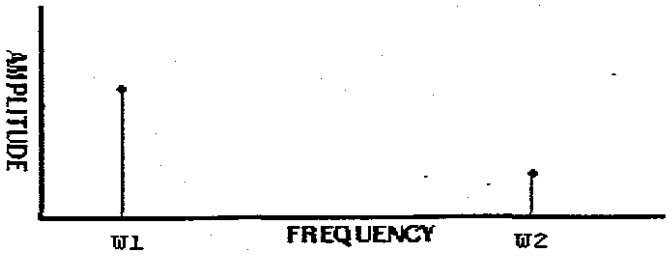

Figure 10: Fourier Amplitude - Frequency representation

Two amplitudes at their corresponding frequencies are clearly visible. Hence Fourier analysis gives us important information about a signal in the frequency domain that is not immediately obvious in the time domain. Fourier analysis gives us a well developed arsenal (Fourier series, Fourier Transforms, Inverse Transforms), backed by sound mathematics, to evaluate signals and are extensively used in the modern DSP (Digital Signal Processing) approach. In order to decompose signals into their frequency domain components, a fast algorithm, the so-called Fast Fourier Transform (FFT) is used, which is the equivalent of the mathematical Fourier transform.

2.3.2 Analysing time variant signals:

For most time-invariant signals, the Fourier techniques suffice. Very often, however, signals are time variant, and this information is not adequately represented by the Fourier transform. The signal shown in Figure 11 is a typical example.

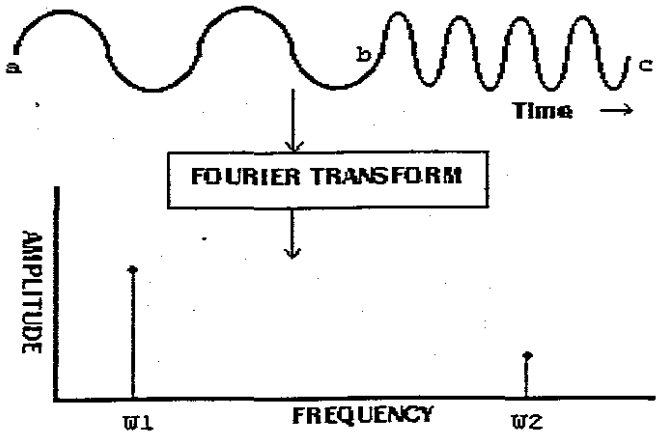

Figure 11: Fourier transform without windowing of a time variant signal.

Note that the Fourier transform looks almost identical to the one in figure 10, albeit for two very different signals in the time domain! This is because Fourier analysis provide a spectral representation that is independent of time. It is **time invariant.** A key feature of the Fourier series representation of periodic signals is the description of such signals in terms of the frequency content given by the sinusoidal components. The Fourier representation is therefore a superposition of sines and cosines, of which the coefficients represent the contribution of each sine and cosine function at any specific frequency. Non periodic or *aperiodic* signals can also be described in terms of frequency content. But as could be seen above, certain time information is lost in the frequency domain.

Vibration processes does not necessarily however always exhibit non-stationary behaviour. Such processes can therefore not be adequately described by classical Fourier analysis. In order to do effective analysis a number of **time variant** methods have evolved namely,

1) the Short-Time Fourier transform (also called the Windowed Fourier transform) - an adaptive technique
2) Wigner-Ville Distributions - a time-frequency technique
3) Wavelet transforms - a time-scale procedure

2.3.3 Wavelet analysis

With wavelets we enter a whole new mindset or perspective in processing data. It is ideally suited to processing of signals by numerical means. Wavelet analysis essentially breaks down a signal into **local functions** (wavelets - which are finite in time), instead of decomposition into **global functions** (harmonics- functions which are not localised in time). With this analysis we are analysing to scale in the time domain. In other words the scale that we use to look at data plays an important role. With the wavelet transform (WT) we cut up data into different frequency components and then study each component with a resolution matched to its scale.

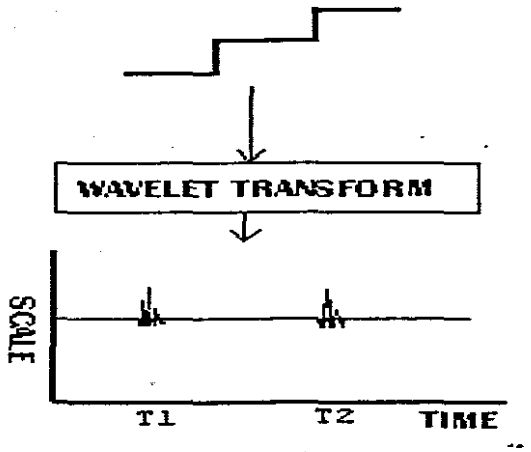

Figure 12 Wavelet transform- time scale representation

2.3.3.1 Mathematical Background:

The continuous wavelet transform is defined as

$$W_g^x(a,b) = 1/\sqrt{a} \int x(t) g_{a,b}(t) dt \qquad 2.1$$

This is a linear transform that decomposes a given function x(t) into a superposition of elementary functions $g_{a,b}(t)$, derived from an analysing wavelet g(t) by scaling and translation.

Thus

$$g_{a,b}(t) = g^* ((t-b)/a) \qquad 2.2$$

* = complex conjugation

b = translation parameter

a = dilation or scale parameter

As mentioned earlier the major difference between the classic Fourier analysis and wavelet analysis is in the Space (time) localisation's of the wavelet transform. In contrast to Fourier Analysis, where sine and cosine waves are used as a set of basis functions, the wavelet transform may have any of a set of infinite possible basis functions! (the wavelets) Mathematically the analysing wavelet must satisfy the admissibility condition

$$0 < C_g = \int \frac{|g(f)|}{f} df < \infty \qquad 2.3$$

and also locality

$$\int |g(t)| dt < \infty \qquad 2.4$$

which requires that **g(t) decays at infinity**.

From here one can obtain the synthesis formula for the wavelet transform:

$$x(t) = \frac{1}{C_g} \iint \frac{W_g(a,b)}{\sqrt{a}} \left(\frac{g^*\left(\frac{t-b}{a}\right)}{a^2} \right) dadb \qquad 2.5$$

A common wavelet used in signal analysis is the Morlet wavelet, defined by

$$\Psi(t) = e^{(i2\pi f|t|)e^{\left(\frac{-|t|^2}{2}\right)}} \qquad 2.6$$

This is illustrated below:

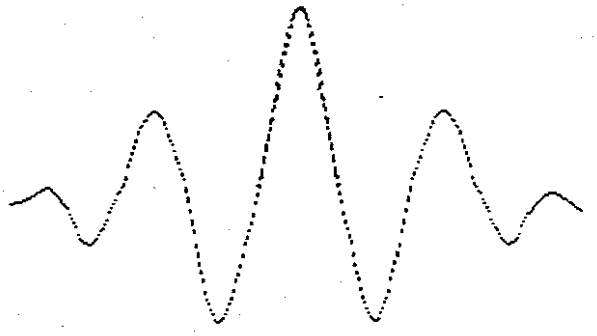

Figure 13: The Morlet wavelet.

2.3.3.2 Analysing with wavelets

Let us begin by analysing a signal, this time with wavelet transforms. Consider an analysis of the following **time variant** signal:

$K_{[a,b]}(t)\, e^{jw1t} + G_{[b,c]}(t)e^{jw2t}$ represented in figure 11.

As seen before, the Fourier analysis of this signal, without windowing , does not adequately reflect the time domain events. Analysing this signal using the wavelet transform gives us the representation shown in figure 14a. The discontinuity is clearly visible in this first pass. Using different levels of analysis we can also isolate the low and high frequency components of the signal. The power of this time/scale tool is really seen in the detection of breakdown in signals that appear to be smooth but is not. Figure 14b illustrates this graphically.

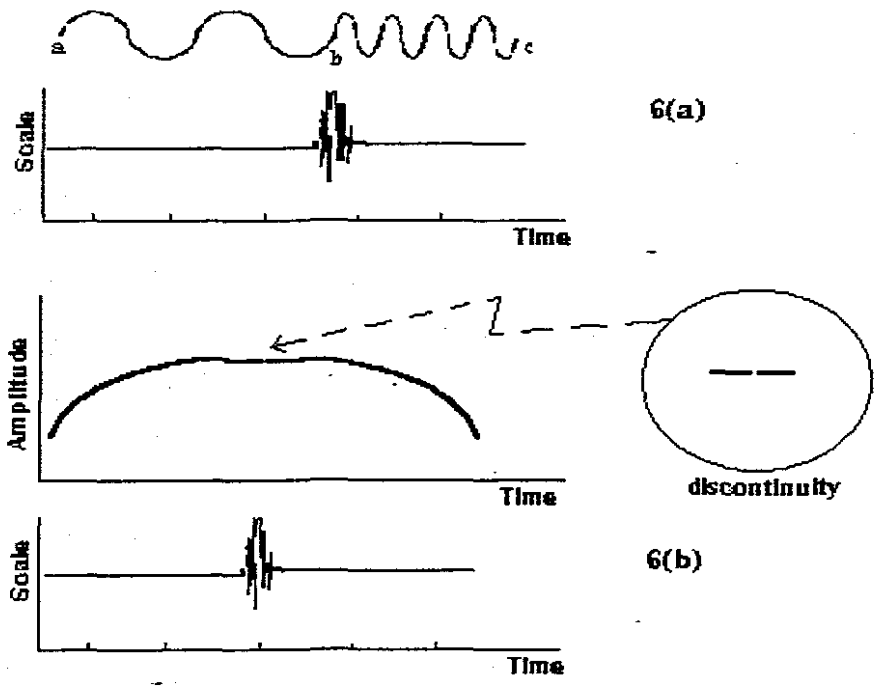

Figure 14 a &b Scale Time representation of signal and signal with discontinuity.

2.3.3.3 Compression and multi-resolution

An important consequence of wavelet analysis is signal compression and feature detection. In this example we wish to clean up a square looking wave. Looking at figure 15 a shows a signal U(n) which is transformed into sums and differences (15b) by W(n). Notice how the small differences in 15a is accentuated by the transformed representation. To perform **compression** all we do is set to zero the small numbers 15b, giving us the compressed signal in 15c. By performing an inverse transform , our **reconstructed** signal 15d is obtained! The signal with the small differences between one time frame and another becomes a uniform square wave after compression and reconstruction.

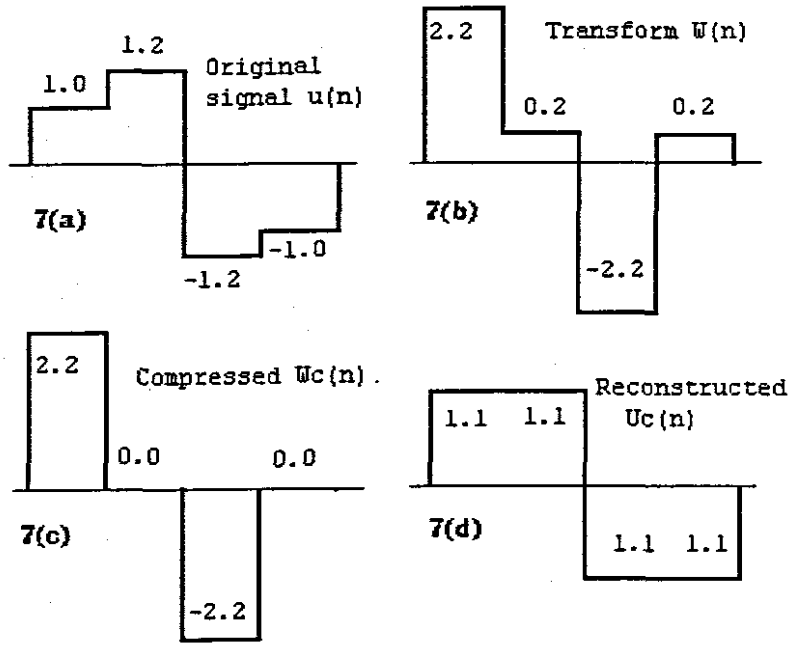

Figure 15 Compression and decompression

Again referring to figure 15, we notice that in the transformed signal 15b the sums and differences was well accentuated. This is obviously the finest scale. An even larger picture can be gained by recursion, ie taking sums and differences again. Averages and details will appear at different scales. This is the idea behind multi-resolution. Multi-resolution analysis is possible with many wavelets as basis functions.

2.4 CONTROL METHODOLOGY FOR SMART STRUCTURES

TECHNOLOGY REVIEW

2.4.1 Control of smart structures

The smart materials age is changing the way in which structures are viewed today. A structure that in general can sense, and not only sound an alarm but also adopt a temporary or permanent course of action to restore things back to "normal", is the class of structure that one can classify as "intelligent." Intelligent structures require robustness, both in terms of the sensor technology as well as the proposed control system. Control theory applied to a structure is again relatively new, and is of course implicitly linked to adequate sensor technology, as discussed previously.

2.4.2 The theory of control

Control theory have found a wide spectrum of applications which are of major technological importance. A control system generally have the components outlined below in figure 16.

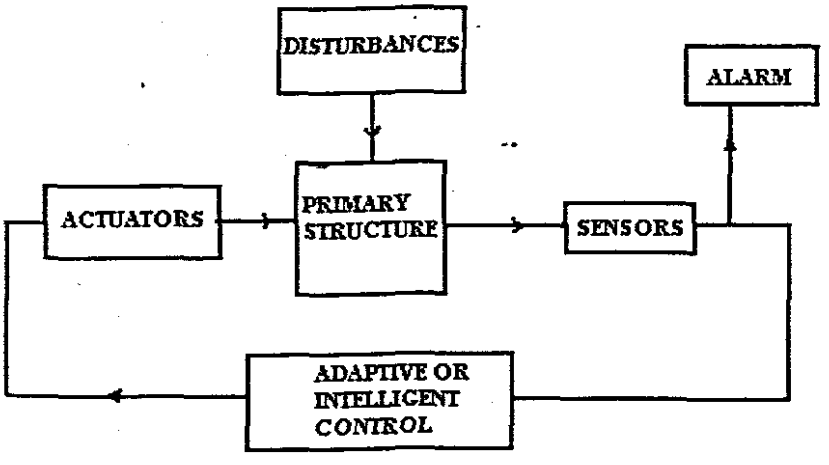

Figure 16: Closed loop control system

Disturbances acting on the structure causes conditions that are sensed by the photonic sensors. The sensor response is fed back to the controller, programmed or designed with a control law that determines what actuator response is needed to

keep the disturbances from degrading the structure. In classical control theory, the stability of a negative feedback closed loop system, outlined in figure 16, is well established.

In order to design a control system, a reasonably accurate **model** of the structure and its dynamics must be attained. Generally, feedback design of large systems without model approximations is unrealistic. It is usually unnecessary because the input/output behaviour of large systems can usually be approximated with lower order models. The model order here refer to the order of the differential equations governing the dynamic behaviour of a structure.

Implementing a classical control methodology to structure would typically follow the steps outlined in figure 17.

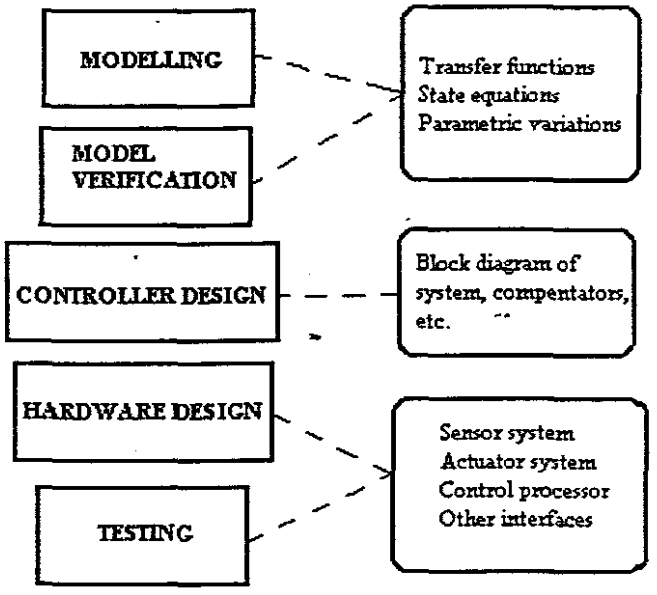

Figure 17: Steps in the design of a control system

2.4.3 Neural networks for control

Obviously the need to achieve fast, accurate and stable control is the aim of all control systems design. The term neural network (more properly : artificial neural network) have a specific meaning in that it refers to any architecture that has a massively parallel interconnection of basic processors. A neural network or processor is generally made up of "neurones", which forms the basic computational element of the processing system. Neural nets (NN's) are not, properly speaking, just an extension of artificial intelligence (AI). A neural network can be trained and on the basis of this training make generalisations and decisions. This is not the realm or objective of AI systems. A general neural network is illustrated below in figure 4.

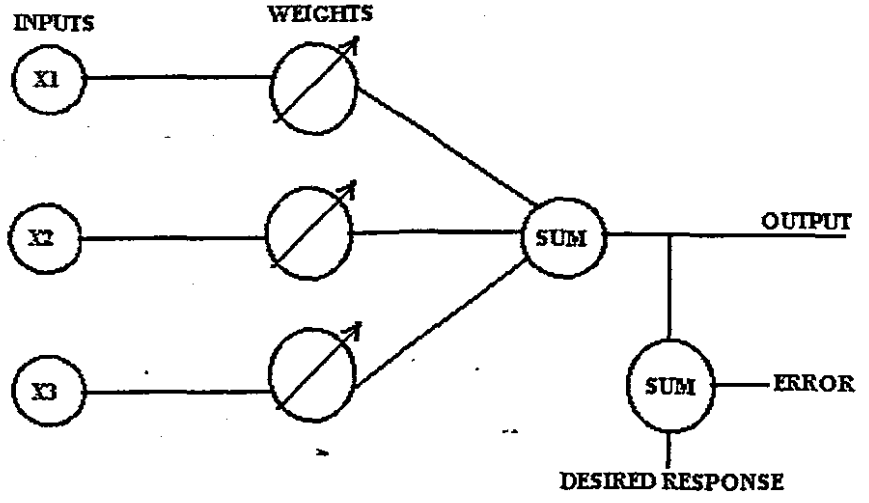

Figure 18: A three input neural network

From the above illustration, one can see that NN's are ideally suited for complex non-linear systems with multiple inputs and various degrees of uncertainty in the approximate model of the system to be controlled. The main advantages of neural networks in the control of intelligent civil structures are:

- the ability to accept and process multiple sensor inputs

- *the ability to adapt*
- the ability to provide a truly "model free" controller

Neural networks already found applications in simple manufacturing processes such as regulation in the manufacture of rebars for reinforced concrete construction.[6] In another application , damage assessment, employing photonic sensors and neural network processors have also been demonstrated. [7] Thus far, neural network generalisation techniques have found more applications in modelling, design and estimation procedures for civil engineering [8][9], than in prospective control applications, although the IEEE literature reports a rapid increase in publications dealing with Neural Networks in control applications lately.

2.5 Problems solved in this chapter

- The concept of an intelligent or smart structure, both on the micro and macro level were introduced.
- The importance of sensing as a key element in smart structures were emphasised.
- An introduction to opto-electronic techniques, such as that employed by fibre optic sensors were shown as a way towards improved sensor design for smart structures.
- A review of signal processing techniques applicable to effective processing of sensor data were researched. In this regard both time domain, frequency domain and time-scale procedures were introduced.
- Control theory applicable to smart structures were researched and a suggestion as to the applicability of neural networks in such a case was made.
- The overall chapter provided the background to the smart structure sensor system to be developed in the chapters that follow.

2.6 CONCLUSION

The development of effective control techniques can enhance the development of complex structures that are intended to be classified as "intelligent." In order to generally develop a large intelligent structure, the need for an appropriate sensor technology, such as that provided by photonic sensors, would be ideally suited for this type of application. Applying control theory to a structure is essential if degradation is not only intended to be monitored but acted upon by the structure itself. Finding a systems model for controller development could however be demanding. Present applications of neural networks to the control processes of systems are dependent on a fair amount of heuristics. The advantages of using neural networks in the control of complex systems are however not to be treated lightly. Together with photonic sensors, it is the next step in the evolution of an acceptable and optimal control architecture for complex systems such as a structure.

Wavelet analysis applications are growing by strides as more an more people begin to realise its power. By no means will it replace Fourier analysis, but it will certainly complement it. At least three, by now well established, wavelet analysis applications are listed below:

- Denoising
- Feature detection
- Audio and video compression and reconstruction

These applications are in itself of vital importance to the development and improvement of optimised sensors. With wavelet analysis the way signals are represented and analysed have changed. By combining wavelets (finite waves) we can represent any signal, especially signals which are time variant.

Opto-electronic sensor technology, being fairly new and under continuous development, will expand and probably dominate the sensor markets in the era beyond 2000. Intelligent structures, both terrestrial and those intended for aerospace applications , will be enhanced by such sensor technology in a way that traditional instrumentation simply would not be able to surpass.

Chapter 3

THEORETICAL DEVELOPMENT OF A NMLFPE [non-monochromatic lightwave fabry-perot etalon]

3.1 Introduction

As mentioned earlier, demands for new generations of materials for aerospace, military and industrial applications fuelled the development of smart materials research. These composite materials, and or structures are generally composed of fibrous polymers in which are embedded sensors and actuators. Based on structural design and basic loading criteria, continuos fibrous composite materials can be tailored to carry the applied loading in a structure, typically that of an aircraft wing. Because of the basic lamination concept and building of a structure with multiple laminates, continuous fibre structural composites are perfectly suited for embedded sensors to monitor and measure structural response. The result of

such a combination is an intelligent or smart skin. Piezo-electric sensor mechanics, and related problems associated with the embedding of such material in composite structures gave impetus to the research topic of this chapter of the thesis (which culminated in a paper that was written for IEEE Journal on Aerospace & Systems Engineering). In this regard the development of fibre-optic based sensors which can be embedded in composites, together with a technique for low cost manufacturable applications, would be extremely appropriate [70]. Fibre-optic interferometric sensors can be designed as compact and robust transducers. In general the transduction mechanism involves the phase modulation of coherent or monochromatic light propagating through a fibre-optic cable, and detecting the changes in the energy that is associated with this phase change. A review of technology suggests that the four different interferometric sensor configurations, namely the Michealson, Mach Zehnder, Sagnac and Fabry-Perot interferometers, have been most popular in fibre-optic sensor development. In the Fabry Perot etalon the sensing element is the optical cavity defined by the two reflecting surfaces. This sensor configuration can be easily constructed by extrinsic as well as intrinsic means, and renders itself a viable candidate for an embeddable sensor technology.

3.2 Problems associated with monochromatic fibre-optic interferometry

In previous designs based on interferometry, laser light sources have generally been used. In such applications expensive helium-neon lasers as well as semiconductor lasers have been employed. Semiconductor lasers, although more readily available nowadays, still need to adhere to stringent requirements before successful operation can be achieved in a sensor configuration. Appendic 5 gives a comparison of opto-electronic sources It is found that sensors using semiconductor lasers need Faraday isolators between the fibre and the source in order to eliminate feedback effects, a requirement for temperature stabilisation, as well as expensive single-mode laser action devices. In addition, there is often a need to compensate for thermally induced shifts in the emission of wavelength of the laser. The use of

non-monochromatic light sources could eliminate all of these effects. Non-monochromatic sources produce light with a wide spectral width. They generally have the advantages of low temperature sensitivity and is completely insensitive to back reflections, which is common in fibre-optic sensors. The incoherent emitted light is also insensitive to optical interference from such reflections.

The use of a non-monochromatic interferometer using the Sagnac configuration have been described before. In other interferometric configurations it is usually found inconvenient to use a non-monochromatic sources since it is not often possible to keep the path-length differences shorter than the coherence length. In most instances an interference effect cannot be predicted using non-coherent light. In the discussion below, a theoretical development of a Non-Monochromatic Lightwave Fabry-Perrot Etalon is achieved.

3.3 Energy of a Photon emitted from a non-monochromatic source

A semiconductor non-monochromatic source such as an LED produce light by spontaneous emission. This occurs when high energy conduction band electrons changes place to a low energy valence band and releases a photon in exchange for the energy loss. The energy E of a photon, is determined from the physics as proportional to its frequency f.

$$E = hf \qquad 3.1$$

The proportionality constant h is called Plank's constant, and has the numerical value of

6.624×10^{-34} joules/second

Since the speed of light c= fλ we can re-arrange such that $f=c/\lambda$ and substituting back into 1, giving

$$E = hc/\lambda \qquad 3.2$$

and therefore

$$\lambda = hc/E_g \qquad 3.3$$

Where Eg = eV (electron volts) = energy

h = Planck's constant

c = speed of light

Thus spontaneous hole/electron combination in the light emitting semiconductor, causes light emission due to recombination radiation and can also be represented by

$$\lambda = 1.24 / E_g \ um \qquad 3.4$$

The wavelength of semiconductor LED's as well as Laser Diodes (LD's) are both governed by equations 3 and 4 above. If we differentiate (2) with respect to the wavelength then

$$\frac{dE_g}{d\lambda} = -hc\lambda^2 \qquad 3.5$$

and taking infinitesimals as approximations yield

$$\frac{\Delta E_g}{\Delta\lambda} = -\frac{hc}{\lambda^2} \qquad 3.6$$

Thus

$$\Delta\lambda = \frac{\lambda^2 \Delta E_g}{hc} \qquad 3.7$$

Equation 3.5 gives us the spectral width of a semiconductor light source such as an LED. The coherence length Lc $\approx \lambda^2/\Delta\lambda$ is the minimum length required for the production of an interference signal. This will determine the typical extent of a Fabry Perot etalon. This result was used in the LED selection for the sensing NMLPFE.

Figure 19 shows the spectrum of the light emitting diode. This indicated a broad distribution of wavelengths calculated by the above equation. The spectral width can be graphically determined by looking at the half-power points of the spectrum. Values that are typical for full width at half power may (as seen with some LED's) range from 20 to 130nm.

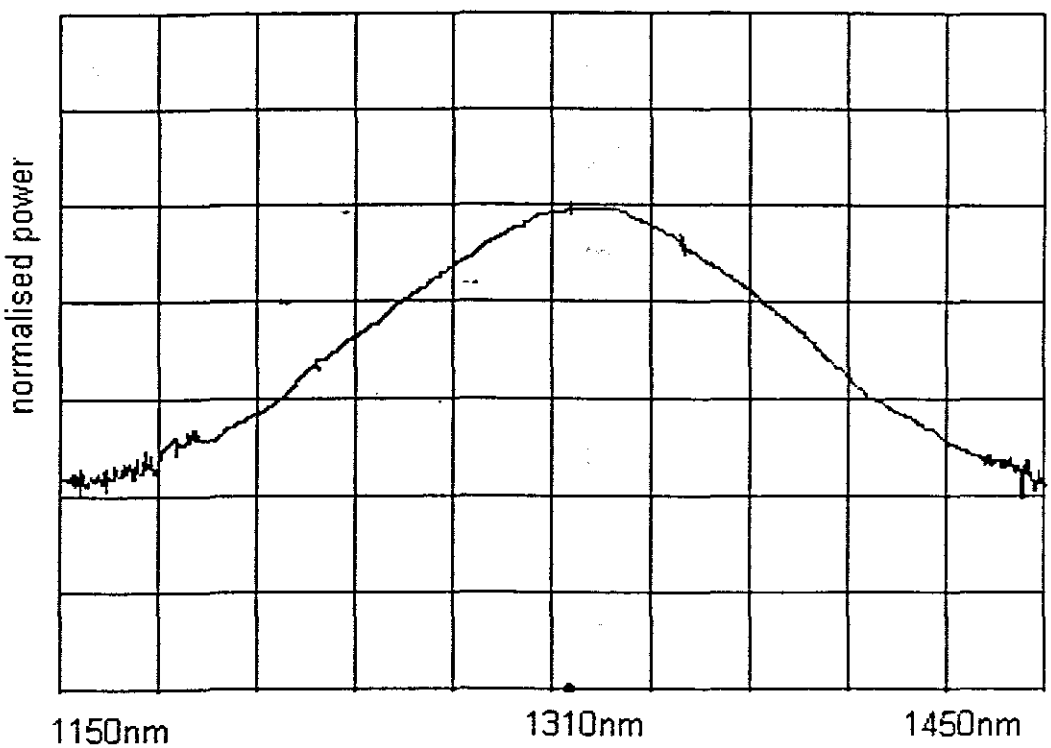

Figure 19 Spectrum of light emmiting diode

The HFBR 1315TM single mode fibre-optic transmitter (see appendix 7), made by Hewlett Packard contains a 1300nm E-LED (edge emitting LED). This non-monocromatic source has a spectral width of typically 100nm, and can be coupled efficiently for launching optical power into single mode fibre by means of a ST type connector. The coherence length calculated for this device turns out to be approximately 20um.

3.4 The Fabry Perot Etalon

The Fabry-Perot etalon is an optical cavity defined by two reflecting surfaces, and forms the main transduction mechanism for the sensor developed from the principles established here. This is illustrated in figure 20.

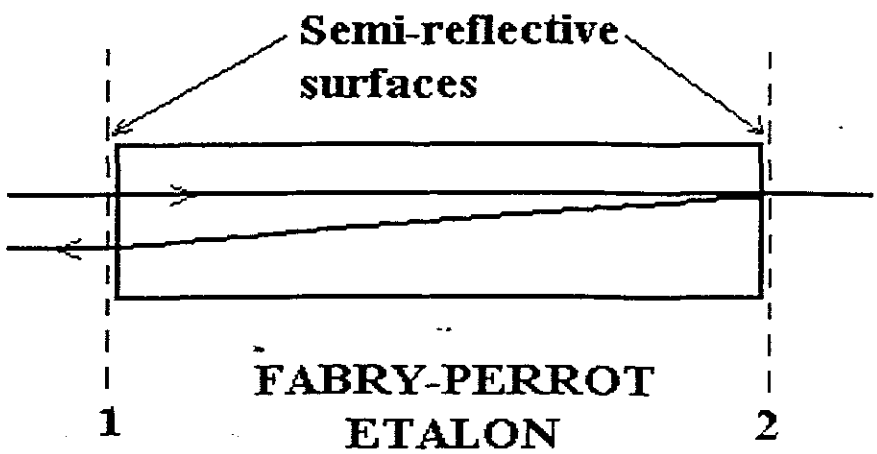

Figure 20: The Fabry Perrot etalon

Assuming that the reflectivity is 80% at each mirror interface, then 80% of light from the source will be reflected back towards it and 20% will be transmitted in the etalon. This light would in turn be reflected and transmitted back and forth between the semi-reflective mirrors. The various reflected beams would cause an optical signal intensity to occur that would be the vector sum of the electric fields

of the various transmitted beams. Conventionally, the analysis of such a cavity is based on the infinite summation of a series of multiply reflected optical waves. In the block diagram method proposed by [71] the analysis of the etalon becomes:

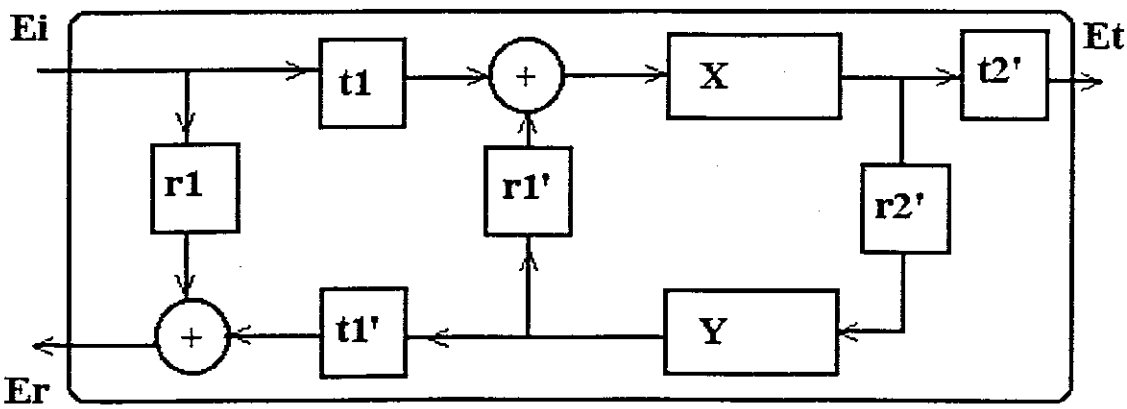

Figure 21: Block diagram of etalon

where t_i and r_i are , respectively , the amplitude transmission and reflection coefficients for optical waves travelling from a surrounding medium to the cavity medium.

$$X = [J_{12}\ ]e^{j\theta}$$

$$Y = [J_{21}\ ]e^{j\theta}$$

From here

$$E_r = [H_r]\, E_i \qquad 3.9$$

where

$$[H_r] = r_1[I] - t_1 t_1' r_2'[J_{21}]\{[I] - r_1' r_2' e^{j2\theta}[J_{12}][J_{21}]\}^{-1}\,[J_{12}]e^{j2\theta} \qquad 3.10$$

is the reflected amplitude transfer matrix. This result holds for all cases including media where the cavity reflective index differs from that of the fibre-optic medium. In cases where the cavity medium is isotropic, and the medium outside the mirror has the same refractive index (often the case where fusion splice FP cavities are formed), it stands to reason that

$$[J_{12}] = [J_{21}] = [I] \qquad 3.11$$

where $r_1 = r_2 = r$ $\qquad r1' = r2' = r'$ *and* $r' = -r$

$t1 = t2 = t$ $\qquad t1' = t2' = t'$

In this case $[H_r]$ reduces to

$$[H_r] = \frac{(1 - e^{2j\theta})\sqrt{R}}{1 - \mathrm{Re}^{2j\theta}},\ R = r^2 = (r')^2, \qquad 3.12$$

$$R_{11} = [H_r]^2 = \frac{4R\sin^2\theta}{(1-R)^2 + 4R\sin^2\theta}. \qquad 3.13$$

The reflected amplitude transfer characteristic is plotted against phase perturbation in figure 22

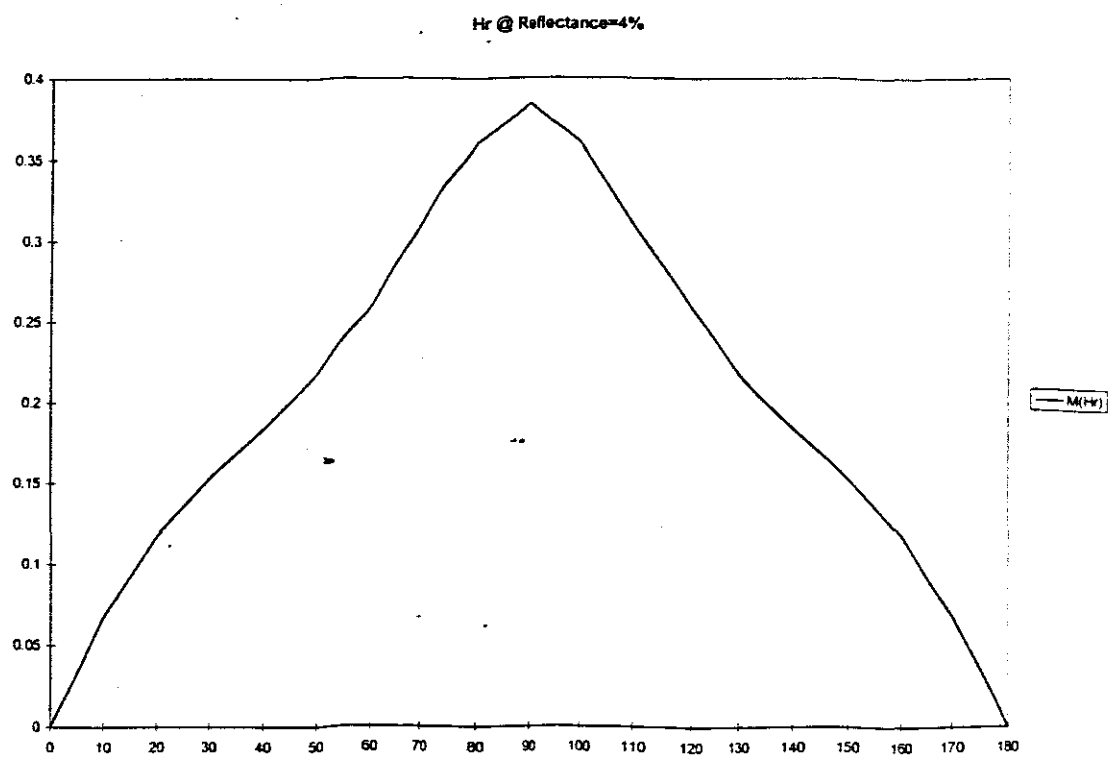

Figure 22 :[Hr] at lower than 10% reflectance

For a low finesse FP etalon, with reflectivity less than 10% for the reflecting surfaces, it is reasonable to ignore multiple reflections within the cavity. In a two

beam approximation, in which the cavity response approaches a cosinosoidal function, the returned light intensity can be represented [72] , as

$$E_r = kE_i(1+V\cos\theta) \qquad 3.14$$

Where E_r is the returned light intensity, and E_i the incident light intensity. V indicates the cavity specific visibility and k the effective mean reflectivity. A theoretically expected transfer characteristic would look as illustrated in figure 23.

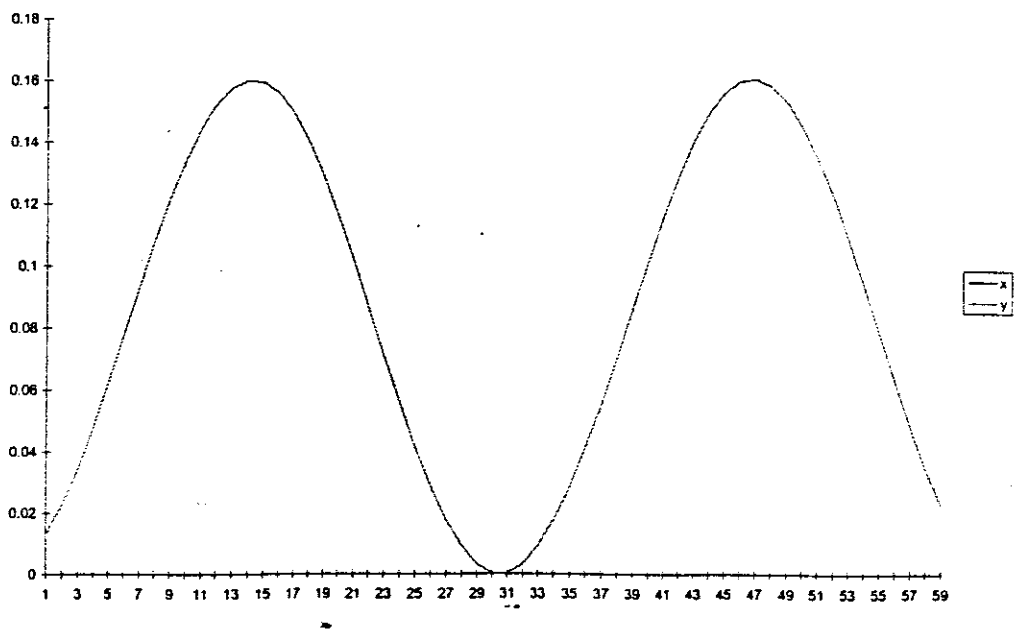

Figure 23 :Theoretically expected transfer characteristic

The optical phase of the cavity is determined by

$$\theta = (4\pi nL)/\lambda \qquad 3.15$$

Where n is the refractive index of the fibre core or cavity, L is the length of the cavity, and λ is as before the wavelength of the lightwave. This may also be represented by

$$\theta = (4\pi fnL)/c \quad \{c=f\lambda\} \tag{3.16}$$

The round trip phase shift in the etalon can then be written as

$$\Delta\theta_s = \theta + \Delta\theta_p \tag{3.17}$$

Where θ_p is due to any perturbation.

3.5 The Monocromatic Fabry Perot interferometric sensor

A host of sensors have been developed that use the following standard FP topology in sensor design. In this analysis I will use the block diagram method to analyse this sensor. By analogy the non-monocromatic FP interferometric sensor would be identical except that the simplification of the coherent source is dispensed with

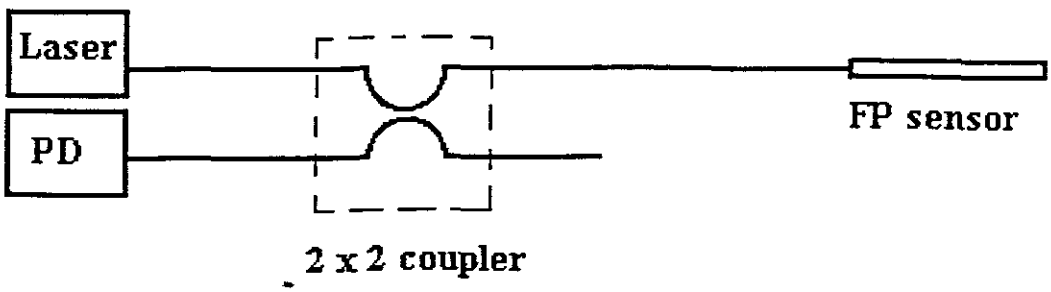

Figure 24 : General Fabry Perot based sensor

It was seen before in the analysis of that the Fabry Perot cavity behaves like an optical resonator, which can be utilised to provide spectral modulation of the incident light. In order to couple light from the sensor a 2x2 coupler is required.Fibre optic couplers are important optical fibre components. The block diagram of such an element can be described by three basic elements, namely, branching, combination and linear transformation. This coupler is modelled, using Jones [73][74] matrix algebra as

$$[K]_{2x2} = t_c \begin{bmatrix} [K_{A1}] & [K_{A2}] \\ [K_{B1}] & [K_{B2}] \end{bmatrix}, \qquad 3.18$$

where $[K_{ij}]$ are in general 2x2 complex matrices and t_c is the overall transmittance of the coupler taking into account the losses associated with evanescent wave coupling. Because of the properties of symmetry and reciprocity of the coupler , we have the following relationships

$$[K_{A1}] = [K_{B2}] \quad [K_{A2}] = [K_{B1}], \qquad 3.19$$

A block diagram of such a coupler is illustrated below in figure 25.

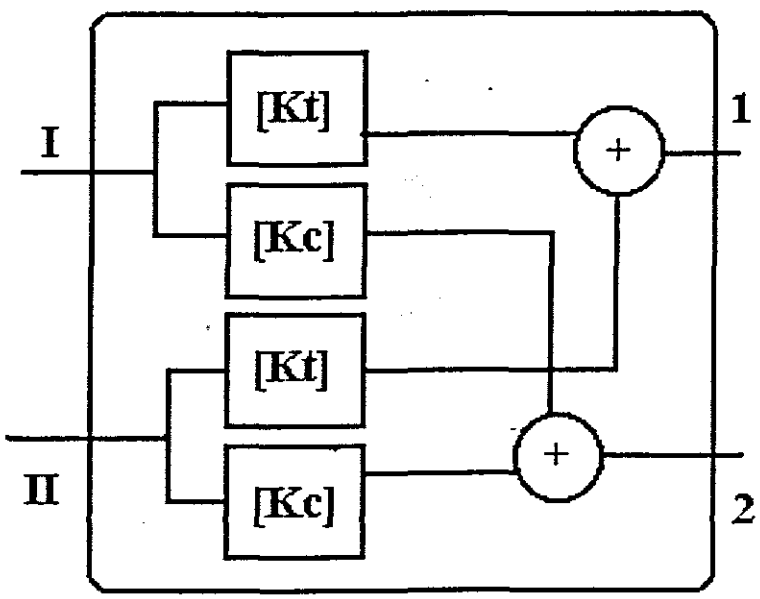

Figure 25: A block diagram of a 2x2 coupler

Therefore the transfer matrix of a coupler becomes

$$[K]_{2x2} = t_c \begin{bmatrix} [K_t] & [K_c] \\ [K_c] & [K_t] \end{bmatrix}, \qquad 3.20$$

where $[K_t]$ and $[K_c]$ are trough coupling and cross coupling matrices respectively. For a polarisation independent fibre, with cross power coupling ratio k, we simply have

$$[K_t] = \sqrt{(1-k)}[I],\ [K_c] = j\sqrt{k}[I], \qquad 3.21$$

Most fusion process fibre couplers are polarization independent. Therefore equation (20) becomes

$$[K]_{2x2} = t_c \begin{bmatrix} \sqrt{(1-k)}[I] & j\sqrt{k}[I] \\ j\sqrt{k}[I] & \sqrt{(1-k)}[I] \end{bmatrix}, \qquad 3.22$$

Couplers that are polarization independent also have a reasonably flat wavelength response as illustrated in figure 26.

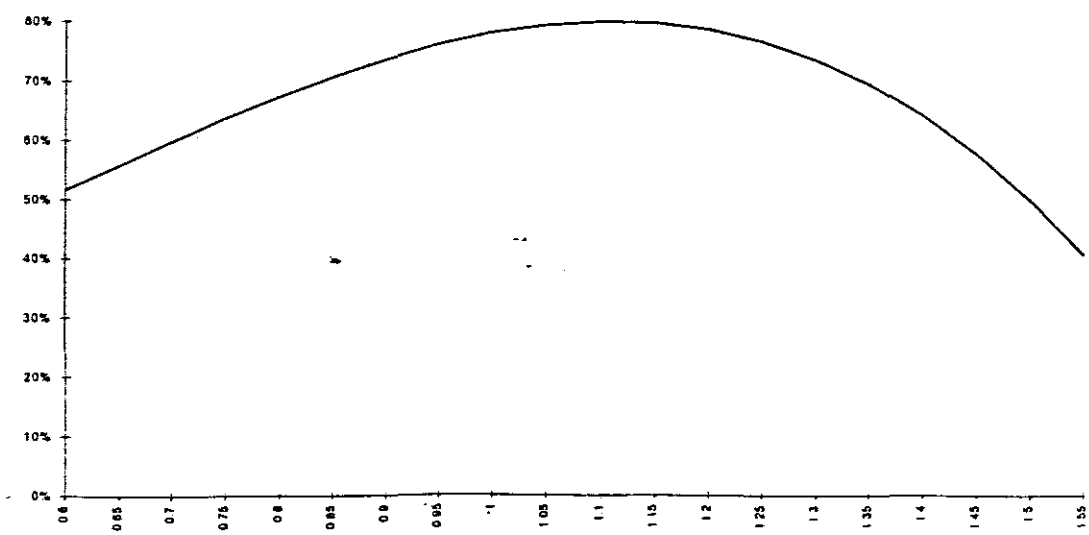

Figure 26: Coupler response over wavelength region

This response is reasonably wavelength independent and would therefore not affect the assumptions of the model. The model of the single FP sensor can now be represented by the block diagram technique as shown below in figure 27.

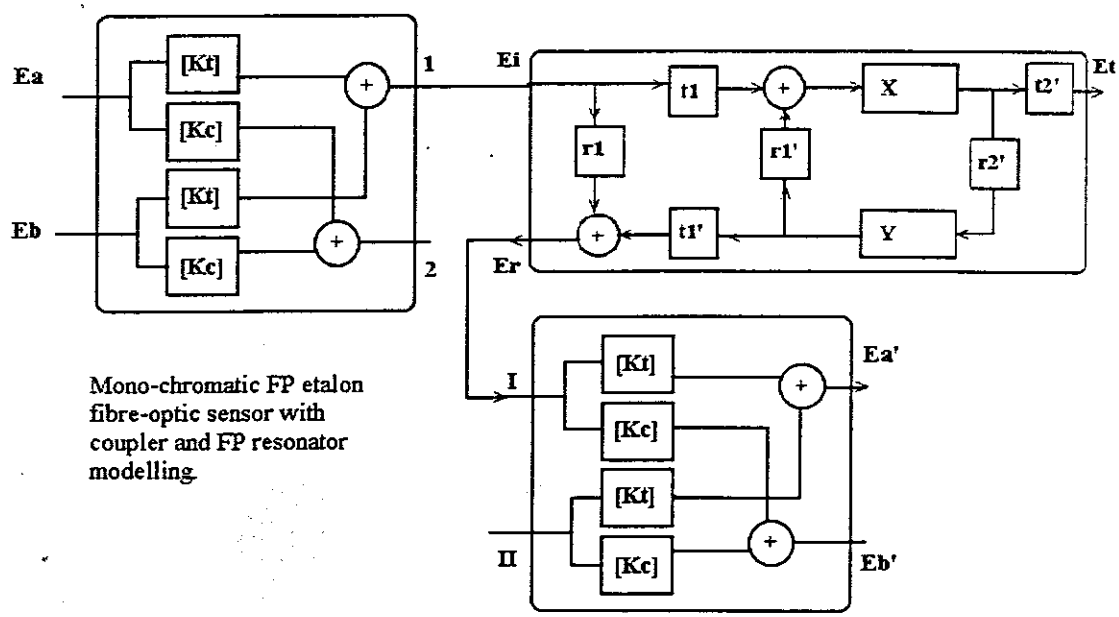

Figure 27 : Block diagram model of FP sensor

From the above figure the input/ output optical wave fields can be deduced as

$$\begin{bmatrix} E_a^{'} \\ E_b^{'} \end{bmatrix} = \begin{bmatrix} [J_{AA}] & [J_{AB}] \\ [J_{BA}] & [J_{BBA}] \end{bmatrix} \begin{bmatrix} E_a \\ E_b \end{bmatrix}, \qquad 3.23$$

where

$$[J_{AA}] = [K_t][H_r][K_t] + [K_t], \qquad 3.24$$

$$[J_{AB}] = [K_c][H_r][K_t] + [K_c], \qquad 3.25$$

$$[J_{BA}] = [K_t][H_r][K_c] + [K_t], \qquad 3.26$$

$$[J_{BB}] = [K_t][H_r][K_t] + [K_c], \qquad 3.27$$

at

$$[E_a^{'}] = [J_{AA}]E_a + [J_{AB}]E_b, \qquad 3.28$$

and

$$[E_b^{'}] = [J_{BA}]E_a + [J_{BB}]E_b, \qquad 3.29$$

The optical power transmittance from the source to the photo-detector would therefore be

$$T_{AA} = \frac{E_A^{*T}[J_{AA}]^{*T}[J_{AA}]E_A}{[E_A]^2}, \qquad 3.30$$

$$T_{AB} = \frac{E_A^{*T}[J_{BA}]^{*T}[J_{BA}]E_A}{[E_A]^2}, \qquad 3.31$$

This describes the transmittance and reflectance of a monochromatic FP etalon based sensor.

3.6 Treatment of a non-monocromatic source

The optical power spectrum of a broadband light source (non-monochromatic) can be represented by

$$E_I(\omega) = E_{in}S(\omega), \qquad 3.32$$

Where E_{in} is the total input power and $S(\omega)$ the normalised optical power spectrum which is assumed to be zero outside the spectrum range. Using equation (14), the power spectral density of the light reflected from the etalon is then

$$\frac{dE_{PR}}{df} = k_p R \frac{dE_{PI}}{df}(1+\cos\theta_s). \qquad 3.33$$

where R is the percentage reflectivity and k_p a constant of proportionality related to the reflectivity. It is assumed that the cavity specific visibility is unity in this case. The total incident power on the etalon is therefore the integral over the spectrum of the light source.

3.7 The effect of a second interferometer

By modifying the basic FP sensor to include a reference interferometer, identical to the first interferometer, we have, in the absence of a disturbance

$$\frac{dE_{PR2}}{df} = k_p R_2 \frac{dE_{PI2}}{df}(1+\cos\theta), \qquad 3.34$$

where E_{PR2} is the reflected power from the second interferometer and R_2 is the reflectance of the mirrors in this interferometer. If R_2 is much less than one (low finesse), then

$$E_{PI2} = \alpha E_{PI}, \qquad 3.35$$

where α is a constant of proportionality representing the optical loss between the interferometers. Combining (33) and (34) leads to

$$\frac{dE_{PR2}}{df} = k_p{}^2 R_1 R_2 \alpha \frac{dE_{PI}}{df}(1+\cos\theta_s)(1+\cos\theta_0). \qquad 3.36$$

Since the total incident power is the integral over the light source spectrum, the result of integrating (36) after some algebraic manipulation , and noting that

$$\int \cos\theta_0 df = 0, \quad \int \cos\theta_n df = 0, \qquad 3.37$$

yields

$$E_{PR} = k_p{}^2 R_1 R_2 \alpha E_{PI}(1-\frac{1}{2}\cos\theta_P). \qquad 3.38$$

3.8 Problems solved in this chapter

- In this chapter the problems associated with monochromatic fibre optic interferometry, the basis for the smart structure sensor, were outlined.
- The Fabry-Perot etalon, as an interferometer were analysed from first principles with the motive of developing a interferometric model of this as a monochromatic lightwave sensor
- This model, inclusive of the optical anciliaries such as coupler and losses in the fibre, were then used to determine the basic transfer characteristic of a Fabry-Perrot etalon.
- A non-monochromatic source were then introduced and the model extended to produce an interferometric transfer characteristic.
- A second reference Fabry-Perot etalon successfully produced a desired prediction of an interference pattern that means that a Fabry-Perot based sensor could be operated with an LED instead of a laser. A best fringe visibility of 0.5 was predicted, for perfectly matched mirrors in the cavities and pathlenghths of the lightwaves. This is a conclusive problem solved that would mean an easier implementation of a sensor that would be simpler to construct and much more versatile in smart structure applications than previous laser based sensors based on such interferometry.

3.9 Conclusion

Thus from (38) one can deduce that the power reflected from the second interferometer shows a sinusoidal dependence on the phase shift θp due to a perturbation that might be applied to the sensing interferometer. The result in 3.38 suggests that an interferometric sensor can be operated with a non monochromatic source by using a second interferometer to modulate the frequency spectrum of the light before it is detected by a photodetector. This second interferometer is meant to be a reference and should by itself not be subjected to any perturbation.

Chapter 4

VIBRATION SENSOR DESIGN

4.1 Introduction:

Accelerometers have long been recognised as the primary transducer used to measure dynamic characteristics of vibrating structures. They maintain excellent linearity over a wide frequency range, have self generating capabilities and are compact. However accelerometers generally are electromechanical transducers that need electrical interfacing. Also as each different type of accelerometer is designed they may contain desirable or undesirable properties that make them application specific. One undesirable characteristic, inherent in accelerometer design is the Eigenfrequency of the device, which must be avoided in its operation. In the design presented in this chapter of the thesis, the opto-electronic technique developed in chapter 3 would be aimed at to transduce vibration, instead of an accelerometer.

Mechanical vibrations are oscillatory motions, either transient or continuous, of structures. The undesirable effects of vibrations on mechanical systems can be severe. The excitation of resonance in a structure can cause damage, but so too can exposure of a mechanical structure to vibrations of frequencies away from

resonance. In the latter case the damage caused will be by the mechanism of fatigue.

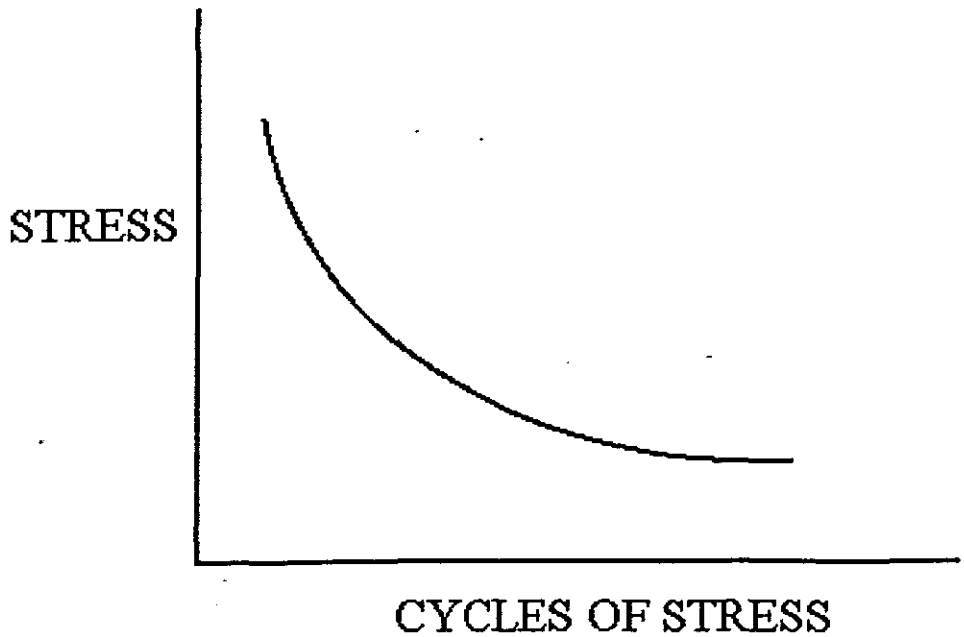

Figure 28: Structure failure due to fatigue

Another undesirable side effect of vibrating structures is the generation of audible noise. Such noise can be psychologically damaging to human beings and can even render normal communication impossible.

4.2 Vibration Measurement:

As mentioned in the introduction, accelerometers, and associated electrical instrumentation are most generally used to measure vibrations. The basic components of such a measurement system is shown in figure 29.

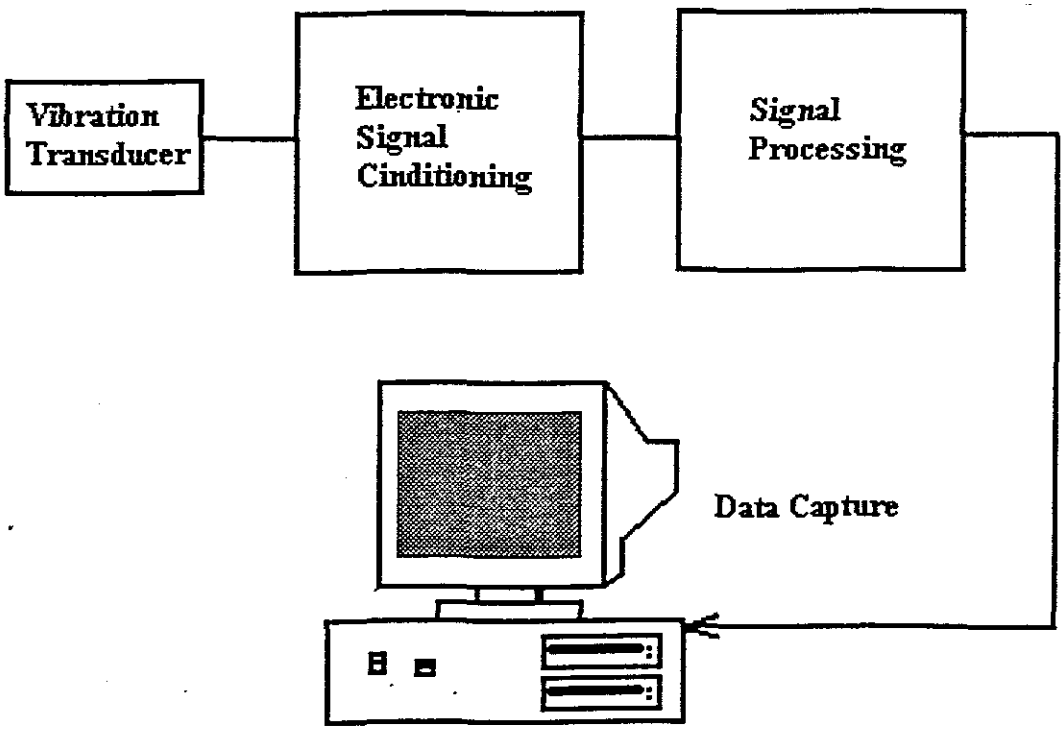

Figure 29: generalised laboratory data capture

4.3 Overview of vibration transducer operation

Vibration transducers are commonly modelled as shown in figure 30 It consists of a spring mass combination contained within a rigid container. The upper end of the spring is attached to the container and the motion of the mass is used to transduce the appropriate electrical signal. The casing is attached to the surface of the item whose vibrations are to be measured.

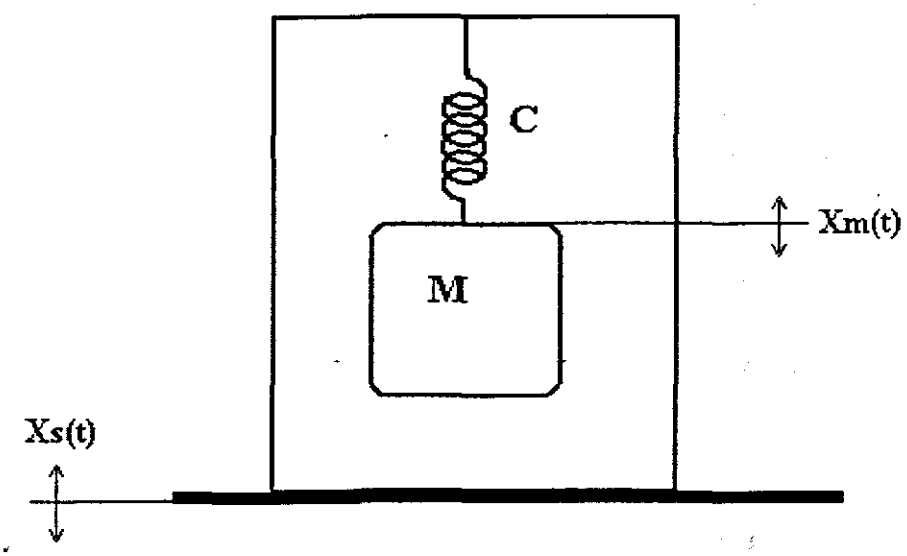

Figure 30: Mass-spring accelerometer model

The force equation for such a mass M under sinosoidal excitation $x_s=A_s\cos\omega t$ is then

$$M(dx_m / dt) + C(x_m - x_s) = 0 \qquad 4.1$$

whose solution is

$$-\omega^2 A_m\cos\omega t + \omega_0^2(A_m - A_s)\cos\omega t = 0 \qquad 4.2$$

such that

$$A_m = \left(\frac{1}{1 - E_m^2}\right) A_s \qquad 4.3$$

where

$$Em = \omega/\omega_0$$

is the ratio of the frequency of vibration to the undamped free oscillation of the mass spring combination. If the ratio of mass displacement amplitude to surface displacement amplitude is plotted as a function of the frequency ratio *Em*, one obtains the graphic illustration in figure 31.

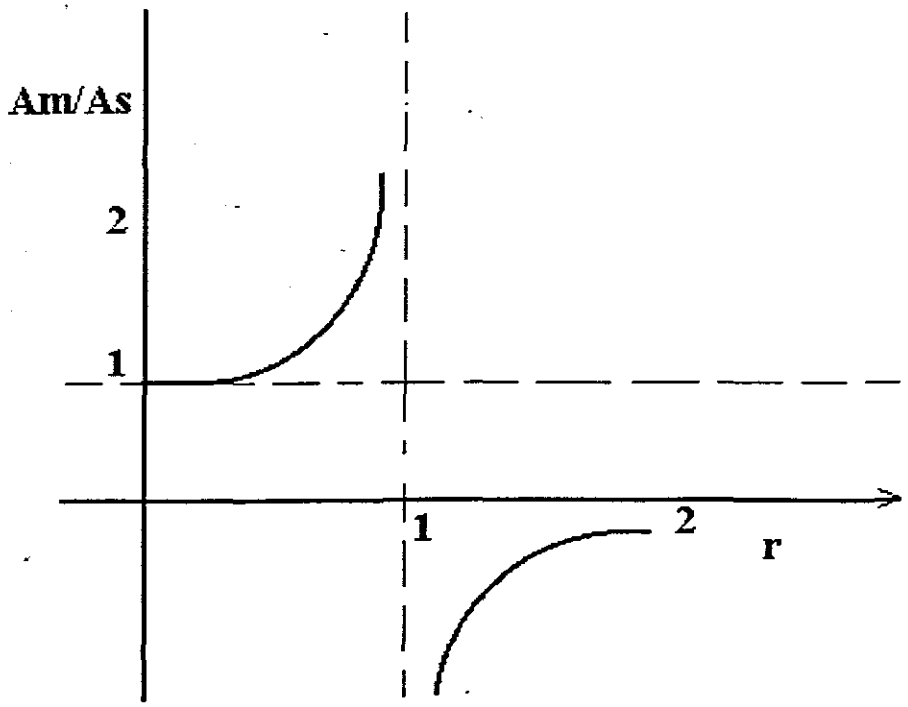

Figure 31: Accelerometer response

From this diagram it is obvious that $A_m=A_s$ for $Em<1$. The output of this transducer would therefore be exactly the motion of the vibrating surface.

4.3.1 A microbend fibre-optic accelerometer

In the technology review it was described that fibre optic cable is sensitive to microbending. It has been shown that some fibres are more sensitive to this optical power loss phenomenon than others. A microbend transducer is generally quite simple to design and Bucaro et al have shown that there is an optimal spacing l_o for microbend deformations that will produce the greatest change in transmission loss T for a given depth of deformation. Such a transducer is illustrated in figure 32.

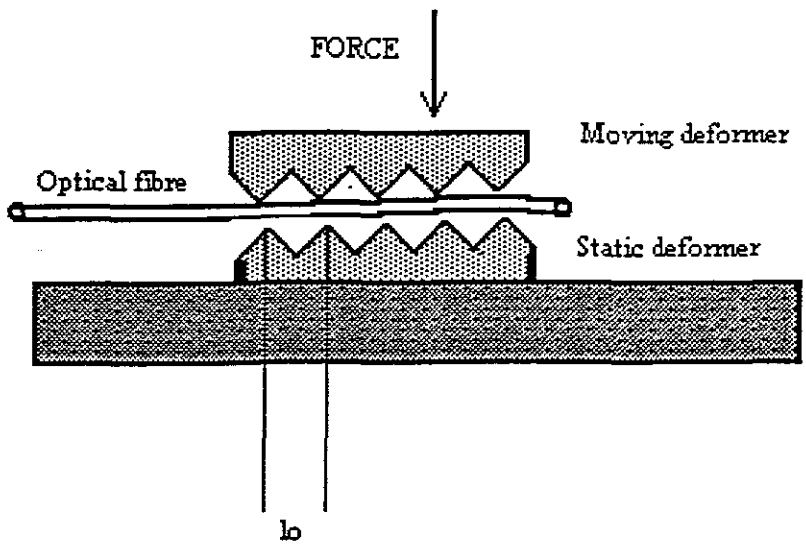

Figure 32: Microbend transducer

For step index fibre the critical length that gives the greatest change in transmission loss is given by

$$l_o = sqrt(2)\ \pi na/N \qquad 4.5$$

where n= refracrive index of the core

a_c= core radius

N_a=Fibre Numerical apeture

For typical step index multimode fibre (ATC) a_c= 60um and N_a = 0.2. The refractive index of the core is 1.46. The value of the deformation spacing is then calculated from 4.5 to be 1.95mm and represent the critical spacing used in the sensor. For practical implementation of such a sensor the number of deformations have to be optimally chosen. The more deformations the more mechanically stiff the sensor will become. In such a design the same mass spring analogy will suffice in modelling the design of the sensor to operate as an accelerometer.

4.4 Vibration signal processing considerations

In assessing the usefulness of vibration measurement parameters in smart structures , we must consider the following:

- Ease of measurement
- Ease of signal processing

The vibration transducer must therefore be designed to take into consideration the signal processing technique that would be useful for feature detection in the structure. In this regard (as mentioned in chapter 2) various options were available to me. The techniques presented below will be done comparatively so as to point to a particular hardware implementation of the sensor head.

4.4.1 Time Domain techniques

Perhaps the easiest signal processing technique is time domain processing. Time domain techniques, if subjected to digital computer processes are computationally efficient and fast. Various hardware interfaces are available off the shelf that requires only signal conditioning.

4.4.1.1 RMS Vibration measurement

If a vibration from a transducer has a pure tone, it is completely described by its amplitude and frequency. A more common way of describing the magnitude of pure tone displacement is to use the root mean square (RMS) value of the displacement.

Measurement of RMS vibration is one of the simplest techniques available. If structural damage is meant to be assessed, then as the damage increases, the RMS level is expected to change. However, such a technique is ineffective if early damage or non comparative tests are envisaged. A measurement of a structure in good condition is required to establish a reference level. As an aside, one may also consider RMS measurement as a statistical measurement since the RMS value of an alternating signal is equivalent to the standard deviation.

4.4.1.2 Peak Vibration levels and Crest Factor

A more reliable anomaly or defect analysis technique would be to measure peak vibration levels. This is done by normalising the peak values by dividing them by the RMS value of signal. The result is a parameter called the crest factor. A signal processor capable of measuring true RMS and peak values is all that is needed for such an application.

4.4.2 Frequency Domain Techniques

If a vibration signal is more generally periodic, it may be Fourier analysed into its spectral components. A frequency analyser or spectrum analyser can perform this analysis on the time domain signal to yield a spectrum. Knowledge of the spectral composition of a vibration can often be used to pinpoint the root causes of these spectral components. As with time domain techniques the interfacing for frequency domain analysis is readily available for use with personal computers for data acquisition and analysis.

4.4.3 Non periodic vibrations

In many situations random vibrations are produced whose sources of vibrations are not harmonically linked. A subgroup of random vibrations are stationary random

vibrations whose statistical characteristics are time invariant. For such vibrations a useful parameter is the probability density function

$$p(x) = \lim_{\Delta x \to 0}\left(\frac{P(x+\Delta x) - P(x)}{\Delta x}\right) \qquad 4.6$$

where P(x) is the distribution function of the variable x. The probability of having a value of x within the interval Δx from x to $x+\Delta x$ is

$$P(x+\Delta x) - P(x) = \int_{x}^{x+\Delta x} p(x)dx \qquad 4.7$$

$$= (\Delta t_1 + \Delta t_2 + \Delta t_3) / T$$

$$= \frac{\sum_k \Delta t_k}{T}$$

This calculation may be easily calculated from a computer data capture algorithm by choosing a long enough T. The mean value of x may be calculated as

$$\bar{x} = \int_{-\infty}^{\infty} x p(x)dx \qquad 4.8$$

and the variance as

$$\sigma^2 = \int_{-\infty}^{\infty} (x-\bar{x})^2 p(x)dx \qquad 4.9$$

Although various probability density functions may occur, for a random vibration , a normal or Gausian distribution applies. Here of course the corresponding probability density function describes the condition adequately.

$$P(x) = 0.5 + erf\left(\frac{x-\bar{x}}{\sigma}\right) \qquad 4.10$$

4.4.3.1 Cross correlation

Cross-correlation is a measure of the similarity between two signals. It is used to detect time-shifted or periodic similarities. In other words, the cross correlation of two signals is the sum of the scalar products of the signals in which the signals are displaced in time with respect to one another. The displacement is the independent variable of the cross-correlation function. For instance, for two input signal *x(n)* and *y(n)*. The cross-correlation between the two is given by:

$$R_{xy} = \sum_{n=0}^{N-K-1} (x(n) * y(n+k)) \qquad 4.11$$

where N = number of samples used for both inputs.

N-K-1 = number of overlapping samples at the displacement K.

From the above definition,

(1) The result depends on the number of sampling points taken.

(2) There could be zero indication of correlation due to the two signals being out of phase.

To correct (1), an average of the sum of products is done. To avoid (2), it is necessary to shift (lag) one of the wave-forms with respect to the other, as follows:

$$R_{xy} = 1/N \sum_{n=0}^{N-1} (x(n) * y(n+k) \qquad 4.12$$

This allows for easy numerical implementation on a computer. Considering two finite energy signals f(t) and g(t) such that

$f(t) \leftrightarrow F(w)$

$g(t) \leftrightarrow G(w)$

the cross-correlation between the two signals is defined as

$$\rho_{fg}(\tau) = \int_{-\infty}^{\infty} f(t)\, g(t+\tau)dt \qquad 4.13$$

The above relation is called the *Wiener-Kintchine theorem* for finite energy signals.Figure 33 shows two signals which, though not identical, bear a degree of similarity to one another. To evaluate the correlation between the two signals, we first shift g(t) to the left by τ , then form the product of the result with f(t) and integrate over the range [$-\infty$, $+\infty$]. ρ_{fg} (0) is initially 0, but $\rho_{fg}(\tau)$ varies with τ, increasing as τ increases from 0 to *a*, reaching its maximum at $\tau = a$. Consequently, τ may be interpreted as a scanning parameter used to reveal the similarity between the two signals. If $\rho_{fg}(\tau)$ is zero for all τ, the two signals are uncorrected.

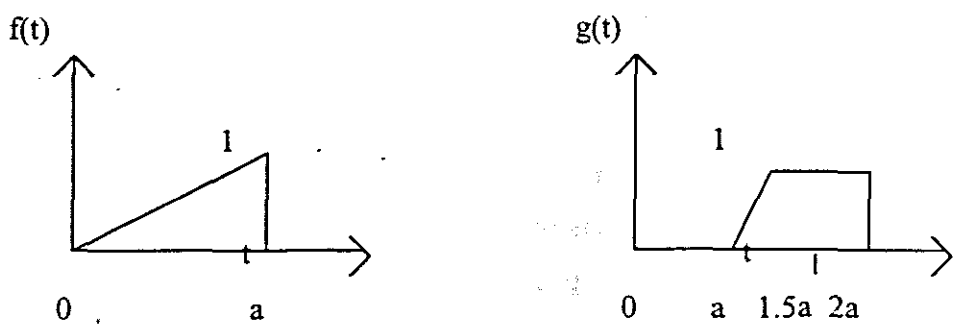

Figure 33: Cross correlation

4.4.3.1 Autocorrelation

The autocorrelation is the convolution or correlation of a signal with itself, and can be used to find periodicity in a signal. Thus

$$R(\tau) = \lim_{T\to\infty} \frac{1}{T} \int_0^T x(t)x(t+\tau)dt \qquad 4.14$$

When the superposition between x and x+t is good, the autocorrelation produces a high value, and vice versa if there is a poor fit.

4.4.3.2 Cepstral Analysis

The cepstrum of a signal is defined as the inverse Fourier transform of the log of the Fourier transform of a signal. The simplest way of utilising this analysis is to use the cepstrum to detect signal harmonics. Should a signal consist of a sine wave and its harmonics then cepstrum of the signal will show a peak at the time corresponding to the period of the signal. This peak in the cepstrum might be easier to detect than multiple peaks in a power spectrum, and thus provide a simpler method for defect analysis. When used in this way the cepstrum is very similar to the autocorrelation function, but with the log function providing greater dynamic range.

With the above in mind , it was necessary to develop the sensor head to operate over a wide frequency range with minimal dependence on eigenfrequencies. In this regard a transduction mechanism was envisaged to operate over the 0-20kHz range with no resonance considerations that needed to be taken into account.

4.5 The Fabry-Perot Efalon Vibration Sensor head

The idea for the sensor head development of this chapter was sparked by a report in "Optical Engineering Reports-1997" , in which a non-interferometric fibre-optic microphone similar in operating procedure to the principle in 4.3.1, was mentioned. It was decided for the purpose of this research to investigate the applicability of such a technique to cause a phase perturbation in the non-monochromatic Fabry-Perot etalon described in chapter 3, and thereby to produce a very sensitive vibration sensor. It was decided to use an external (no splicing) Fabry-Perot etalon as the micro interferometer using mirror tilting as the transduction mechanism to change the mechanical input into phase modulation of the sensing lightwave.

Readily available fibre ferrules was chosen as external components in creating a cavity. In a conceptual design, the ferrules were collinearly adjusted by a cylindrical spring which in turn is fixed in an adapter piece of a single mode fibre connector. The polished end faces of the single mode fibre in the ferules, if separated would form the air gap for the low finesse FP etalon. Two of these devices needed to be constructed, one as the sensing element and one as the reference, in order to produce the desired interference pattern using a non-monochromatic light source. From the concepts expounded in chapter 3, the Fabry-Perot etalon created in this manner would produce the periodic interference signal :

$$E_{PI} = kR_1R_2(1 + 0.5\cos(\theta) \qquad 4.15$$

The response function for this sensor, normalised to input power, is shown in figure 34.

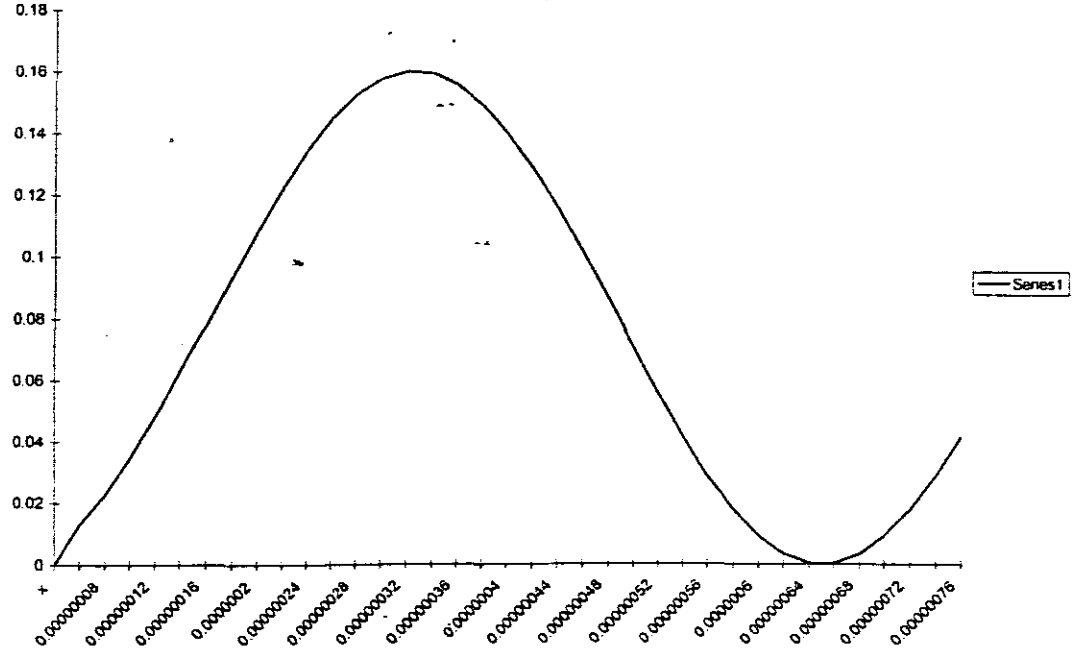

Figure 34: Theoretical interference at photo-detector

4.6 Pro Engineer for improved part design.

Pro-engineer is a C language Cad package written for mechanical component design and or system design and modelling. The present versions of Pro-Engineer is still dependent on a VI editor for the graphics interface and is not making any use of say a Visual C++ platform.

4.6.1 Pro-Engineer program script

There are four basic sections into Pro-Engineer program script.:

- the information section - contains the Pro-Engineer version number and the applicable user Revision number.
- the Input section where information is put into the program from several possible sources. (direct or fickle based)
- the Relations section:-this is the working part of the Pro-Engineer program in which most parameters are defined.
- The Feature Part and assembly section: This contains descriptions of components and turns them on or off.

Pro-engineer was investigated as an alternative to design an improved sensor head for future applications.

4.7 Sensor head design specifications

The following design specifications were chosen to design the vibration sensor.

Operating wavelength λ = 1310nm (See Appendix 7)

Mean reflectivity R = 4% at ferrule to air interface

$\Delta\theta << \pi$

$\Delta E_{PR} << 4R$

Ferrule diameter D= 2.5mm

Lightwave spectral width $\Delta\lambda$ =100nm

These specifications were met by using a standard single mode ST fibre-optic connector and its associated zirconate ferrule supplied with the connector. Figure 35 shows the detail of the ferrule based Fabry Perrot sensor head

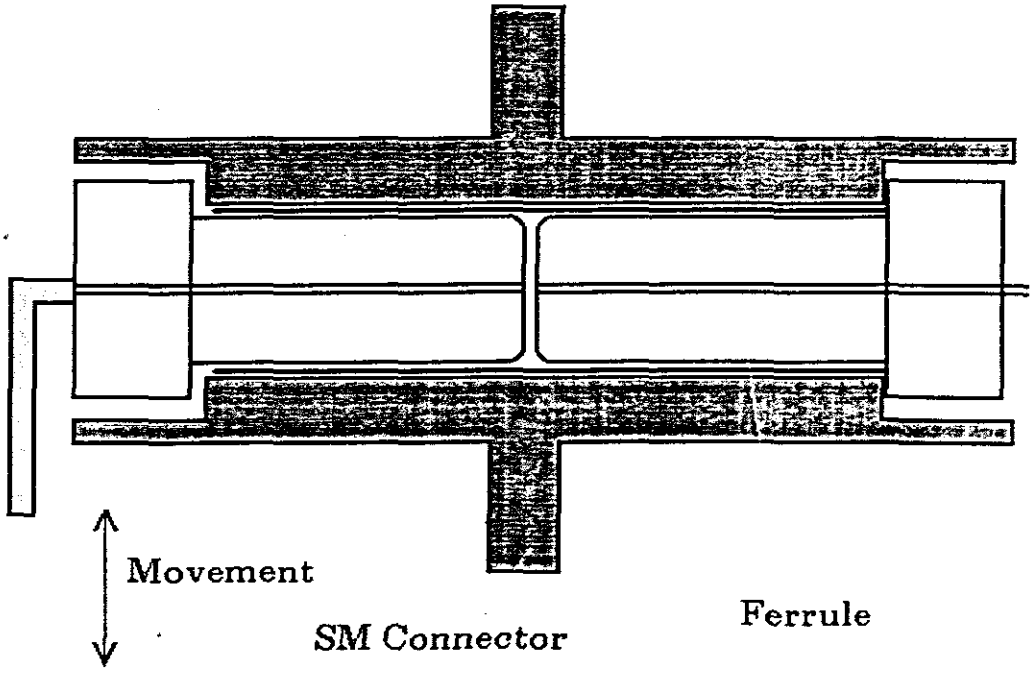

Figure 35: Ferrule and ST connector

Differentiation of the interferometer characteristic (equation 4.15) with respect to L yields at $\theta q = 4\pi L/\lambda = \pi/2$ (where $cos(90^0) = 0$) the resultant change in L is 20nm. With a ferrule diameter of 2.5mm the maximum tilt angle of the cavity formed by the ferrules are approximately 20nm/2.5mm = 16 x 10^{-3} mrad. This is approximately 1milli degree. This tilt angle detail is illustrated in figure 36.

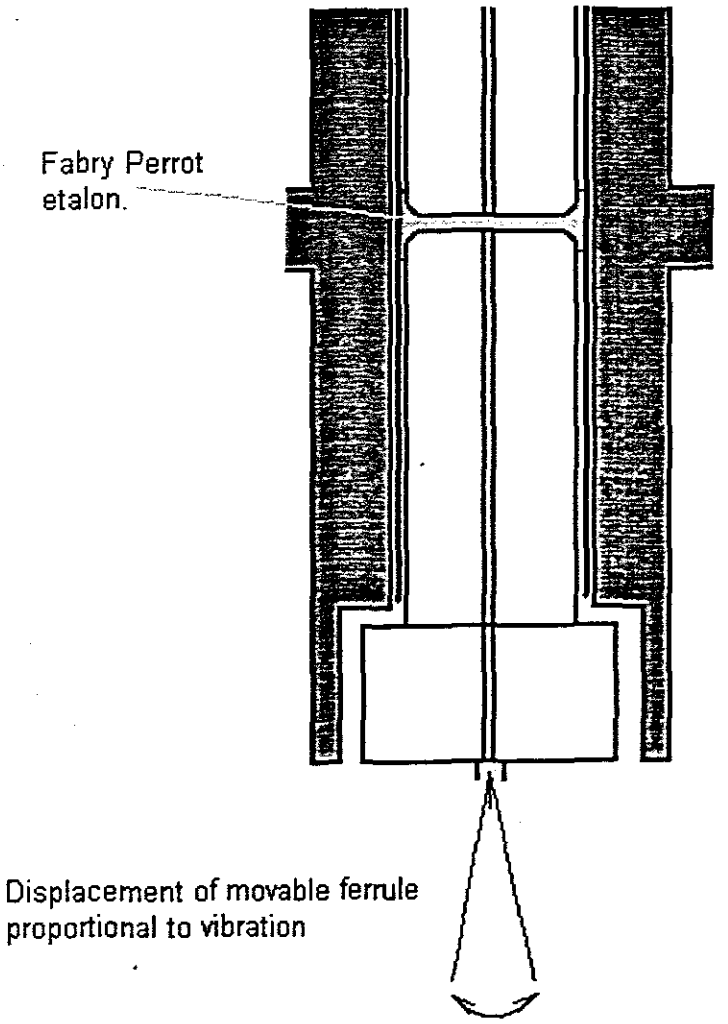

Figure 36: Tilt angle of movable ferrule.

From figure 36 the tilt angle variation can intuitively be seen as creating a variation in Fabry-Perot cavity length. The plotted distance variation as depicted in figure36 correspond to large variation in ferrule tilt angle. In practice the contraints offered by the single mode connector rendered such a variation unlikely The movable ferrule was attached to a membrane of 3cm diameter (standard speaker cone), then the ferrule tilt angle was calculated as

$$\varphi = q/M \qquad 4.16$$

where q = membrane displacement and M_r = membrane radius. The Fabry-Perot cavity variation can the be calculated as

$$\Delta L = qD/M_r \qquad 4.17$$

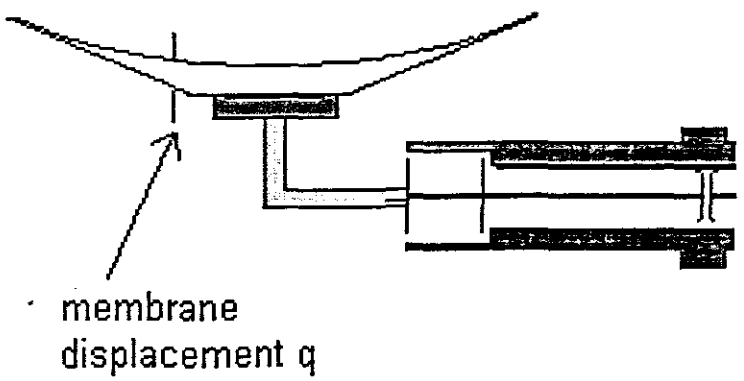

Figure37: Membrane displacement

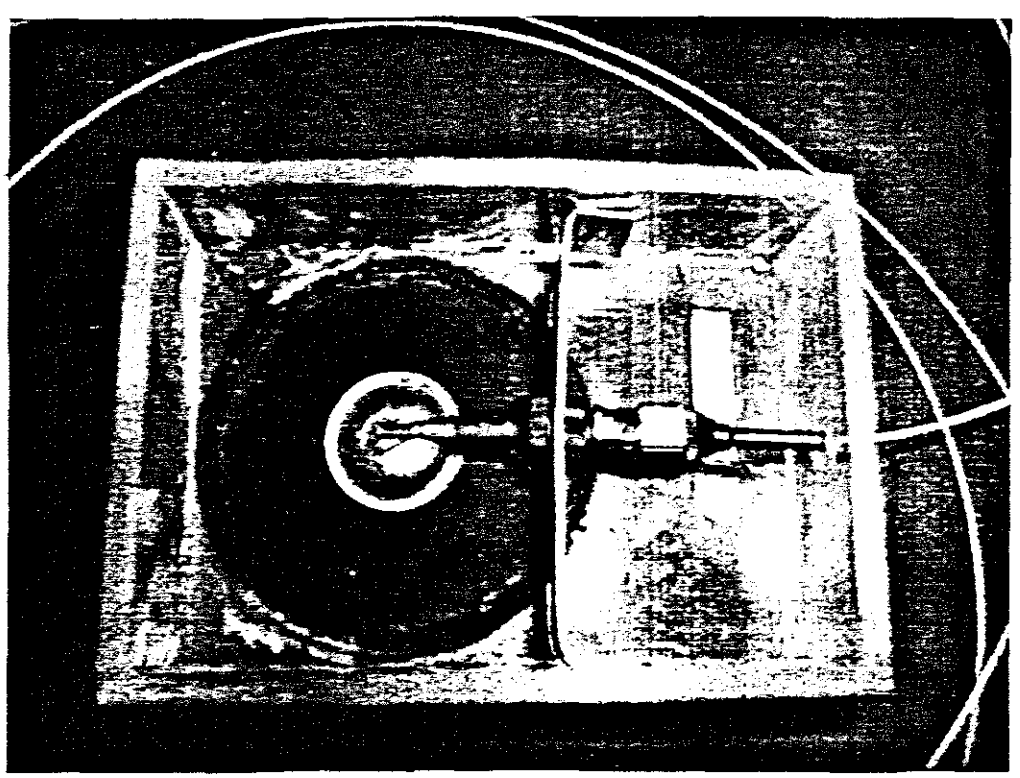

Figure 38: Sensor head detail (picture)

This change in Fabry Perrot cavity length is directly translated into a phase perturbation as required for the operation of the sensor technique of chapter 3. In the optical interconnect diagram of figure 39, the complete sensor head and associated opto-electronics are shown. Figure 40 is a picture of the actual set-up. Here a reference ferrule was kept a reasonable distance away from the sensing ferrule (FP) cavity. Due to certain construction deficiencies (the sensor head was manufactured from a used speaker cone and a perspex box, and there was difficulties in aligning the ferule to the cone base) the sensor head did not perform as expected in the testing phase. This will be discussed in chapter 5. Results were however reasonable for proof of concept consideration.

4.8 Problems solved in this chapter

- In this chapter the sensor technique developed in chapter 3 were applied to the development of a structural sensor, to enable the design of a transducer to measure the dynamic characteristics of vibrating structures.
- Mechanical vibrations and the associated classical transducer operation and measurement systems were analysed.
- Vibration signal processing considerations were taken into account
- An extrinsic Fabry-Perrot etalon vibration sensor head was developed , analysed and constructed to enable prototype sensing.

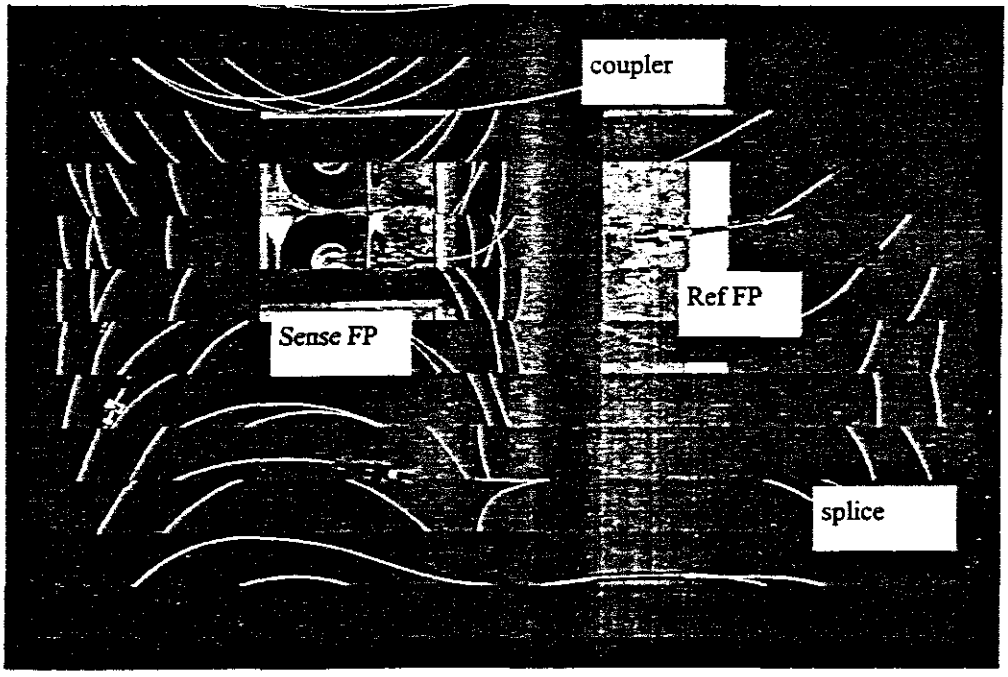

Figure 40: Picture of sensor setup

Chapter 5

MEASUREMENT SYSTEM DEVELOPMENT

5.1 Introduction

The previous chapters have concentrated on a technology overview of smart structures and smart sensing, the development of a fibre optic sensor both from the lightwave as well as mechanical aspects for vibration measurement, and related signal processing techniques. This chapter deals with the development of a real time signal conditioning, processing and measurement system design for fibre-optic sensor experimentation.

The system design consisting of, signal conditioning circuitry, a data acquisition card and a personal computer formed the heart of the development station. In recent years industrial PC based data acquisition products have become increasingly reliable. The Dictionary of Scientific Terms of 1978 refers to data acquisition and automated testing as **"the phase of data handling that begins with the sensing of variables and ends with the magnetic recording of raw data."** In this chapter a description of a easily modifiable photonic data acquisition

will also be described and may find application in later laboratory work at the Technikon. Ancillary equipment such as stable laboratory power supplies, digital storage oscilloscopes, lightwave meters and fibre optic accessories formed part of the general experimental equipment.

5.2 Micro-interferometer detector module

5.2.1 Photodiode operation

When light enters a semiconductor material the photon energy of the light waves is converted into an electric signal by releasing hole electron pairs. This causes the release of accelerating current conducting carriers within the semiconductor.This condition is shown in figure41.

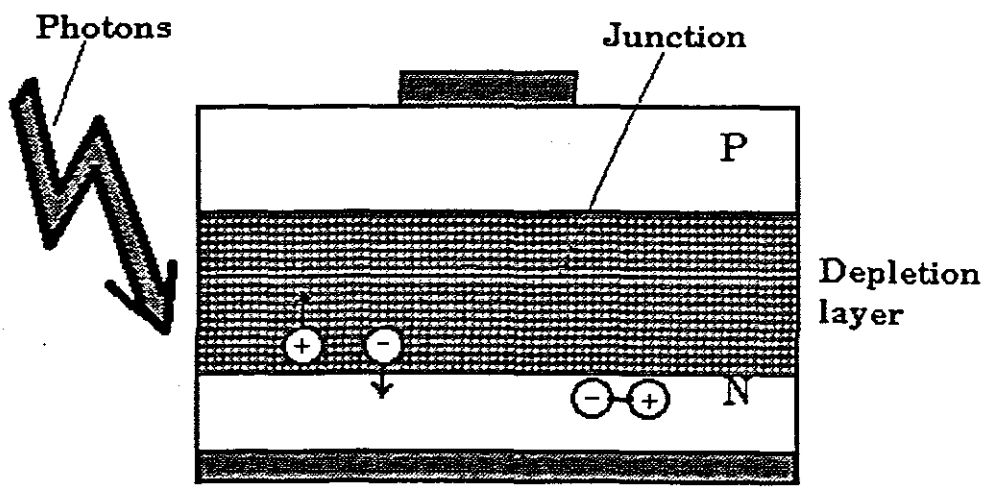

Figure 41: The PN semiconductor junction.

All photodetectors obey a characteristic as illustrated in figure 42.

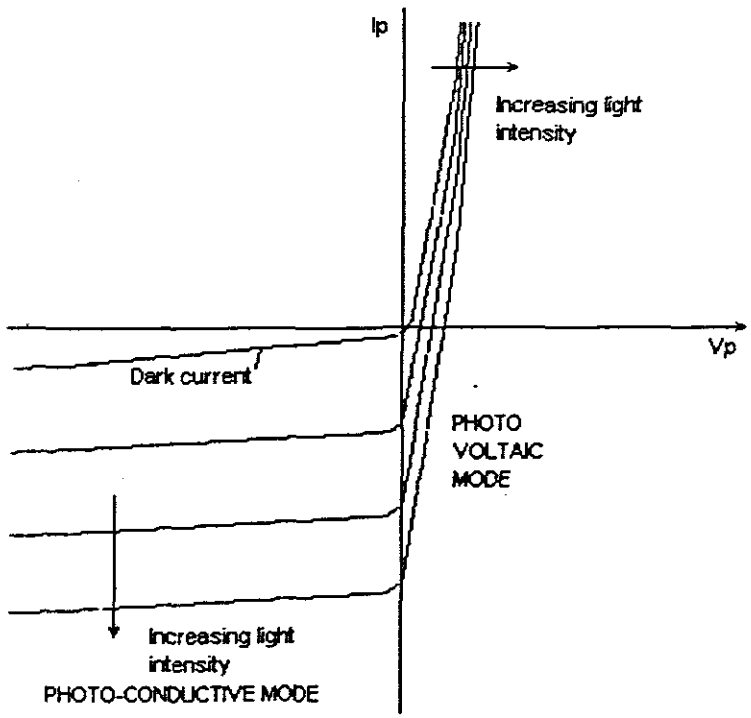

Figure 42:Photodiode characteristic

In the photo-voltaic mode ip flows through the diode to produce

$$e_p = v_t \, Ln(i_p/I_d) \qquad 5.1$$

where $v_t = kT/q$

i_p varies linearly with illumination intensity ϕe as expressed by

$$i_p = r\phi_e \qquad 5.2$$

giving

$$e_p = kT/q(Ln(r\phi/I_d) \qquad 5.3$$

From this it is evident that the voltage is logarithmically related to light intensity. In the photo-conductive mode the current I_t tends to increase linearly with increasing light intensity. Hence this would be the preferred method of photo-diode operation.

5.2.2 Detector design considerations

The appealing simplicity of the photo-voltaic mode of photo-diode operation does not justify its application because the interferometic signal produced by the NMLFPE is intensity modulated, and would in that case render a non-linear output.

The current mode (transresistance) operation of the photo-detector is easily converted to a voltage by means of a current to voltage converter. Current mode operation requires that the monitor circuit present zero load impedance to the photodiode and that the circuit itself absorb the diode current without producing a voltage across the diode. The generalised op-amp circuit shown in figure 43 closely approximates this condition.

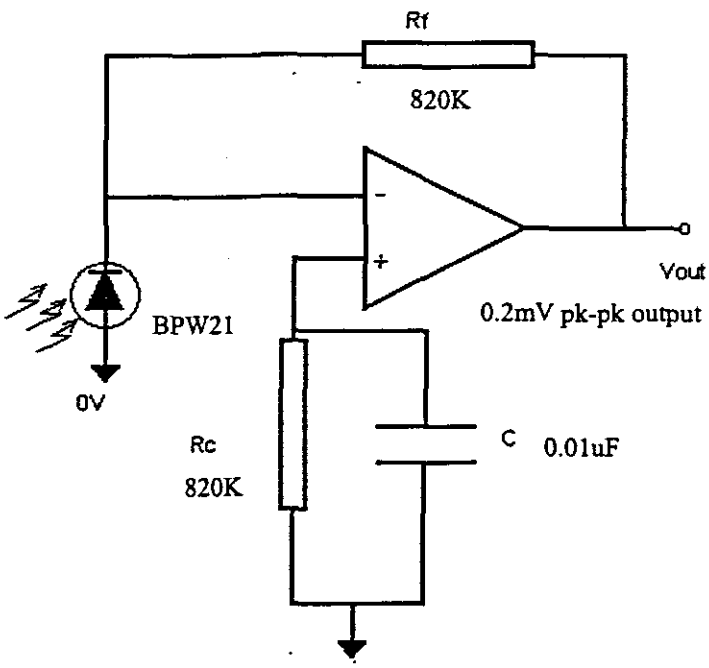

Figure 43: Op-amp current to voltage converter

In initial experiments for this thesis a plastic fibre-optic cable(POF) (see Appendix 7) was interfaced to a photo-detector (BPW21) and a good linear response was observed. The set up illustrated in figure 44 was constructed. Here a 660 nm LED was interfaced to the POF after suitable cutting and polishing of the fibre. The interface is a solid butt-coupler arrangement and allows excellent optical power transmission to the fibre. The detector was connected to the POF by means of a tube which was adhered to the glass face of the detector with cyanoacrylate.

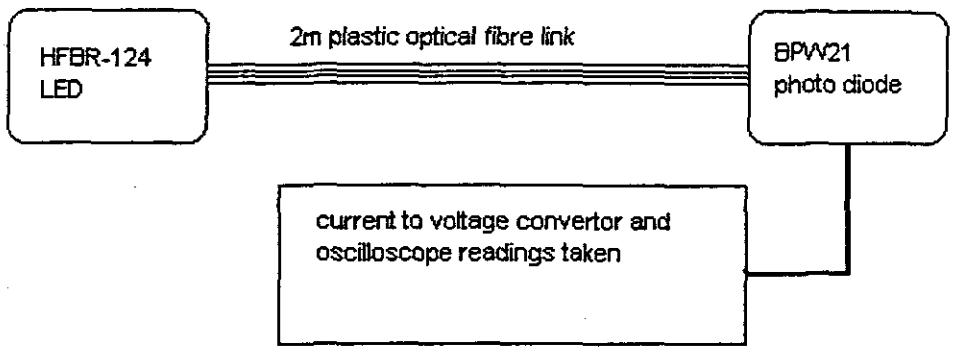

Figure 44: POF photodiode amplifier test circuit development setup

At 33na per lux responsivity of the photodiode, the LED current was modulated with a sine wave and the waveform in figure 45 was observed.

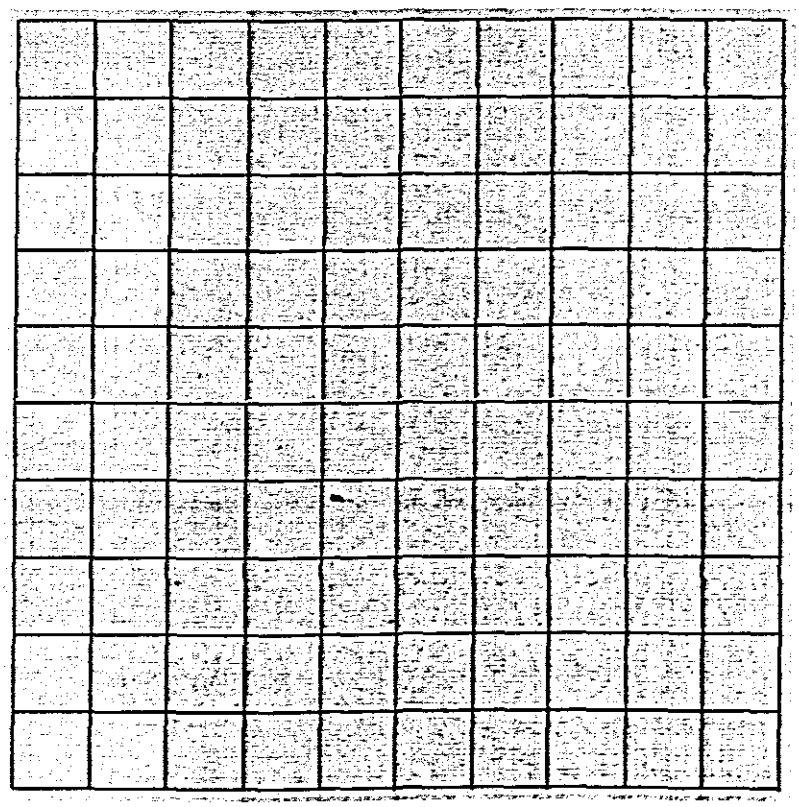

Figure 45:1kHz waveform observed from photo-amplifier after 10X amplification.

5.2.2.1 Dc offset effects:

It was observed from these experiments that the current to voltage convertor developes a dc offset primarily through two error currents. Both the input current of the amplifier and the leakage current of the photodiode flow through the feedback resistor. By making Rc equal to Rf, the offset was reasonably compensated.

5.2.2.2 Bandwidth

The junction capacitance restricts the signal bandwidth for most photo diode amplifiers. Any signal voltage developed across the diode react with this capacitance which essentially shunts the diode photocurrent. The BPW 21 photodiode used in the initial experiment to develop an adequate photo-detector had a junction capacitance of 400pF. An improvement to this initial experiment was the selection of a photodiode with a smaller junction capacitance.

5.2.3 Noise reduction in the detector

Effective noise reduction in optical amplifiers results from restricting noise bandwidth without reducing signal bandwidth. Unlike most op-amp circuits, the high gain transresistance photo-diode amplifier discussed above produces a bandwidth distinction for signal and noise. Several op-amp specs were investigated and it as concluded that a reduction in opamp open loop bandwidth decreases noise without affecting signal. By reducing the amplifier bandwidth to the same frequency as the signal band width limit, noise performance is optimised. A brief survey revealed that op-amps that have provision for external phase compensation, automatically offer this option. The limited provision of this option however restricts amplifier choices and it was preferred to design a general purpose high gain transresistance amplifier that could produce the desired signal and noise (co-

incidently) bandlimited, without restrictions. An amplifier configuration that was investigated as a choice for low noise specifications is illustrated in figure 46.

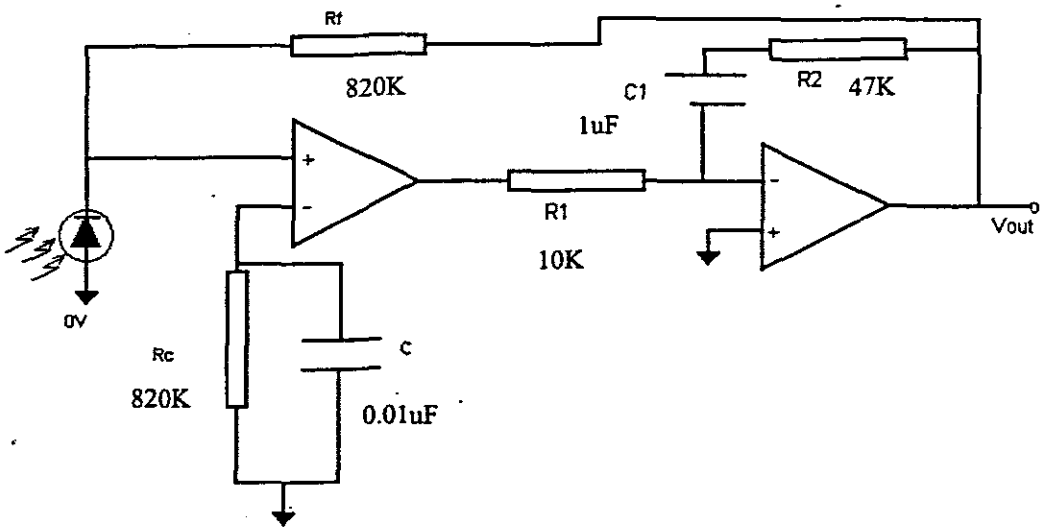

Figure 46: Composite amplifier.

This amplifier essentially minimised noise by means of the second op-amp for noise bandwidth control. The offsets voltages were however difficult to control with the selected op-amps and the idea was abandoned for the following improved amplifier.

5.2.4 **Final module and results**

By constructing the circuit of figure 47, a single stage, high gain photo-diode amplifier was achieved. This circuit worked well and produced up to 8V peak to peak swing on the output for light intensity variations. The photodiode used in testing this case was the FID3Z from Fujitsu, a Galium Arsenide PIN device with excellent responsivity in the 900 to 1600nm wavelegnth. This fitted well within the specifications of the LED lightwave source that the sensor system was designed to operate at in chapter 3. The photo diode in this case is bootstrapped by removing the load's signal voltage from the photodiode. The photodetector signal becomes a common mode signal at the amplifier's two inputs and common mode rejection virtually removes the signal from the diode. This condition leaves the diode responsivity virtually unchanged and avoid a forward biased diode state that could produce latching in the composite amplifier case.

In this case current gain is effectively:

$$i_o = \frac{R_f}{R_1} i_p \qquad 5.4$$

and is essentially linear with regard to light intensity.

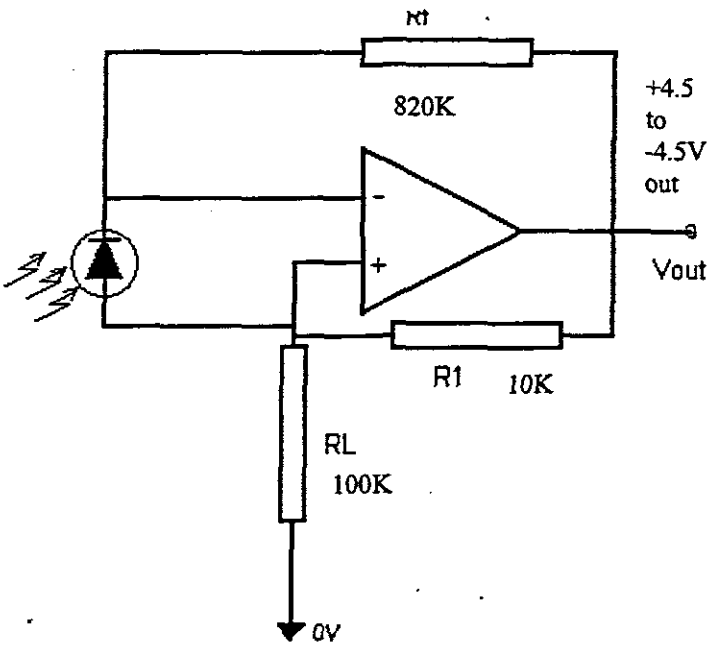

Figure 47: photo current amplifier to improve response due to weak signal

The circuit was subjected to a biased analog light intensity signal and produced an easy 6Vpk-pk swing as shown in the captured result of figure 48.

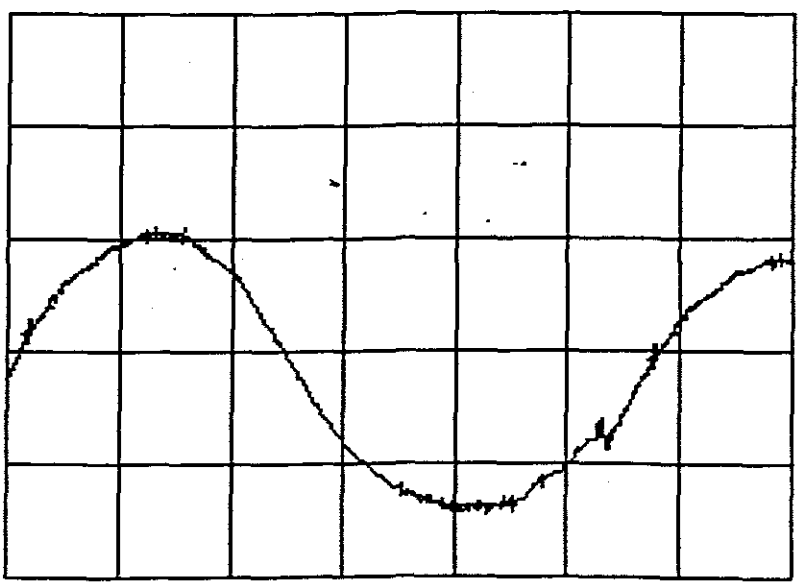

Figure 48: Lightwave measurement with photo-detector

5.3 Anti-aliasing signal conditioning filter module

Signal conditioning circuits improve the quality of signals generated by transducers before they are converted into digital signals by the PC data acquisition hardware. Examples of signal conditioning include signal scaling, amplification, linearisation, filtering and attenuation. One of the most frequently used signal conditioning circuits are amplifiers. Amplification expands the range of transducer signals so that they might match that of the input range of the A/D converter for maximum resolution. The amplifier, which in this case was the high current transresistance amplifier described above is then followed by a low pass active filter to reduce unwanted electrical interference, appropriate to bandwidth of course, as well as anti-aliasing operations in the A/D card.

5.3.1 Why anti-Aliasing?

Aliasing although not always bad in analogue electronics, where it is often referred to as mixing or heterodyning to produce tuning in common household televisions, can be disastrous for this application if vibration damping in a closed loop would be attempted in later research. Since we will have data acquisition and hence sampling of the analogue signal to produce a digital equivalent of the input, the sample rate must be greater than twice the highest frequency in the input. This well known criterion , known as the Nyquist Criterion, dictates that we may ideally overcome the errors due to aliasing in a measurement system. Unfortunately the real world rarely restricts the frequency range of its signals. The only way to be really certain that the input frequency range is limited is to add a low pass filter before the sampler (A/D). This type of filter is called an anti-alias filter.

5.3.2 Anti-alias filter design parameters.

The ideal anti-alias filter will have a "block" low pass characteristic as shown in figure 49. It should according to that characteristic, pass all desired input frequencies with no loss and completely reject any higher frequencies, which could otherwise alias into the input frequency range. In a tight design anti-alias and anti-imaging filters typically approximate ideal low pass characteristics.

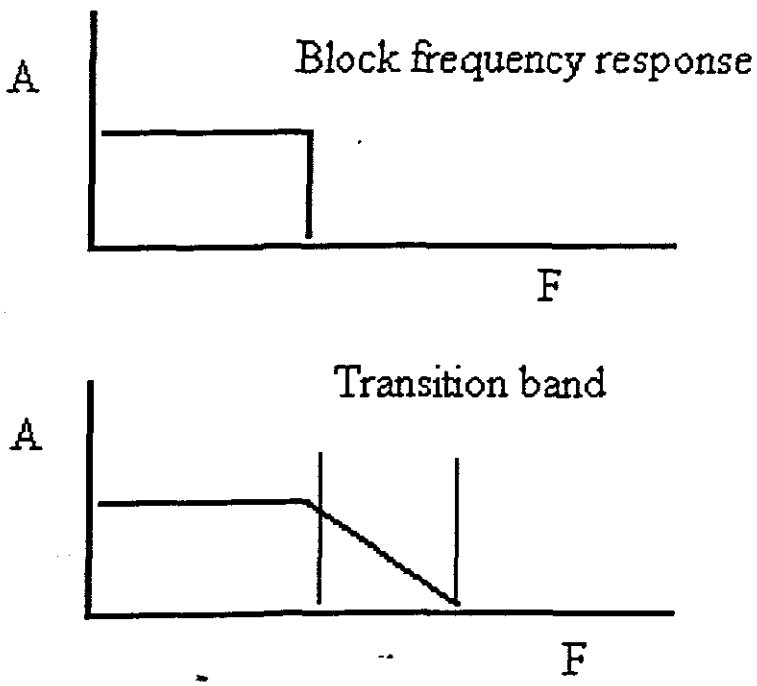

Figure 49: ideal anti alias and a realistic filter

In order to avoid aliasing the sampling frequency often has to be higher than twice the highest frequency of the transition band. The vibration sensor head was designed to typically operate in the 19kHz audio band. In this case the transition band, if essentially steep could still allow a realistic sampling frequency choice in order to keep the cost of the data acquisition card low. The following table shows the specifications to which the anti-alias filter was designed for:

Passband attenuation	3dB
Stopband attenuation (Min)	60dB
Passband edge	19kHz
Stopband edge	22kHz

Table 5.3.2

5.3.3 Analog prefiltering vs digital pre-processing

Digital filters are commonly designed by transforming an s-domain transfer function to the z-domain, using the well known bilinear transform. In recent years however , many powerful filtering algorithms have been developed that operate entirely in the discrete time domain. Examples of such digital filtering algorithms are certain classes of non-linear filters and some prediction and estimation algorithms [78][79]

Although DSP's re increasingly used, analog signal processing can provide advantages in applications where power consumption and simplicity is critical. Furthermore, anti-aliasing filters is needed for bandlimiting the sensor signal before sampling and A/D conversion. The drawback of the conventional AA filter is that it also ads a DELAY (due to low pass filter action) which is sometimes more harmful in data acquisition than the aliasing phenomenon. In closed loop control applications this can lead to instability as well.

In researching the design of a novel anti-alias filter for use in the measurement system, it was decided to use the interesting idea of Viano and apply it to the anti-alias filter. In the application for this chapter the design took the following steps.

5.3.4 Development of a low delay AA filter

A delayless filter is most easily designed in the discrete time domain, where one can use efficient methods of extending FIR forward predictors into predictive IIR filters, thus making the necessary model for conversion to the continuos time domain. FIR filters can be designed for prediction of time domain signals using the Lagrange multiplier method expounded in [78][79]. The design specification for FIR predictors is

$$y(n)=\sum_{k=0}^{M-1} c_k x(n-k)=x(n+N) \qquad 5.5$$

where M is the FIR filter length, x(n) is the input signal with specified characteristics and y(n) is the output. The prediction step length is represented by N. Depending on the nature of the incoming signal to be predicted, the FIR predictor coefficients are based on a polynomial model. This model is a modification of Golay filters as given by [79] and is given by this reference as:

$$F(z)=\sum_{k=0}^{M-1} c_k\, z^{-k} \qquad 5.6$$

and therefore

$$H(z)=\frac{\sum_{m=0}^{M-1}[c_m z^{-m}\prod_{r=0}^{m}(1-b_r)]}{1-\sum_{l=0}^{M-1} c_l b_l z^{-N-1}-\sum_{i=1}^{M-1}\{c_i z^{-N-i}\sum_{j=1}^{i}[b_{i-j}\prod_{k=1}^{j}(1-b_{i+1-k})]\}} \qquad 5.7$$

This is essentially the transfer function of an IIR predictor formed from that of a FIR. Conversion of this IIR filter was done by using the inverse bilinear transformation

$$z=\frac{1+(T/2)s}{1-(T/2)s} \qquad 5.8$$

where T represents the sampling interval. The frequency mapping in transformation is given by

$$\Omega = \frac{2}{T}\tan(\omega / 2) \qquad 5.9$$

representing the discrete and continuos time frequencies respectively.

5.3.4.2 **Analog filter implementation**

After the inverse transformation is complete an RC active filter wasdesigned to implement the idea. The general cascaded active RC filter can be represented by the transfer function:

$$H(s) = \prod_{i=1}^{q} K_i \frac{b_{2i}s^2 + b_{1i}s + b_{0i}}{a_{2i}s^2 + a_{1i}s + a_{0i}} \qquad 5.10$$

This can be easily implemented by the by the state variable biquadratic filter or first order RC inverter networks as realised by the following equations:

$$H(s) = K\frac{s^2 + b_1 s + b_0}{s^2 + a_1 s + a_0} \qquad 5.11$$

or

$$H(s) = K\frac{s + a}{s + b} \qquad 5.12$$

Prototype circuits were designed and built to test the idea. A LM348 operational amplifier was used to breadboard the following circuit to the design parameters outlined below. Viano gives $F(z) = c_0 + c_1 z^{-1}$ as a sufficient function to obtain the very basic IIR transfer function

$$H(z) = \frac{c_0 - c_0 b_0 + (c_1 - b_0 c_1 - b_1 c_1 + b_0 b_1 c_1)z^{-1}}{1 - b_0 c_0 z^{-1} - (b_0 c_1 - b_0 b_1 c_1 + b_1 c_1)z^{-2}} \qquad 5.13$$

I arbitrarily chose say $F(z) = 2 - z^{-1}$ such that

c0 = 2

$$c1 = -1$$

$$b0 = 0.861$$

and $$b1 = -0.950$$

and obtained after the bilinear transformation of ( ) the following analog transfer function:

$$H(s) = \frac{(0.00695 + 0.54905s)(1 + s)}{0.00695 + 0.5421s + 3.45095s^2} \qquad 5.14$$

This was a transfer function with real poles and zeroes and of second order. This implementation circuit was the state-variable biquad shown below:

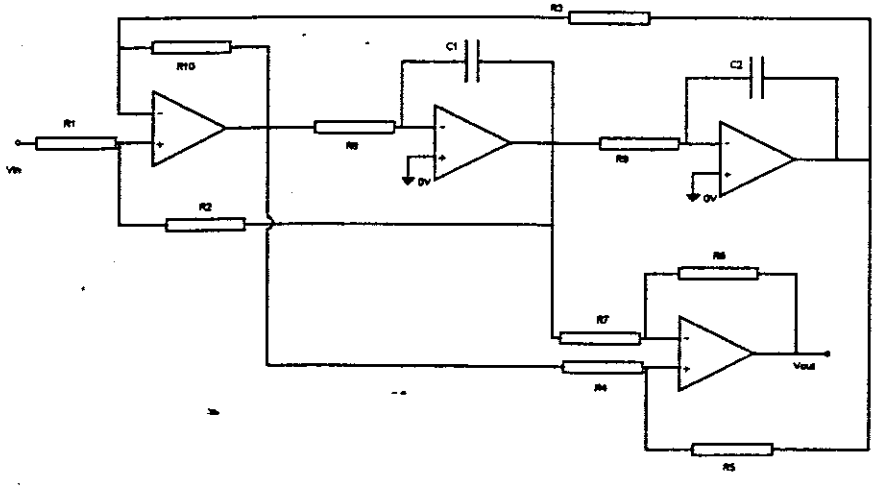

Figure 49: State variable filter

Component choice for practical implementation:

Choosing R1=R2=R3=R8=R9=R10= 1Ω , the capacitor values become C1=6.36F and C2= 78F according to [80]. The impedences were further scaled by 10^5 and

frequency denormalised to give a cut-off frequency at 19kHz. This circuit is shown in figure50.

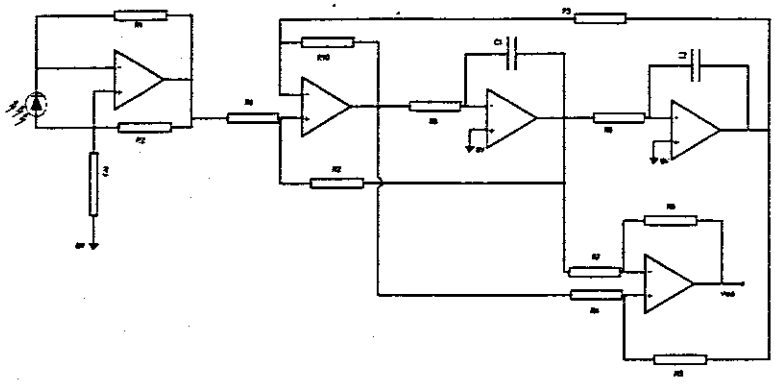

Figure 50: Final amplifier and statevariable filter

The frequency response of the circuit was tested using Monarch filter response software and a data aquisition system, kindly provided by Tellumat for testing purposes. The Monarch logo and corresponding test result is shown in the illustrations that follow (figure 51 and 52).

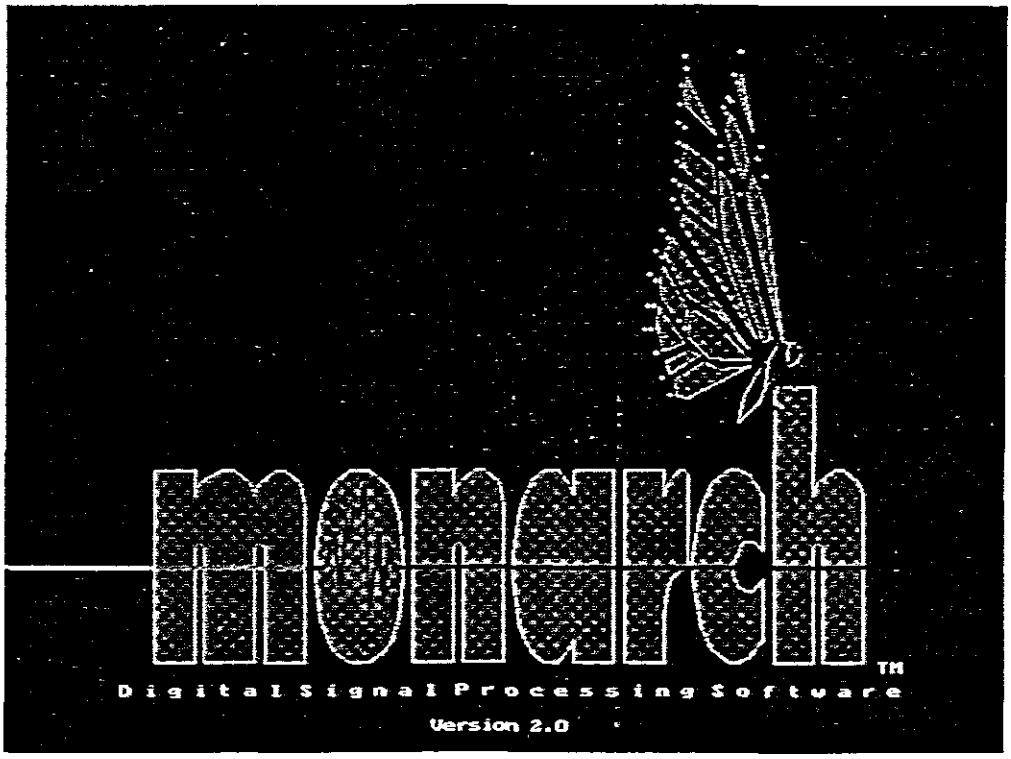

Figure 51 Monarch software

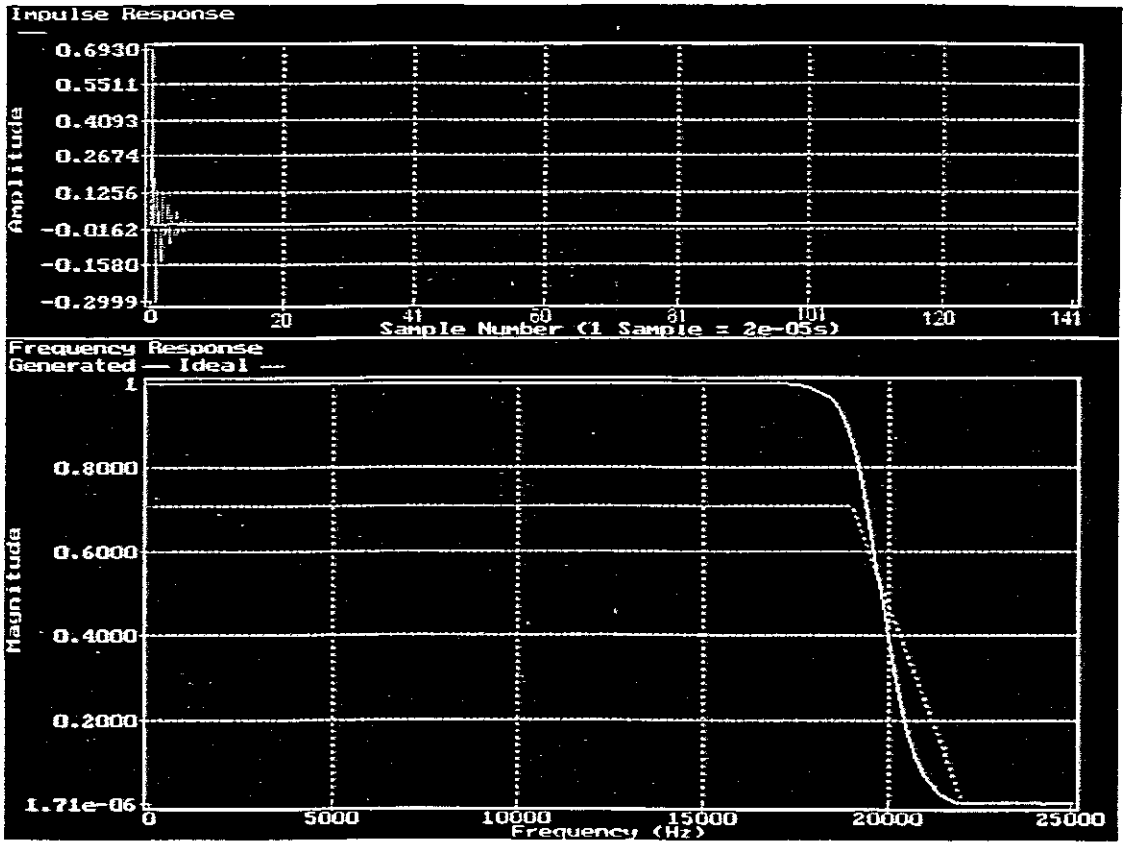

Figure 52 Anti-alias filter response as tested with Monarch

It can be seen that the delay in the time domain is very much smaller than would be expected of an equivalent filter designed in the analog domain. The cut-off frequency was somewhere at 18kHz, due to component spread in the actual breadboarded filter, which was implemented with LM324 operational amplifiers.

5.3.4.2 Development of a GIC based filter

In the following design a very sharp roll-off Cauer filter was designed to implement the requirement, based on GIC(general impedance converters) as the active elements. GIC's, in combination with 1/s transformations are well suited to high order low pass filter design. An example of the GIC elements used is illustrated below in figure 53. This circuit exhibited a low sensitivity to component tolerances and amplifier characteristics.

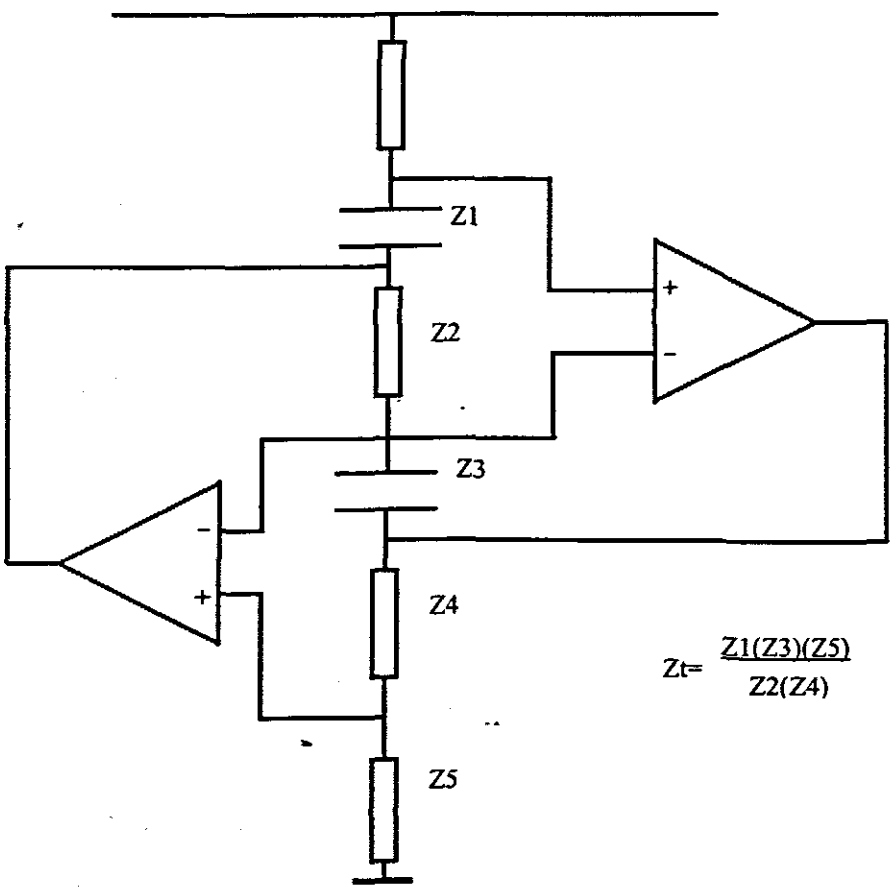

Figure 53: Generalised impedence convertor

By substituting RC combinations of up to two capacitors for Z1 through Z5 a variety of impedences can be simulated with the above circuit.

From table 5.3.2 the steepness factor for the anti-alias filter was calculated as

$$As=fs/fc \quad =22/19 =1.15$$

Since an extremely sharp filter is required, an elliptic function type filter was selected. From the filter tables in appendix 10, a filter corresponding to C1120, $\theta=60^0$ was chosen. This filter had the following parameters.

N (order) = 11

$\Omega s = 1.154701$

A_{min} = 91dB (better than 60dB)

The normalised circuit corresponding to the dual filter is taken from the table in appendix 10, and shown in figure 54.

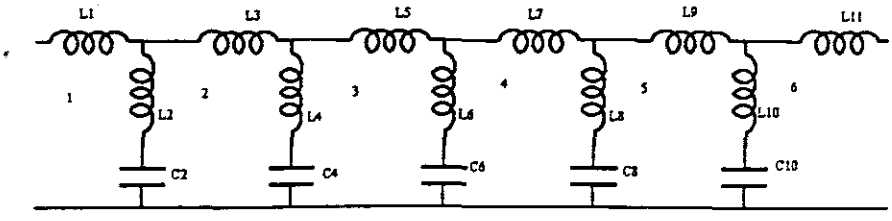

Figure 54:Normalised filter

The 1/s transformation was applied to this circuit and the result was the modified circuit of figure55. Here all inductors were transformed to resistances, capacitors to D elements, and resistors to capacitors of value 1/R.

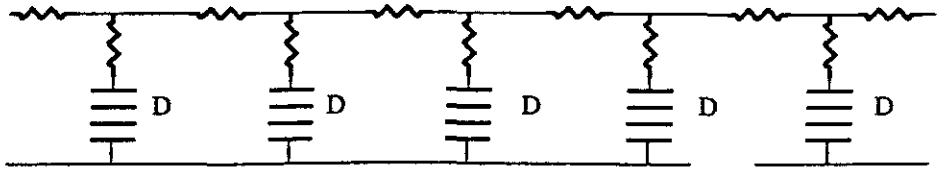

Figure 55: Modified circuit

The D element is realised by the GIC circuit. The result is the circuit shown in the circuit of figure56.

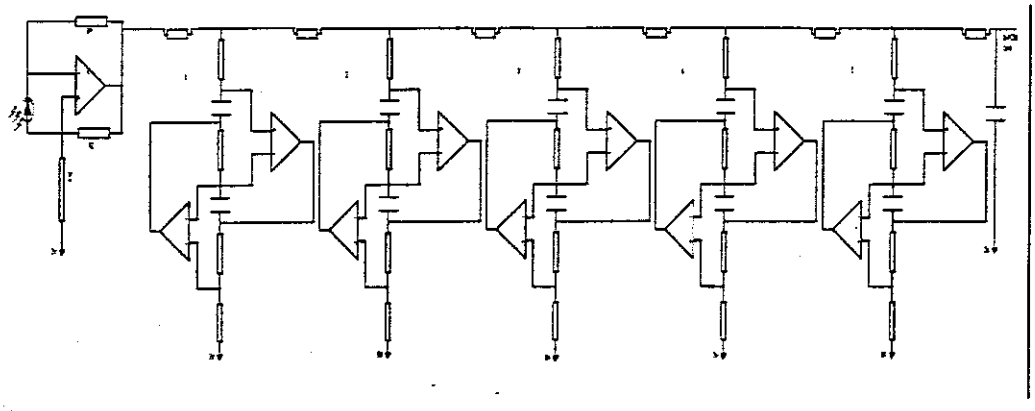

Figure 56 GIC implementation of filter.

The physically realisable circuit shown here were obtained by impedance scaling according to the formula

$$Z = C/(FSxC') = 1/(FSx0.1x10^{-6})$$

where FS = $2\pi f_c$ and fc= 19kHz The table below shows the transformation and scaling of impedences to achieve the final circuit.

L1	1.287 (H)	1.287 (Ω)	150k
L2	0.0796	0.0796	91k
L3	1.825	1.825	220k
L4	0.5308	0.5308	62k
L5	1.370	1.370	160k
L6	0.9528	0.9528	18k
L7	1.239	1.239	150k
L8	0.7991	0.7991	91k
L9	1.542	1.542	180k
L10	0.3042	0.3042	36k
L11	1.098	1.098	130k
C2	1.327(F)	1.327 (D)	150k
C4	1.030	1.030	200k

C6	0.7795	0.7795	91k
C8	0.8530	0.8530	100k
C10	1.100	1.100	130k

Table 5.3.4.2

The completed circuit diagrams for both detector and filter is shown in appendix8. Tests on this circuit in conjunction with the high current photodiode amplifier were done using a PC based measurement system and Monarch analysis software. A rudimentary Labview interface was also done to facilitate testing, the requirements and specifications of which is given below.

5.4 General purpose PC based measurement system

Today's rapidly growing industrial PC market offers a variety of industrial PC hardware and peripherals. Different applications require different system performance levels: 286, 386, 486 and Pentium CPU's are now available , allowing the user to select system performance ranging from a landmark speed of 20Mhz to over 200Mhz. Most measurement and process control applications usually need no more than a 80386 CPU. However the software available today are making such slow processors obsolete by being totally incompatible with the latest versions of software. Faster PC's therefore become a necessary choice.

5.4.1 Hardware specifications

A Pentium or equivalent PC was chosen, which is economical and suitable for most general purpose data acquisition uses. In particular, a system as described here would be useful for high speed and high volume sampling processes as well. A data acquisition card system were chosen with the following specifications

- sixteen A/D conversion single ended inputs
- or eight double ended inputs
- two D/A channels
- at least 40 000 samples per second conversion speed
- 12 bits (1/4096) conversion resolution
- software selectable gain
- gain selectability via software for each individual channel

This specifications were met by the PC30 Data aquisition card.

A laserjet printer were chosen for data printouts.

5.4.2 Software components

The driving force behind any data acquisition control system is software control. Programming a data acquisition and control system can be accomplished in three ways:

- hardware level programming
- driver level programming
- and package level programming

Commercially available general purpose data acquisition driver level software was chosen to be compiled into a user friendly panel controlled package. In this case the natural, choice of software was Labview. This software offered the following features, amongst others:

- compatible with selected data acquisition cards as well as similar cards
- allows graphical programming and is easily menu and console driven
- Output data files are easily portable
- variety of data display formats available
- data presentation can be viewed in real time
- analysis capabilities including, differentiation, integration, basic spectral analysis are available.

Other software that were more application specific were also used to conduct the proof of concept tests.

5.5 **Test results of the sensor head .**

It was decided to conduct tests on the sensor set-up using acoustic emissions as a signal source. Low power signal from a signal generator coupled to a 2W audio amplifier did not affect the Fabry Perrot cavity significantly. The reasons for this was explained in chapter 4. Qualitative tests on the sensor head was meant to be compared with a standard microphone in the audio range, but the sensitivity of the initial unit was too low. In an improved and more accurately constructed prototype, such tests could be done as a comparative and qualitative assessment of the sensor head. The following proof of concept tests were performed on the existing sensor head prototype.

5.5.1 Acoustic vibrations of motor car engine.

As an example of a practical application, figure57 shows the result of the acoustic spectra obtained with the sensor head mounted on a motor car engine. Tests were also done using an electric drill as a noise source. This data represented a time domain signal and clearly shows that the sensor concept can work.

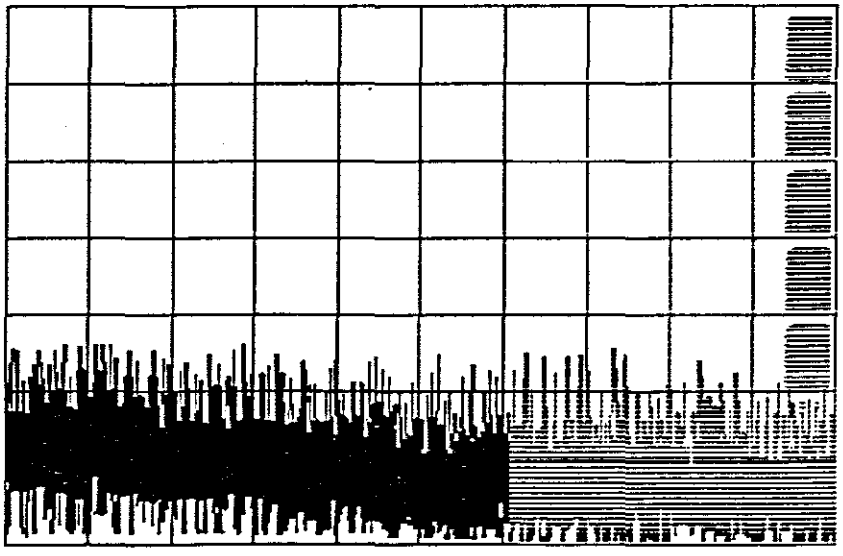

Figure 57: Signal obtained from measurement of engine noise

Data from the photo detector and GIC based anti alias filter were sampled at 50kHz. and a spectral representation of the signal was done using Monarch. This is shown in figure 58 and figure59. As expected from a qualitative interpretation of the different noise sources, the spectra clearly discriminate between that of the motorcar engine and that of an electric drill .

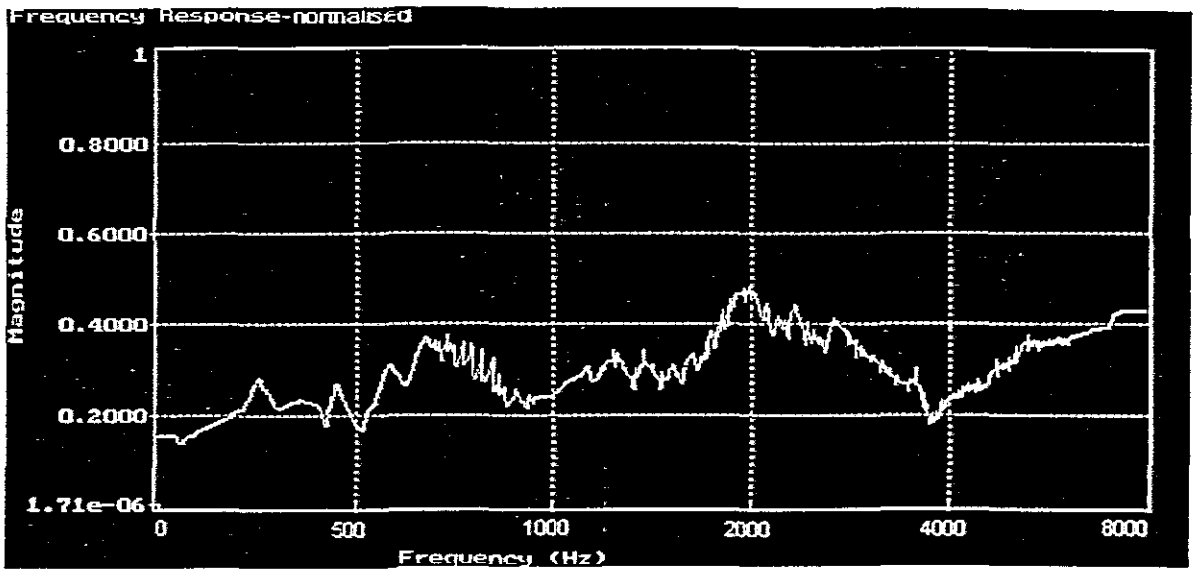

Figure 58:Frequency response of engine data with sensor prototype

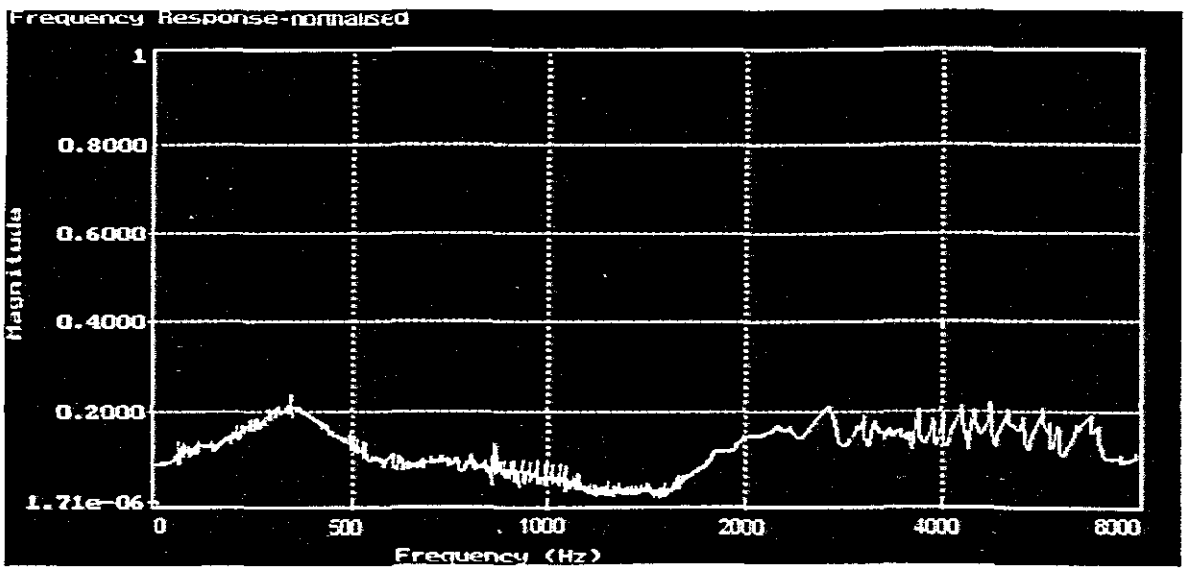

Figure 59: Data of an electric drill sensed by prototype

The spectra compare reasonably well with those obtained from a conventional condensor microphone as seen in figure 60. The difference in frequency response

here is primarily due to the poor construction of the prototype sensor head, which I believe lead to the lower sensitivity.

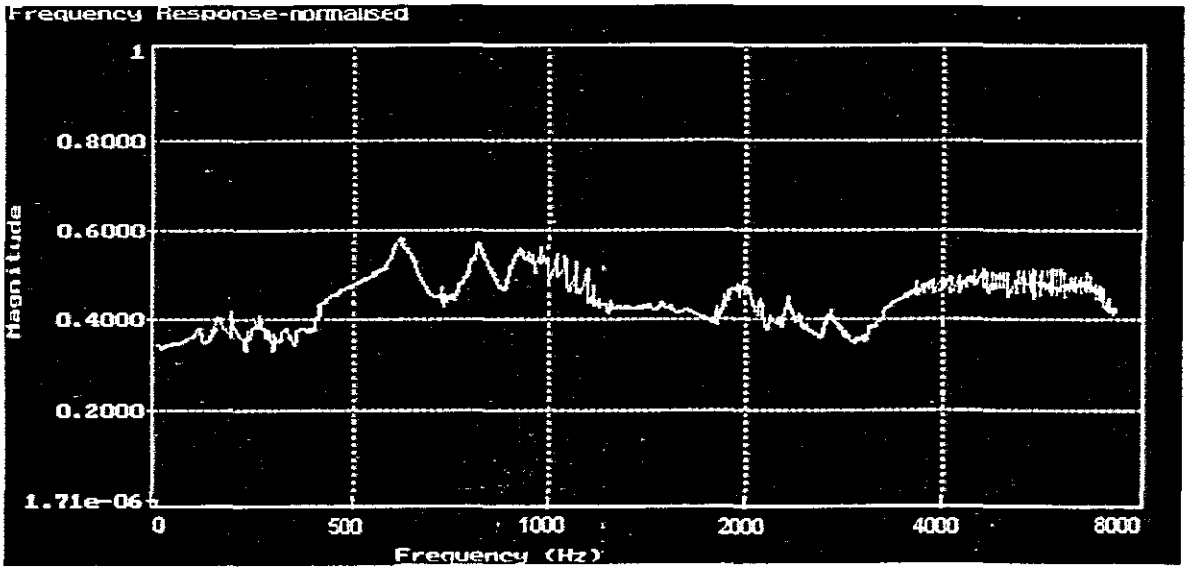

Figure 60: Response of condensor microphone to engine data

5.6 Overall conclusions and recommendations based on the tests performed.

A different approach to acoustic band vibration sensing for smart structures was investigated, using fibre-optic sensor technology. This sensor was based on non-monochromatic LED light sources and external Fabry-Perrot etalons, to produce a micro-interferometer for transferring the phase modulation of the sensing lightwaves as induced by mechanical disturbances (vibrations, acoustic emissions), into intensity modulation of the interference signal. Experiments performed agreed in principle with that expected from the theoretical considerations. The theoretical design, as developed in chapter 3, indicated that a sensitive lightwave sensor could be manufactured using non-monocromatic sources. Developement of the sensor head, as outlined in chapter 4, implemented the design with standard optical fibre ferules as the extrinsic Fabry Perrot cavities. With the measurement system

developed and discussed in this chapter, techniques were analysed and implemented to create a high responsivity, low noise, photodetector pre-amplifier and an adequate anti-aliasing filter as appropriate signal conditioning circuitry for a general data acquisition system. This system was intended to be Labview based. Tests were also performed using as standard software data analysis package to obtain meaningful test results from the data acquisition process. These tests indicated that the sensor technique is viable, and discrepancies in comparison with a condensor microphone, indicated that the sensor head construction could be improved. Further improvements to the measurement system could be a fully Labview based data acquisition and instrument driver system (the specifications for such a system have been developed in this chapter.). As it is only a rudimentary interface was built and another software package (monarch) was used to do test data analysis. In conclusion the concept of a lightwave sensor, which is based on fibre-optics, and therefore capable of being embedded in composite materials and structures, is possible from a thorough theoretical foundation as well as initial prototype tests. Interferometric performance have been predicted and demonstrated in an extrinsic fibre-optic sensor that made use of two Fabry Perrot cavities to modulate the spectrum of LED emission. A best fringe visibility of 0.5 was predicted, for perfectly matched mirrors in the ferrules and pathlenghths of the lightwaves. It was found that interferometric performance still occurred despite difficulties, albeit with a much reduced fringe visibility. Further work on this project could continue merely to improve the overall effectiveness of the transduction mechanism and data capture system.

BIBLIOGRAPHY

1 Crawley F.C. "Intelligent structures for Aerospace", AIAA Journal, Vol. 32 No.8, 1994, pp1689-1699

2 Palazzolo AB, Alexander Rm, Kascak AF, Montaue J, "Piezoelectric Pushers for active vibration control of rotating machinery", Transactions of the ASME, Vol. 111, July 1989, pp 298 -305.

3 Culshaw B, Michie C, and McGown, "Smart structures and Applications in Civil Engineering," Proceedings of the IEEE, Vol. 84 No1, January 1996, pp 78-86.

4 Yellin JM and Shen IY, "a self sensing active constrained layer damping treatment for a Euler-Bernouli beam," Smart Mater , Struct. 5, 1996, pp 60-67

5 Lesieutre GA and Lee U, "A finite element for beams having segmented active constrained layers with frequency dependent visco-elastics," Smart Mater, Struct.5, 1996, pp 615-627

6 Petersen K, "Micromechanical Accelerometer integrated with MOS detection circuitry," IEEE Transactions on electron devices, Vol. 29, No 1, January 1982, pp 23- 27.

7 Lynne Mr, "A batch fabricated silicon accelerometer", IEEE Transactions on Electron Devices, Vol. Ed 26, No 12, December 1979, pp 1911-1917

8 Puers B, "A new uni-axial accelerometer in silicon based on the piezo-junction effect," IEEE Transactions on electron devices, Vol. 35 No 6, June 1988, pp 764-770.

9 Udd E, " Fibre-optic smart structures," Proceedings of the IEEE, Vol. 84, No 1, January 1996, pp 60- 67.

10 "Microsensors react to small pressures," Eureka transfers technology, May 1996, pp 31-32.

11 Voss KF and Wanser KH, "Fibreoptic strain-displacement measurement sensor employing non-linear buckling," Applied optics, Vol. 36 No 13, May 1997 , pp2944-2946.

12 Sakai I, "Multiplexing of optical fibre sensors using frequency modulated source and grated output," Journal of Lightwave Technology, 1987, LF5, pp 972 -940

13 Lee CE and Taylor HF, "Interferometric optical fibre sensors using internal mirrors," Electronics Letters, Vol. 24 No4, February 1988, pp193 -194.

14 Yu A and Siddiqui AS, "Theory of a novel high sensitivity optical fibre gyroscope," IEE Proceedings-J, Vol. 140 No 2, April 1993, pp150 -155

15 Urquart P, "Review of rare earth doped fibre lasers and amplifiers," IEE Proceedings, Vol. 135, Pt J, No 6, December 1988, pp 385-407.

16 Tingye LI, "The impact of optical amplifiers on long distance lightwave telecommunications," Proceedings of the IEEE, Vol. 81 No 11, November 1993, pp1568 -1578.

17 Soref R, "Silicon based opto-electronics," Proceedings of the IEEE, Vol. 81 No 12, December 1993, pp 1687- 1706.

18 Kahn MTE, "Intelligent structures with opto-electronic sensor systems," Elektron SAIEE Journal, September 1997

19 Kamen EW and Heck BS, "Fundamentals of Signals and Systems," Prentice Hall, 1997

20 Cohen A and Kovacevic J, "Wavelets: The Mathematical Background," Proceedings of the IEEE, Vol 84, No 4, April 96

21 Mallat S, "A theory for multiresolution signal decomposition: the wavelet representation," IEEE Transactions on Pattern Analysis and Machine Intelligence, Vol 2, No 7, 1989

22 Stang G and Nguyen T, "Wavelets and Filter banks," Wellesey-Cambridge Press, 1996

23 Hess N and Wickerhauser MD, "Wavelets and Time frequency analysis", Proceedings of the IEEE, Vol 84, No4, April 96

24 Kekana M and Sun B, "A Technical review of Smart Materials and Structures. Part 1: An Introduction," Submitted to Journal of SA Mechanical Engineers, June 1997.

25 Spillman WB, "Smart Structures," Optical Engineering, Vol 36, No 7, July 1997.

26 Garret JH, Smith FC, "AI Applications in Structural/ Construction Engineering," IEEE Expert, August 1996, pp 20-22

27 Turkiyyah GM, Fenves SJ, "Knowledge-Based Assistance for Finite-Element Modelling," IEEE Expert, June 1996, pp23 - 32.

28 Culshaw B, Michie C, Gardiner and McGown, "Smart Structures and Applications in Civil Engineering," Proceedings of the IEEE, Vol 84, No.1 January 1996, pp78 -86

29 Dunston PS, Ranjithan S, "Neural network Model for the Automated Control of Springback in Rebars," IEEE Expert, August 1996, pp45- 49.

30 Grossman B, Gao X and Thursby M, "Composite damage assessment employing a neural network processor and an embedded fibre-optic sensor array," SPIE Vol.1588, 1991, pp64-69

31 Teh CI et al, "Prediction of Pile Capacity using Neural Networks," Journal of Computing in Civil Engineering, April 1997, pp129 -132.

32 Mukerjee A and Despande JM, "modelling initial design process using Artificial Neural Networks," Journal of Computing in Civil Engineering, Vol 9, No 3, July 1995.

33 MTE Kahn, " Sensing and control in the evolution of intelligent structures for civil engineering," Electricity and Control Journal, pp 47-50 , Nov 1997

34 D. Biswas, "Characterization of polyimide-coated optical fibres, "Journal of Optical Engineering Vol 30, No 6 ,pp722-725 , 1991

35 D. Biswas, "Aging behaviour of polyimide/acrylate coated fibtres in harsh envirinments," Journal of Optical Engineering, Vol 36,No 8, pp 2167-2170, 1997.

36 GR Kurkjian, JT Krause, MJ Mathewson, " Strength and fatigue of silica optical fibres," Journal of Lightwave Technology, Vol 7,No 9, pp1360-1370, September 1989

37 G Das, SN Sarkar, " Estimation of dispersion parameters involving the Peterman II spot size using Gausian type approximation in single mode graded index fibres," Journal of Optical Engineering, Vol 36, No 9 , pp2425- 2428, September 1997.

38 SC Rashleigh, "Origens and control of polarization effects in single mode fibres," Journal of Lightwave Technology, Vol 1, No 3, pp 312- 317, June 1983.

39 JT Krause, CR Kurkjian, "Fibre splices with perfect fibre strength of 5.5Gpa," Electronics Letters, Vol 21, pp533- 535, 1985.

40 K Chen, D Krepps, "Coupling efficiency of surface emmiting LED's to single mode fibre's," Journal of Lightwave Technology, Vol LT-5, No 11, pp1600-1604, November 1987.

41 T van Muoi, "receiver design for high speed optical fibre systems," Journal of Lightwave Technology, Vol LT-2, No 3, pp243 246, June 1984.

42 FC Crawley "Intelligent structures for Aerospace", AIAA Journal, Vol. 32 No 8, pp1689-1699, 1994

43 E. Udd , " Fibre-optic smart structures," Proceedings of the IEEE, Vol 84 , No 1, pp 60- 67, January 1996.

44 MTE Kahn, "Intelligent structures with opto-electronic sensor systems," SAIEE Elektron Journal,pp35-37, September 1997.

45 KF Voss and KH Wanser, "Fibreoptic strain- displacement measurement sensor employing non-linear buckling," Applied Optics, Vol. 36 No 13, May 1997 , pp2944- 2946.

46 B Culshaw , C Michie , and McGown, "Smart structures and Applications in Civil Engineering," Proceedings of the IEEE, Vol. 84 No1, January 1996, pp 78-86.

47 D.X Wang, WL Anderson, MA Karim, Y Li, " Self referenced two fibre sensor for micro-displacement measurement," Journal of Optical Engineering, Vol 36, No 10, pp2809-2813, October 1997.

48 CE Lee, HF Taylor, "Interferometric optical fibre sensors using internal mirrors," Electronic Letters, V24, No4, pp193-192, Feb 1988.

49 L Yanbaio, S Qinxia, "optical fibre Mach-Zender interferometer for smart skins," Fibre optic Smart Structures and Skins V, SPIE Vol 1798, pp 186-191, 1992

50 I Sakai , "Multiplexing of optical fibre sensors using frequency modulated source and grated output," Journal of Lightwave Technology, Vol LF5, 1987, pp 972 -940

51 WB Spillman, LB Maurice et al, "Quasi distributed Polarimetric Strain sensor for smart skin applications," SPIE Vol. 1170, Fiber optic Smart structures and skins II, 1989, pp483-494.

52 HW Haslach, JS Sirkis, "Strain or stress component separations in surface mounted interferometric optical fibre strain sensors," SPIE vol. 1170, Fiber optic smart structures and skins II, 1989, 452-461.

53 SD Dyer, DA Christiansen, "Dispersion effects in fibre-optic interferometry," Journal of Optical Engineering, Vol 36, no 9, pp 2440-2447, September 1997.

54 AYu and AS Siddiqui , "Theory of a novel high sensitivity optical fibre gyroscope," IEE Proceedings-J, Vol. 140 No 2, April 1993, pp150 -155

55 P Urquart , "Review of rare earth doped fibre lasers and amplifiers," IEE Proceedings, Vol. 135, Pt J, No 6, December 1988, pp 385-407.

56 LI Tingye, "The impact of optical amplifiers on long distance lightwave telecommunications," Proceedings of the IEEE, Vol. 81 No 11, November 1993, pp1568 -1578

57 AD Kersey, "Recent progress in interferometric Fibre sensor technology," Proceedings of the SPIE, Vol. 1367, No 2, 1991

58 A Dandridge, AB Tveten, AD Kersey, "Multiplexing of Interferometric sensors using phase generated carrier techniques," Journal of Lightwave Technology, Vol LT-5, pp947-950, 1987

59 J Mlodzianowsky, " A simple frequency domain multiplexing system for optical point sensors," Journal of Lightwave Technology, Vol LT-5, pp 1002-1006, 1987

60 HS al-Raweshedy, "Spread spectrum techniques for passive multiplexing of interferometric fibre-optic sensors," Proceedings of the SPIE, vol 1314, pp 342,
1990

61 BV Dasarathy, "Sensor Fusion Potential Exploitation-Innovative Architechtures and illustrative applications," Proceedings of the IEEE, Vol 85, No1, January 1997, pp24-38

62 R Soref , "Silicon based opto-electronics," Proceedings of the IEEE, Vol. 81 No 12, December 1993, pp 1687-1706.

63 E. Udd, et al, "Fibre optic sensor systems for aerospace applications,"SPIE Vol.838, Fibre Optics and Laser Sensors V, pp162-168, 1987

64 R.L Wood, A Tay, DA Wilson, "Design and fabrication for omposite structures with embedded fibre optic sensors," SPIE vol.1170, Fibre optic smart structures and skins II, pp160-170, 1989

65 C. R Lowe, "Biosensors," Trends in Biotechnology, Vol 2, pp 59-65, 1984

67 Y Rao, DJ Web et al, "In fibre Bragg grating temperature sensor system for Medical applications," Journal of Lightwave Technology, Vol 15, No 5, pp779-785, May 1997

68 RS Marks, E Basis et al, "Chemiluminescent optical fibre immunosensor for detecting cholera antitoxin," Journal of Optical Engineering, Vol 36, No 12, pp 3258-3264, December 1997

69 CH Mazel, "Diver operated instrument for in situ measurement of spectral fluorescence and reflectance of bethnic marine organisms and substrates," Journal of Optical Engineering, Vol 36, No 9, pp 2612-2617, September 1997.

70 Wood, RL et al, "Design and fabrication for composite structures with embedded fibre optic sensors," SPIE Vol.1170,1989, pp160-170

71 Lu , A and Siddiqui, AS, "Theory of a novel high sensitivity optical fibre gyroscope," IEE Proccedings Journal, Vol 140, No 2, 1994, pp249- 256

72 WN MacPherson, "Phase demodulation in optical fibre-Fabry Perot sensors with inexact phase steps," IEE Proceedings Journal, Vol 144, No3, 1997, pp130-133

73 Jones RC, "A new calculus for the treatment of optical systems (I-III)," Journal of OSA, Vol 31, 1941, pp 488-503

74 Jones RC, " A new calculus for the treatment of optical systems(IV)," Journal of OSA, Vol32,1942, pp 486-493

75 O. Viano and SJ Ovaska, "Tachometer signal smoothing with analog discrete time polynomial estimators," IEEE Transactions on Industrial Electronics, Vol 41, pp147-154, April 1994

76 P. Heinonen, " FIR median hybrid filters with predictive FIR substructures,"IEEE transactions on Acoustics, Speech and Signal processing, Vol 36,pp892-889, June 1988

77 P Steffen, On digital smoothing filters,IEEE Circuits, Systems and SignalProcessing, Vol 5, no.2, pp 187-210, 1986.

78 O. Viano and SJ Ovaska, "Tachometer signal smoothing with analogue discreet time polynomial estimators," IEEE Transactions on Industrial Electronics, Vol 41, pp147-154, April 1994

79 P. Heinonen, " FIR median hybrid filters with predictive FIR substructures,"IEEE transactions on Acoustics, Speech and Signal processing, Vol 36,pp892-889, June 1988

80 WK Chen , "Passive and Active Filters", NewYork, John Wiley & son,1986

APPENDIX 1
PAPER DELIVERED TO ICCSS98

"ELECTRO-OPTIC TECHNOLOGIES FOR SENSOR APPLICATIONS"

M.Tariq Kahn
Faculty of Engineering
Department of Electrical Engineering
Peninsula Technikon
P.O. Box 1906
Belleville,7535
SOUTH AFRICA
e-mail: khan@eleceng.pentech.ac.za

ABSTRACT

Fibre-optic communications technology is now a firmly established field in telecommunications. The fact that fibre-optic communication systems could be installed in hostile environments, gave impetus to the present research into sensor systems based on fibre-optics. At the present moment there is still a large research task to produce sensors that would become industrially acceptable since photonic sensors must compete on both technical and cost grounds with traditional sensors. This paper offers a basic overview of the technology involved in the development of such sensors.

1 PHOTONIC SENSORS FOR INDUSTRY- INTRODUCTION

The increasing demand for sensitive, low cost sensors for industrial applications is the driving force behind many present research efforts. Photonic sensors for industry offers another exiting and logical application of this new and quite possibly far superior class of sensor technology, which is essentially a spin-off from both telecommunications and aerospace - smart structure research. Fibre-optic based sensors have the potential of being used in a diverse range of applications, including chemical analysis, process control, oil refineries, food processing, manufacturing facilities and even hospitals.

Research developments in the field are focusing on the developments of a variety of physical and chemical parameters, including temperature, pressure,

flow, strain, position, rotation rate, thickness, chemical reaction rates and many more. The acceptance of many of these sensors by the process monitoring and control industry have been reasonably slow, understandably because of current competing and existing technology that can meet the needs of industry. This is an area in which research can benefit enormously from a closer relationship with industry to develop an understanding of the user requirements for the evolution of standardised photonic sensors.

Photonic sensors have advantages over traditional techniques in that:

- Extensive interconnection requirements using twisted wire cables and coaxial cables are considerably reduced.
- Prohibitive electrical power requirements are reduced
- simpler signal conditioning and greater integration are possible
- Sensors could easily be mounted in a potentially hostile environment.

These sensors operate by measuring parametric changes in light between a light source and a detector due to external physical factors. Modern photonic sensors may generally require only a fibre optic cable interconnection and can be embedded in a structure. With the revolutionary changes that took place in the last decade in fibre-optic cable technology, as well as research into viable point and distributed photonic sensors, these techniques are set to dominate instrumentation in the next century.[1]

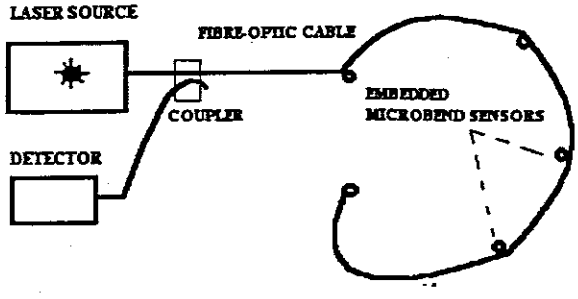

Figure 1: Photonic sensors using only fibre-optic cable embedded in a structure

2 OPTICAL FIBRE TECHNOLOGY

2.1 Fibre-optic cables

In reviewing optical fibre technology one finds that the choice and effective utilisation of optical fibres plays an important role in sensor design. Great progress has been made in the manufacturing of long lengths of strong silica lightguides since the 1970's.

Optical fibres are required to maintain stable performance under severe conditions. The long term stability conditions, wide bandwidths and low transmission loss is an essential requirement for practical lightwave

transmission systems [2]. Fibre-optic cables, which may be comprised of single or multimode optical fibres, can be manufactured in a similar fashion to ordinary electrical cables, of course with several material changes. They can include fibres which are tightly enclosed in various polymer materials under compressive stress, or alternatively in 'loose tube' configurations. Sensor cabling applications must therefore be carefully examined and designed in relation to the operating specifications.

As mentioned before, optical fibres are available in multimode and single mode. This refers to the way that the optical waveguide, the fibre, will transmit the lightwaves by means of total internal reflections. Single mode fibres have very thin cores and hence dispersion and multiple reflections, a characteristic of multimode fibre operation, are not possible. Figure 2 illustrates this operation graphically.

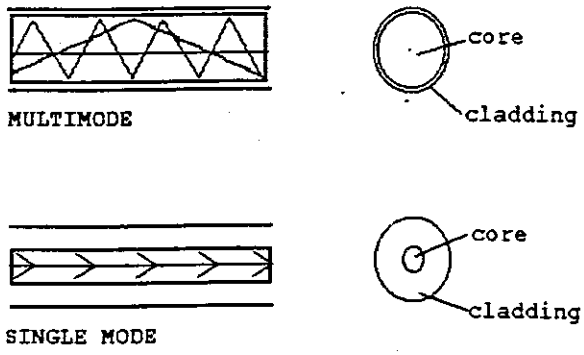

Figure 2: Optical fibre modes and lightwave transmission

In previous laboratory experiments, single mode fibre was chosen for proof-of-concept sensor design. One may however, advance a strong argument in favour of large-diameter multimode optical fibres on the basis that they are preferable for optical sensors because of the increased simplicity of light coupling and launching. The existence of cheap compatible sources,. e.g. incoherent light emitting diodes and superluminescent diodes that can couple to multimode fibre is much more readily available.

From figure 2 one can see that the guiding refractive-index difference is provided by a direct polymer coating of lower refractive index onto the core. Graded-index fibres provide a graded change in refractive index between the core and cladding of the fibre. This reduces the dispersion of pulsed radiation for telecommunications applications and permits increased bandwidth. The fibre cladding, however, plays an important role , not only because of the optical characteristics that it imposes on the fibre, but also because it is expected to endure harsh environments. The cladding is not normally very thick and is dependent on the type of material used. Telecommunications grade cladding is normally acrylate, but recently other types of cladding such as

polyimide, and composite polyimide/acrylate coatings have also been employed. The ageing of such claddings in harsh environments have been the topic of recent study [3].

Plastic clad silica, as the name suggests, is achieved by adding a polymer cladding, with the appropriate lower refractive index, on the silica fibre itself. Most multimode fibres are however coated with a primary coating such as silicone or epoxy acrylate. A secondary plastic coating can then be applied, followed by an added wound strength member. From applications relating to telecommunications, the strength and fatigue of optical fibres have been thoroughly investigated [4]. If special coatings on the fibre for sensor applications is required, this may lead to fibre defects and weakening. In addition, the dispersion parameters of fibres are being more accurately estimated and room for continuous improvement is possible [5]

Plastic or polymer based fibres (also known as POF -plastic optical fibre) are finding increased applications in data communications. This has lead to the idea of sensor development using these material as opposed to glass fibre in sensor research. At the present moment plastic fibre sensor technology is also being researched at Peninsula Technikon. Plastic-cored fibres cannot withstand such high tensile stresses as silica fibres. The bend radius for these rather large diameter fibres may also not be as tight as that of generally available silica fibres. This may change as better fibre manufacturing techniques develop. Attenuation of POF are typically 200 dB/km with pronounced absorption minima in the visible spectral region (around 660nm). What is useful with POF is that easily available visible light sources can be employed . In this regard LED's and solid-state lasers operating in the red visible spectrum can be used. With POF highly simplified jointing and splicing in the field is possible. For optical-sensing systems, with plastic fibres a simple razor-blade splice and butt-coupling with crimping could be employed. A study of short haul plastic fibre sensors for industrial applications must also be envisaged.

Single-mode fibre is now available for longer wavelengths such as 1300 to 1600nm. In this wavelength region absorption is less and therefore less attenuation occurs for long haul sensor applications. With fibre core diameters that are typically 10um, special requirements for detection and launching must be considered. Special requirements such as the polarisation of light in a single mode fibre, with particular application to sensors, have also been investigated [6]. Nowadays fibre pigtailed lasers and detectors are supplied with the fibre already firmly encapsulated next to the laser in a standard package. The cost of single mode components are however more costly than that of multimode devices.

2.2 Fibre-optic connectors, splices and couplers

These devices perform quite different functions, although the names suggest synonymity. Splicing forms a permanent connection between two previously unconnected optical fibres. Connectors are used to provide a demountable joint, therefore semi-permanent, whereas couplers are components which carry out primarily the function of power splitting.

2.2.1 Connectors and splices

Fibre-optic connectors, such as that provided by FIS or GTE are very easy to install and use. These connector technology requires virtually no tools, no adhesives and no fixtures to add an in line connector. A fair percentage of fibre-optic components such as sources and detectors are readily available with fibre pigtails. It is often necessary to make a permanent joint in an unjointed length of fibre. It is also at times necessary to make a joint which may be made and broken many times. For the first application, and especially with single mode fibre, fusion splicing is the preferred technique. This is a well established technique in telecommunications applications. Splicing and the effects on the overall strength of an optical fibre have been thoroughly investigated[7]. In making a splice the fibre is stripped back to bare glass, and the ends to be jointed are cut perpendicularly. The fibres are now aligned between two electrodes and an electric arc fuses them together. Following splicing, the primary and secondary coating of the fibre are restored and a ferrule fitted for added protection. Demountable connectors can be used for semipermanent joints, especially in the field, or in hazardous environments where fusion splicing is unsuitable.

2.2.2 Couplers:

The terminology 'coupler' derives from 'directional coupler' which is an analogous device in microwave circuits. For sensor systems couplers allow multiplexing of several sensors onto a single source and detector. This power splitting operation is essential in many sensor applications. Sophisticated variations of couplers are often employed as wavelength multiplexers and demultiplexers, allowing more than one source/detector pair to operate over the same fibre. Couplers are manufactured by a fusion technique where the fibres are stripped back to the glass for a portion of their length, and then twisted together and stretched over heat from micro burners. This causes the light-guiding cores of the fibres to be brought sufficiently close together for evanescent coupling to take place. Single mode couplers are necessary for interferometric sensors. Since single mode fibre has extremely small cores, it is necessary to continually monitor the coupling ratio during the fusion process. Couplers are specifically manufactured by certain companies that cater for this need in fibre-optic installation and research.

Couplers may affect the total insertion loss in a system and careful light budget calculations must be made before a sensor system is commissioned. Typical coupler losses is in the order of 3dB.

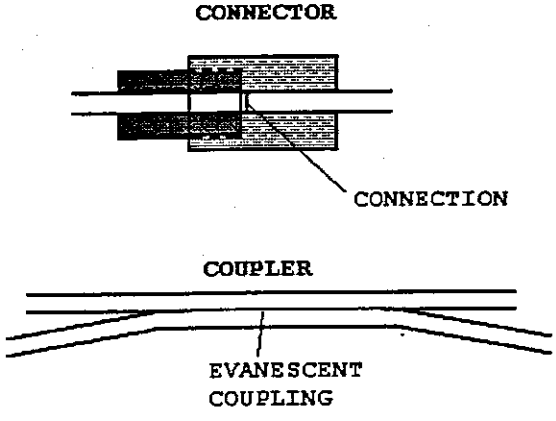

Figure 3: Connectors & Couplers

3. SOURCES AND DETECTORS

For interferometric sensor devices requiring a coherent source, semiconductor diode lasers can be used but for more general systems, semiconductor LED sources are the obvious choice. The expected lifetime of LED's is about 10^7 hours. Presently, laser devices are extremely small and robust and have been also developed to have extremely long lifetimes. With lasers a certain amount of device selection is however required to obtain satisfactory coherence properties. Several laser types have been developed for coherent communications that will maintain the necessary mode stability.

In the discusion on fibre optic cables, section 2.1, it was indicated that in order to obtain minimum loss from silica fibres, the trend for communications applications is to use longer wavelengths at 1300 and 1550nm. This means that sensors will also tend to shift to these wavelengths for reasons of component availability. These devices operate in the infrared range. Changes of power output for a laser diode with temperature dependence need more complicated electronic circuits than that required for an equivalent power LED.

Most LED's emit at short wavelengths (850 nm and below), but devices are now becoming easily available at 1300nm and 1550nm. Light emitting diodes (LEDS) are much cheaper than lasers and can be used for all multimode systems except those requiring transmission over very long distances. The coupling of LED sources to single mode fibre is however not always efficient[8].

Optical detectors present the other half of the electronic interface. The performance of photo detectors and low noise amplifiers affect the efficacy of

a fibre-optic system. At 850 nm cheap and efficient silicon detectors may be used. These are readily available and have very satisfactory performance for most sensor applications. However, beyond the 1.0 um wavelength silicon ceases to function, and either germanium or indium gallium arsenide detectors must be used. These are much more expensive, and germanium, in particular, suffers from a larger dark current which increases system noise levels. The much better avalanche photodiodes, although fast , limits the sensitivity of optical receivers also due to this large dark current. This may require special receiver electronics to provide satisfactory operation in a sensor system [9]. For shorter distance applications, however, there is a strong argument for the use of the cheaper visible laser diodes (i.e. 780 nm) which have become more available with the advent of the video disk. The trade-off between source and detector technology must be accounted for in photonic sensor applications.

4 SENSOR TECHNOLOGIES

4.1 Point sensors

These sensors require a single or more fibre-optic lines to do a unitary measurement at discrete locations.

4.1.1On/off point sensors

These sensors are required to measure parameters at discrete or particular positions. On/off sensors remain one of the easiest and possibly the simplest application of fibre-optic sensors. Other applications include encoders for position and displacement. These types of sensors will be required in increasing numbers, followed of course by multiplexed systems. Already 'fly-by-light' aerospace and defence systems encoders are being evaluated in the USA. These are however only used for specific high-technology aerospace applications [10]. Cheaper devices, competitive with nonfibre-optic technology, will only arrive once volume techniques with accepted multiplexing procedures are employed.

4.1.2 Spectroscopic sensors

Spectroscopic sensors and related optical techniques can assist specific markets in the process control industry. These are essentially sensors based on spectral absorption or emission, and lends itself ideally to opto-electronics based technology. [11] Research in fibre-optic gas sensors, combustion diagnostics, temperature and controlled substance detection are possible application areas. Blackbody radiation detectors have been commercially developed to measure temperatures between 500 - 2000^0 C. Photoluminescence detectors are also commercially available to measure between 0 and 200^0 C with 0.1^0C resolution. [12]In addition the development of absorbent and fluorescent sensor dyes will aid this class of sensors tremendously. Multiplexing considerations will tend to be quite different for such systems, because of the high sensitivities that will be required. Such sensor will therefore tend to be point sensors. Careful light calculations for such measurements will be necessary because of the large sensor insertion

losses. With the increased use and availability of infrared transmitting fibre, spectroscopic sensor applications will be further enhanced.

4.2 Microbend and OTDR sensors

One of the oldest fibre-optic sensors is the microbend sensor. These sensors are generally dependent on the variations in light intensity reaching a suitable photodetector. The opto-electronics and signal processing circuitry for microbend sensors are therefore generally inexpensive and make it ideal for low cost applications. Macrobending, or controlled buckling, optical fibre sensors have been developed for strain and displacement measurements that can complement or surpass traditional microbend techniques [13].

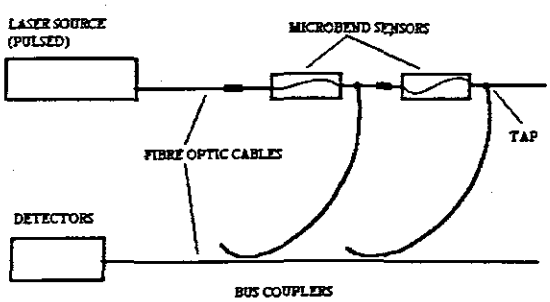

Figure 4 Microbend sensors arrays can be optically addressed

Fibre-optic based OTDR (optical time domain reflectometry) techniques is another well established opto-electronic sensor solution. Rayleigh backscatter methods (OTDR) can be used in distributed sensors, and is essentially a measure of backscatter signature as a function of time, from the launch of an interrogating laser pulse. This is illustrated in figure 5. Coupled with microbend sensors, OTDR have been used in a wide range of applications in Europe, including monitoring of the Berlin-Mansfield bridge, to establish crack growth and dynamic loading. [14]

Other sensors that are based on lightwave reflection or intensity, but does not quite fall under the category of microbend techniques, could be configured to measure parameters such as displacement, strain or pressure. Such experimental work have also recently been described [15].

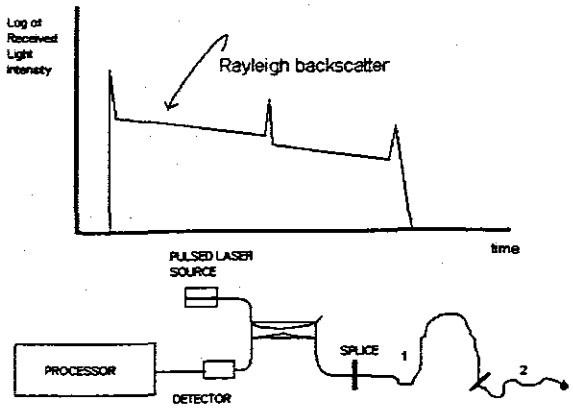

Figure 5 Typical OTDR backscatter signature and sensor configuration.

4.3 Interferometric sensors

Interferometry originally had a purely optical origin and displacement measurements of minute degrees is possible with it. Classical Michealson and Mach-Zehnder interferometers usually required bulk optical components, beam splitters and stable measurement benches. With the advent of lasers and improved optical fibre technology, the bulk optical components was replaced by opto-electronic components. This lead to much more feasible inteferometric sensor applications. These sensors can be configured to be extremely sensitive to certain physical parameters [16] [17] and have proved to be versatile in applications. Even multiplexed Mach-Zehnder sensors have been reported to date. [18]

Interferometric devices for sensors are likely to observe a gradual increase in use with time, with effort at the moment remaining at the development level. The development of passive extended vibration and acoustic sensors will be a useful addition to sensor technology. The use of fibre-optic interferometers for strain measurements have been successfully employed in smart structure skins research, and the literature abound with applications and techniques [19] [20]. Signal processing electronics should however take into account the effects of dispersion in interferometry based on optical fibres. This effects have been highlighted in a recent publication [21].

Yet another technique, that of using internal reflections in a Fabry-Perot cavity, have proved to be of great value in sensor technology. Fabry-Perot interferometers have been configured as temperature sensors for point measurement applications [16]. There have also been proposals for linear Fabry-Perot systems which can be interrogated in the time domain, or wavelength multiplexed distributed sensors

Other interferometric sensors such as the fibre-optic gyro and magnetic sensors can exist as independent devices, and appear to compare favourably in relation to available systems. Perhaps the most famous application of an intererometric sensor technique is that of the Sagnac based fibre-optic gyroscope [22], used in guidance systems.

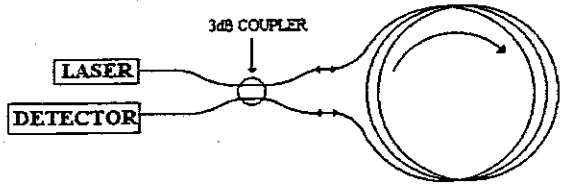

Figure 6 The Sagnac optical fibre gyroscope

The success of the fibre-optic gyroscope depended largely on the degree of miniaturisation and robust packaging that was possible with it. As can be seen in the illustration figure 6, the gyro has thus far been realised with all-fibre and integrated-optic components. Interferometric sensor cost is likely to be the major influence in commercial acceptance, but this factor is steadily diminishing.

5. SYSTEM IMPLICATIONS

Having demonstrated the possibilities as well as the extent of development and research in opto-electronic sensors, one can visualise the next chapter in the development of systems that intend to make use of such sensors. How, for instance would measurement and control signals be coupled, transmitted and processed over long distances? The concept of optical-fibre amplifiers have been advanced [23] [24] and have already found applications in the telecommunications industry. Ebrium doped fibre amplifiers (EDFA) could be used for long distance signal transmission or all optical processor information transfer.

Furthermore, fibre-optic sensors offer unique capabilities when configured in a distributed nature, or arranged in multiplexed networks. Such systems allow sensing at a large number of points by combining fibre-sensing methods with fibre telemetry. Most of the work on practical optical multiplexing systems for sensors has tended to be at the conceptual and experimental level, although progress towards practical systems are continuously advanced [25][26] [27] [28]. The development of sensors are, however, now at the stage where multiplexing and system implications must be taken into account. Sensor information fusion potential for optimal processing in distributed multisensor environments would be a logical part of a systems solution [29]. Applications that would benefit from this technology include civil structural monitoring,

smart structures, military systems, industrial systems and security monitoring and detection, to name but a few.

If the sensor data is digitally encoded , for example, into binary code before transmission, the transmitted data is less susceptible to corruption through attenuation and dispersion effects. Silicon based opto-electronic integrated circuits (OEIC's) [30], hold promise for the development of a completely integrated solution for signal processing of sensor signals. OEIC's is envisioned to outperform electrical circuits and is essentially the outcome of integrating optics and electronics on the same substrate.

There are also possibilities of using wavelength division multiplexing in sensor systems but these methods could be hampered by sensor complications such as: size, robustness, stability and expense of optical wavelength-dispersing components.

6. APPLICATION AREAS

6.1 Defence aerospace

Demands for increased survivability, improved aerodynamics, reduced radar cross section and tactical effectiveness , generated the need for military aircraft and spacebourne structures to include sensors within their composite laminated structures . Advanced aircraft and spacecraft will require fibre-optic sensor systems for structural integrity monitoring [31]. 'Fly-by-light' encoder systems are already installed in military and aerospace applications. Extensive research work on embedded fibre optic sensors (mostly strain related) in composite structures have been undertaken. [19][32]

6.2 Medical

Diagnostic testing in the medical arena gave impetus to development of state-of-the art analytical devices. These medical biosensors , defined by the ability to couple an immobilised biospecific recognition entity to the surface of a transducer which in turn "tranduce" the molecular event into a measurable electrical signal, offer significant advantages to the medical community [33]. The large marketing areas in medical applications of fibre-optic sensors would have to involve 'throw-away' devices for rapid measurement of say. pH, antibody or antigen immobilisation near the patient. The fibre-optic endoscope is already extensively used for in-vivo examination. Probes designed for insertion into blood vessels can be used to monitor flow and heart fluctuations. A temperature probe for medical applications (as distinct from industrial), have also been described [34]. There is extensive research done on fibre-optic immunosensors. In a recent publication an immunosensor capable

of detecting cholera anti-toxin have been described [35]. The advantages of a reduction in time relative to the laboratory analysis of samples are clear both in terms of cost and efficiency using fibre optic sensor technology.

6.3 Marine

Remote sensing of marine activity would benifit from developments of high resolution sensing systems . Sensing systems can be installed on board sea-going vessels largely for safety and immunity to interference reasons. There are indications however, that optical fibres for both sensing and communications purposes will also be increasingly used in an offshore environment such as rigs and platforms. The reduction in weight and volume offered by the fibre cable offer clear advantages, particularly during installation. Biological and ecological studies can benifit by specific fibre-optic sensor developments that could aid studies and research. A diver operated 'in situ' measurement device, described recently in the literature, [36], is one such development.

6.5 Industrial

Fibre optics have facilitated optical access in applications where conventional methods could not be applied due to the often high temperature or hostile nature of the environment. There are obvious advantages to applications of these sensors in the industrial area. Thus far however, this area has moved very slowly, largely because of the component costs for example, the couplers, used in fibre- optic systems. It was discussed in section 5 that single fibres to each sensor, with some electrical multiplexing, may be used in limited installations, pending further research into cheap multiplexing methods. A broad range of industries stand to benefit from the development of faster, more accurate optical monitors, such as the steel, power, petrochemical and glass industries. Further developments for temperature, pressure, flow, rate of reaction etc measurements are clearly application driven. Sensors may also be specifically designed for high power industries such as power plants, where interference effects can be high.

7. CONCLUSION

The field of fibre optic sensors have gained momentum during the last decade but there is still considerable room for innovation. In this paper an overview of the technology applicable in sensor development have been made. Application areas that hold promise have also been demonstrated. Sufficient information is now available for efforts to be directed into the most fruitful areas such as industrial applications. It is important that work on sensors be carried out in conjunction with industry since the replacement of already adequate reliable industrial systems will not occur simply on the basis of purely laboratory experimental evidence. Co-operation with industry is

therefore vital. Sensors which will prove to be successful, are those where proper optical and electro-mechanical systems engineering have been carried out following development of a well-defined interface system.

ACKNOWLEDGEMENT

The author would like to thank the FRD for its financial support (GUN2040624) for the project, Micro-interferometric sensing.

REFRENCES

1 MTE Kahn, " Sensing and control in the evolution of intelligent structures for civil engineering," Electricity and Control Journal, pp 47-50 , Nov 1997

2 D. Biswas, "Characterization of polyimide-coated optical fibres, "Journal of Optical Engineering Vol 30, No 6 ,pp722- 725 , 1991

3 D. Biswas, "Aging behaviour of polyimide/acrylate coated fibtres in harsh envirinments," Journal of Optical Engineering, Vol 36,No 8, pp 2167-2170, 1997.

4 GR Kurkjian, JT Krause, MJ Mathewson, " Strength and fatigue of silica optical fibres," Journal of Lightwave Technology, Vol 7,No 9, pp1360-1370, September 1989

5 G Das, SN Sarkar, " Estimation of dispersion parameters involving the Peterman II spot size using Gausian type approximation in single mode graded index fibres," Journal of Optical Engineering, Vol 36, No 9 , pp2425-2428, September 1997.

6 SC Rashleigh, "Origens and control of polarization effects in single mode fibres," Journal of Lightwave Technology, Vol 1, No 3, pp 312- 317, June 1983.

7 JT Krause, CR Kurkjian, "Fibre splices with perfect fibre strength of 5.5Gpa," Electronics Letters, Vol 21, pp533-535, 1985.

8 K Chen, D Krepps, "Coupling efficiency of surface emmiting LED's to single mode fibre's," Journal of Lightwave Technology, Vol LT-5, No 11, pp1600-1604, November 1987.

9. T van Muoi, "receiver design for high speed optical fibre systems," Journal of Lightwave Technology, Vol LT-2, No 3, pp243 246, June 1984.

10. FC Crawley "Intelligent structures for Aerospace", AIAA Journal, Vol. 32 No 8, pp1689-1699, 1994

11. E. Udd , " Fibre-optic smart structures," Proceedings of the IEEE, Vol. 84 , No 1, pp 60- 67, January 1996.

12. MTE Kahn, "Intelligent structures with opto-electronic sensor systems," SAIEE Elektron Journal,pp35-37, September 1997.

13. KF Voss and KH Wanser, "Fibreoptic strain-displacement measurement sensor employing non-linear *buckling*," *Applied Optics, Vol. 36 No 13, May 1997*, pp2944- 2946.

14. B Culshaw , C Michie , and McGown, "Smart structures and Applications in Civil Engineering," Proceedings of the IEEE, Vol. 84 No1, January 1996, pp 78-86.

15. D.X Wang, WL Anderson, MA Karim, Y Li, " Self referenced two fibre sensor for micro-displacement measurement," Journal of Optical Engineering, Vol 36,

No 10, pp2809-2813, October 1997.
16. CE Lee, HF Taylor, "Interferometric optical fibre sensors using internal mirrors," Electronic Letters, V24, No4, pp193-192, Feb 1988.
17. L Yanbaio, S Qinxia, "optical fibre Mach-Zender interferometer for smart skins," Fibre optic Smart Structures and Skins V, SPIE Vol 1798, pp 186-191, 1992
18. I Sakai , "Multiplexing of optical fibre sensors using frequency modulated source and grated output," *Journal of Lightwave Technology, Vol LF5, 1987, pp* 972 -940
19. WB Spillman, LB Maurice et al, "Quasi distributed Polarimetric Strain sensor for smart skin applications," SPIE Vol. 1170, Fiber optic Smart structures and skins II, 1989, pp483-494.
20 HW Haslach, JS Sirkis, "Starin or stress component separations in surface mounted interferometric optical fibre strain sensors," SPIE vol. 1170, Fiber optic smart *structures and skins II, 1989, 452-461.*
21 SD Dyer, DA Christiansen, "Dispersion effects in fibre-optic interferometry," Journal of Optical Engineering, Vol 36, no 9, pp 2440-2447, September 1997.
22 AYu and AS Siddiqui , "Theory of a novel high sensitivity optical fibre gyroscope," IEE Proceedings-J, Vol. 140 No 2, April 1993, pp150 -155
23 P Urquart , "Review of rare earth doped fibre lasers and amplifiers," IEE Proceedings, Vol. 135, Pt J, No 6, *December 1988, pp 385-407.*
24 LI Tingye, "The impact of optical amplifiers on long distance lightwave telecommunications," Proceedings of the IEEE, Vol. 81 No 11, November 1993, pp1568 -1578
25 AD Kersey, "Recent progress in interferometric Fibre sensor technology," Proceedings of the SPIE, Vol. 1367, No 2, 1991
26 A Dandridge, AB Tveten, AD Kersey, "Multiplexing of Interferometric sensors using phase generated carrier *techniques," Journal of Lightwave Technology, Vol LT-*5, pp947-950, 1987
27 J Mlodzianowsky, " A simple frequency domain multiplexing system for optical point sensors," Journal of Lightwave Technology, Vol LT-5, pp 1002-1006, 1987
28 HS al-Raweshedy, "Spread spectrum techniques for passive multiplexing of interferometric fibre-optic sensors," Proceedings of the SPIE, vol 1314, pp 342, 1990
29 BV Dasarathy, "Sensor Fusion Potential Exploitation-Innovative Architechtures and illustrative applications," Proceedings of the IEEE, Vol 85, No1, January 1997, pp24-38
30 R Soref , "Silicon based opto-electronics," Proceedings of the IEEE, Vol. 81 No 12, December 1993, pp 1687-1706.
31 E. Udd, et al, "Fibre optic sensor systems for aerospace applications,"SPIE Vol.838, Fibre Optics and Laser Sensors V, pp162-168, 1987
32 R.L Wood, A Tay, DA Wilson, "Design and fabrication for composite structures with embedded fibre optic sensors," SPIE vol.1170, Fibre optic smart structures and skins II, pp160-170, 1989
33 C. R Lowe, "Biosensors," Trends in Biotechnology, Vol 2, pp 59-65, 1984

34 Y Rao, DJ Web et al, "In fibre bragg grating temperature sensor system for Medical applications," Journal of Lightwave Technology, Vol 15, No 5, pp779-785, May 1997

35 RS Marks, E Basis et al, "Chemiluminescent optical fibre immunosensor for detecting cholera antitoxin," Journal of Optical Engineering, Vol 36, No 12, pp 3258-3264, December 1997

36 CH Mazel, "Diver operated instrument for in situ measurement of spectral fluorescence and reflectance of bethnic marine organisms and substrates," Journal of Optical Engineering, Vol 36, No 9, pp 2612-2617, September 1997.

APPENDIX 2

ASSESSMENT OF PHOTODETECTOR OPERATION FOR PHOTONIC APPLICATIONS

1. PHOTOCONDUCTIVE DETECTORS :

If a photon of light has an energy greater than the band-gap energy, that photon is capable of raising an electron from the valence band to the conduction band, when the photon is absorbed by a semiconductor. This process will result into the creation of the electron-hole pair.

Since this process results into a pair charges in excess of the thermal equilibrium value, the extra charge can be used to contribute to an electric current, whose value will depend upon the light power falling on the semiconductor. Thus, a small voltage across the photoconductive material layer will give rise to the required, measurable current in an external circuit as shown in figure 1.

Figure 1.1

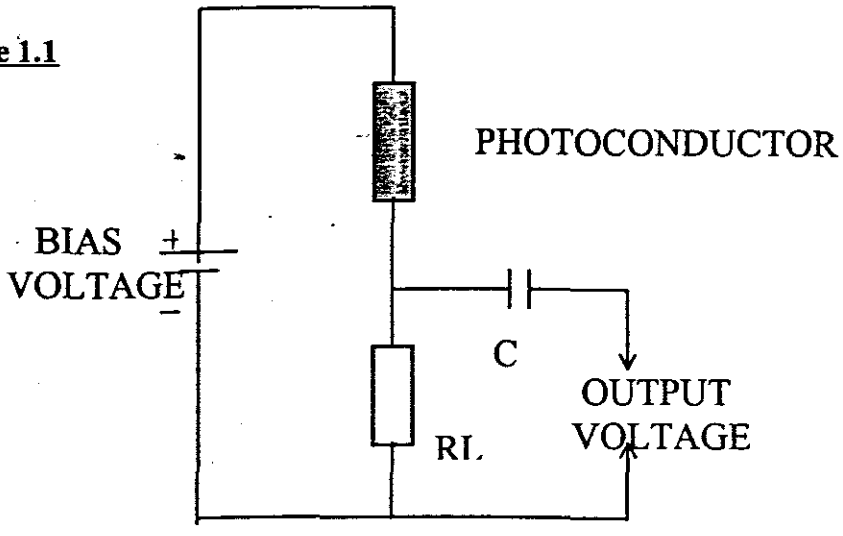

From the photodetection circuit above, all the photons will be absorbed in a thin surface layer and the charge pairs will not be collected

efficiently if the bias voltage is too high. The frequency responsivity spectrum of the photodetector must be matched to the spectrum of the light which is to be detected.

If a person wants to detect a light power of photons of arriving every second on the photoconductive detector and the fraction (n) of these photons produces electron-hole pairs. There will be nP/hv charge carriers are produced every second. If all these charge carriers are collected, the observed electric current is given by

$$I = \frac{enP}{hv}$$

The current (I) resulting from the above equation is proportional to the optical power. Since electrical power is also proportional to the square of the optical power, therefore it is important to know whether the signal-to-noise ratio is given in terms of electrical power or optical power.

Another very important feature is speed of response of the photoconductive detector. If the electron is created in the electron-hole creation process, each electron will continue to contribute to the current flow until it is destroyed completely. If the average time for the recombination of an electron-hole pair in the semiconductor is τ and the transit time across the layer of the semiconductor is τ_o, the average number of times the electron is used in the current is τ/τ_o. Hence the current due to the light flux is given by

$$i_p = \frac{e\,n\,P\,\tau}{hv\ \tau_o}$$

However, the minimum time within which the phoconductive detector can respond to a change in light level is τ, so the bandwidth of the measurement is given by

$$\triangle f = \frac{1}{2\pi\tau}$$

Whereas the sensitivity for the device as the current produced for a given optical power is

$$S = \frac{i_p}{P} = \frac{e\,n\,\tau}{hv\tau_o}$$

The sensitivity expressed by the above equation can be increased by increasing the width of the absorbing layer and changing the geometry as shown in figure 2 on the following page.

Figure 1.2

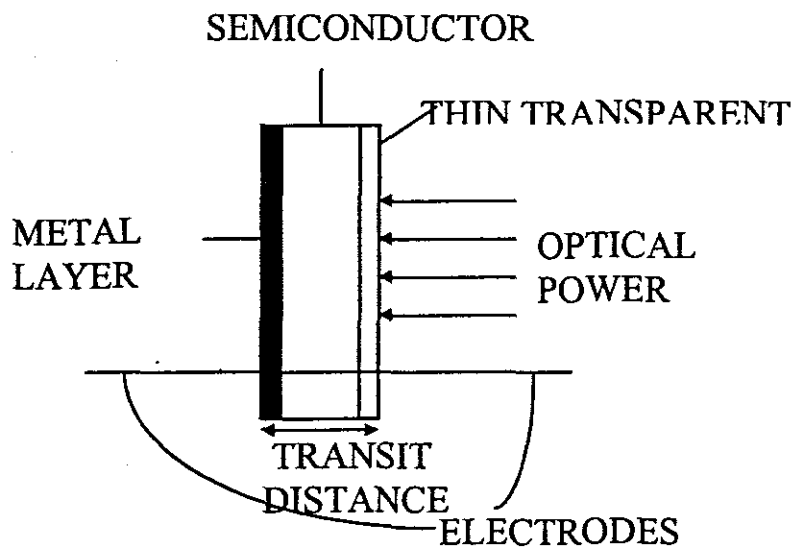

The advantages of photoconductive detectors are that :

(a) They can be used at long wavelengths(approximately upto 20 μm).

(b) They are relatively very cheap

There are two significant disadvantages possessed by photoconductive detectors when compared to other types of photodetectors:

(a) High sensitivity(values of $\tau/\tau_o \geq 10^3$) can only be achieved for response times of approximately 50 ms. This speed is also very slow for most opto-electronics applications.

(b) The electron-hole recombination process is a random one, and thus introduces noise. The recombination noise can be very troublesome in many applications.

Since these devices are very cheap they were often used in domestic cameras as CdS or CdSe cells.

2. PHOTODIODES :

2.1 Junction photodiodes :

If a photon that has its energy greater than the band-gap energy of the semiconductor is incident upon the region of a semiconductor that is exposed to the junction's electric field, the photon will create the electron-hole pair which immediately comes under the action of the electric field. The electron will be swept to the positively charged n-type material and the hole to the negatively charged p-type material. This action will reduce the junction voltage below its equilibrium value.

When a photon flux equivalent to an optical power incident upon the junction, the electron-hole pair created by the electric field acting across the junction, the drift current increases according to the following formula

$$i_p = \frac{e\,n\,P}{hv}$$

Figure 2.1.1

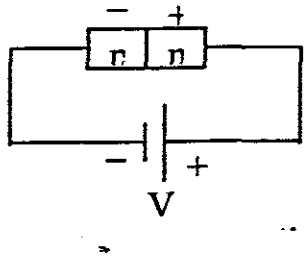

When we take a pn junction and apply to it a reverse bias voltage(approximately 10V) as shown in figure 2.1.1, the two opposing voltage are held low. If the photons are incident upon the depletion region, the electron-hole pairs created are immediately separated into their constituent charges which are quickly drawn to the side of the junction that has opposite charge.

The reverse bias allows only a very small diffusion and drift currents flow in the absence of photogenerated carriers. Essentially the only current which flows is the current due to the charges created by the incoming photons. Hence this current is directly proportional to the input optical power. This method is very common most types of measurements.
The main advantages of the junction photodiodes are as follows:

(a) Charges are quickly separated and almost completely destroyed immediately. Therefore, the greater portion of the randomness of the recombination process is removed. This leads to smaller recombination process and leads to a smaller recombination noise than the in the photoconductive case.

(b) As the reverse bias increases, the drift velocity of the charges will increase until it saturates. At this point, an increase in the bias voltage will increase the depletion region's width without any increase in drift velocity. Since the larger is the depletion width, the greater is the volume available to receive the incoming light and thus there is greater number of the electron-hole pairs that can be created; Hence the junction photodiode has greater sensitivity.

The sensitivity of photodiodes normally is referred to specifically as the **respositivity**, and is defined as the photocurrent produced for a given optical power. Responsivity can be calculated from the following equation

$$R = \frac{ip}{P} = \frac{e\,n}{hv}$$

With the wavelength(λ) in micrometers. The above equation can be written as follows

Figure 2.1.2

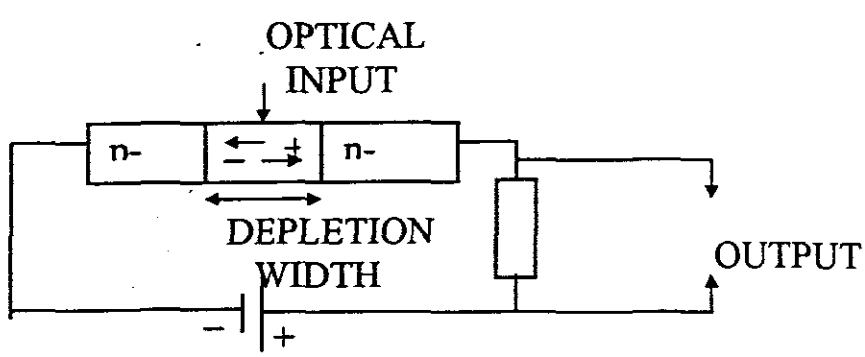

The circuit above shows the response in a junction photodiode depending on the depletion width.

2.2 Silicon photodiode

Figure 2.2.1 below shows the structure of the silicon photodiode.

Figure 2.2.1

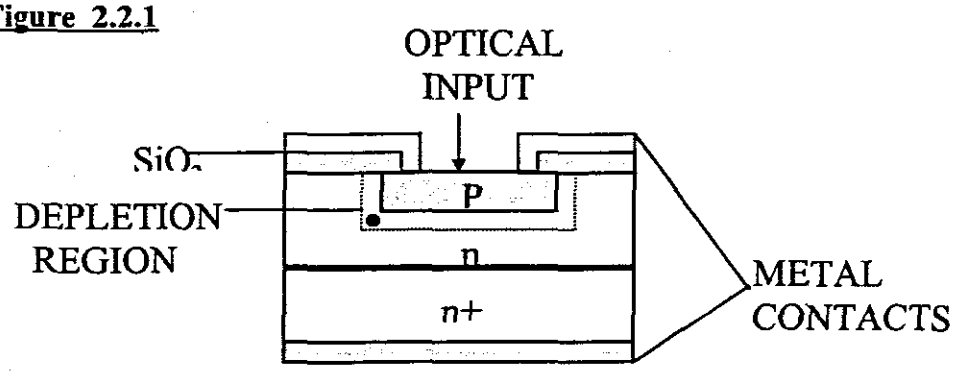

Figure 2.2.2 is the resposivity spectrum for a typical silicon photodiode.

Figure 2.2.2

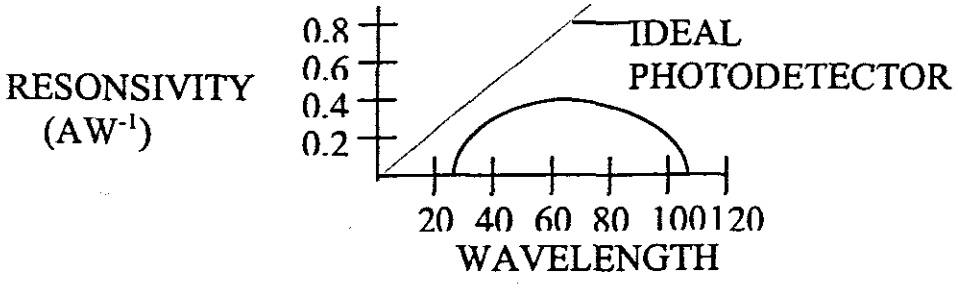

The circuit below is the photodiode circuit with the junction capacitance.

Figure 2.2.3

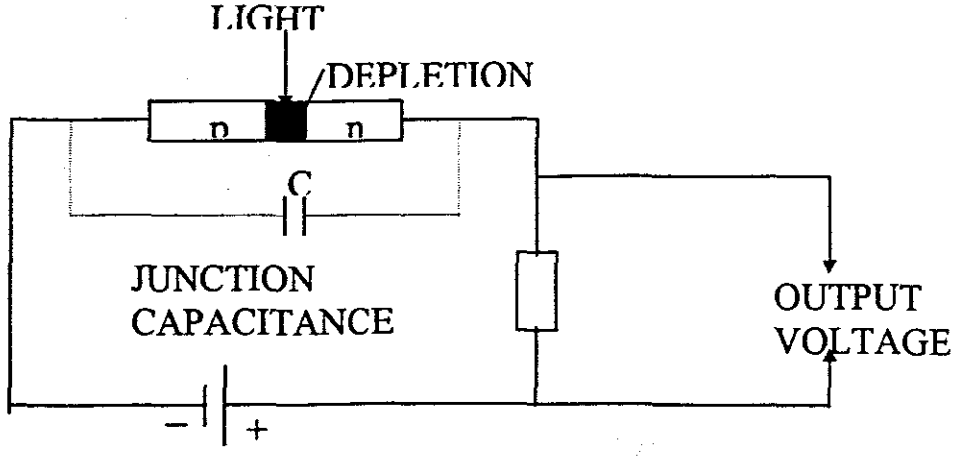

A typical p-n junction capacitance is approximately 25pF, so for a 20GHz bandwidth the required responsivity must be

$$R < \frac{1}{2\pi f c} = 0.32\Omega$$

The voltage generated by the photocurrent will be small as the value of resistance is very small. A good amplifier with large bandwidth, low noise, high gain and properly matched impedance must be employed. In practice the load resistor is approximately 50Ω since this match into standard coaxial cables. These features makes these devices more than sufficient for vast majority of applications, except those applications that include high-bit-rate optical communications.

The source of noise primarily is due to the randomness of the photon arrivals, it can be determined from

$$i_n = (2eBi_D)^{1/2}$$

Where i_n is the noise current, e the electronic charge, B is the circuit bandwidth and i_D the current flowing through the circuit.

$$i_D = i_p + i_d$$

Where i_p is the photogenarated current and i_D is the current which flows in the circuit during the absence of any light input. The noise of the photodiode itself ai usually expressed in the form of the noise-equivalent power(NEP).

$$NEP = \frac{hv(2ei_dB)^{1/2}}{e\,n}$$

A typical value of the NEP for silicon photodiode is approximately 10^{-14} $WHz^{-1/2}$, corresponding to the dark currents of approximately 1nA. The thermal noise power will be 4kTB, so the noise current in a resistor of R will be

$$i_R = [(4kTB)/R]^{1/2}$$

Therefore the total circuit noise current will be

$$i_N = (2ei_dB)^{1/2} + [(4kTB)/R]^{1/2}$$

2.3 The PIN photodiode

The schematic structure of a pin photodiode is shown below

Figure 2.3.1

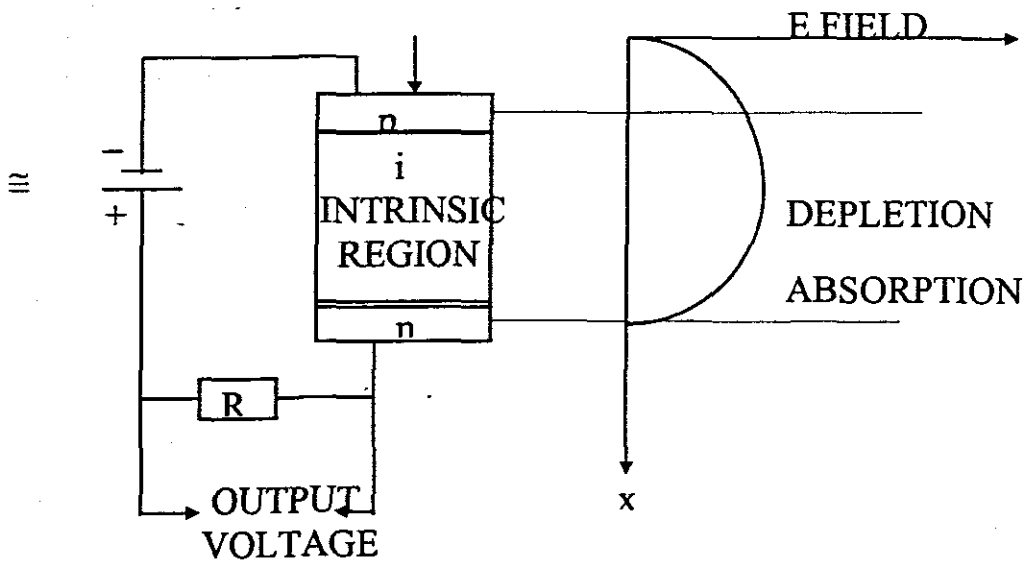

The pin photodiode has a photosensitive region within which an electric field can act to separate and mobilize the carries from the electron-hole pairs as they produced by the incoming photons. Thus the pin photodiodes has greater depletion region leading to a large sensitivity. Two typical designs of pin photodiodes are shown below.

Figure 2.3.1

(a)

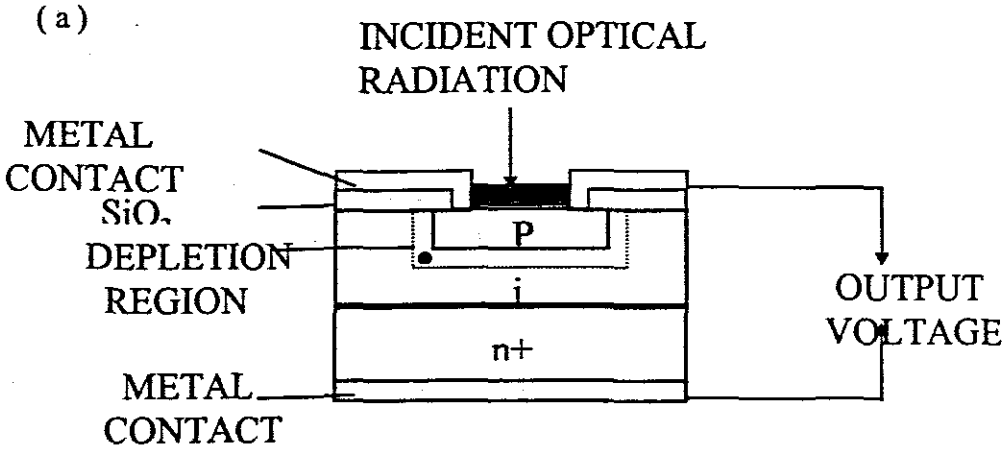

(b)

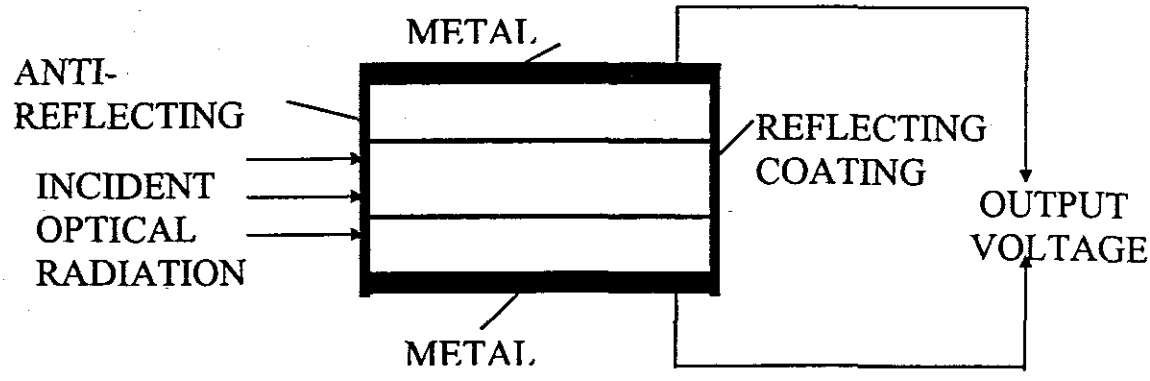

Figure 2.3.1 (a) is the structure of the front illuminated Si pin photodiode and (b) is the side illuminated Si pin photodiode.

The pin photodiode have the advantages of compactness, ruggedness, good temperature stability and low operating voltage (10 - 20). However, they are devices of limited sensitivity. If a very high sensitivities are required we might opt for a photomultiplier.

2.4 Photomultiplier

The circuit for the principle of operation of a photmultiplier is shown below

Figure 2.4.1

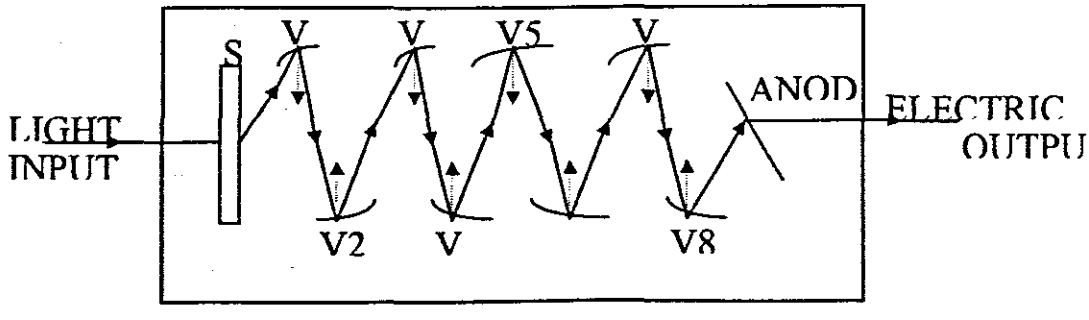

The photons impinging on a suitably chosen sensitive photocathode material that has enough energy to eject electrons from the material into the surrounding vacuum. The electrons are accelerated to another electrode(dynote) by the electric field that exists between the two. On arriving at the dynote, the electrons eject a large number of secondary electrons by energy of impact. This process continues continues for upto an electron multiplication factor of 10^6 to 10^9. Hence a large electric current can result from a very small optical power inputs.

Whilst being very sensitive, photomultipliers have a disadvantage of requiring several kilovolts for their operation and they use bulky vacuum tubes that are vulnerable to damage. They also suffer from agieng problem.

2.5 Microchannel plate

Figure 2.5.1

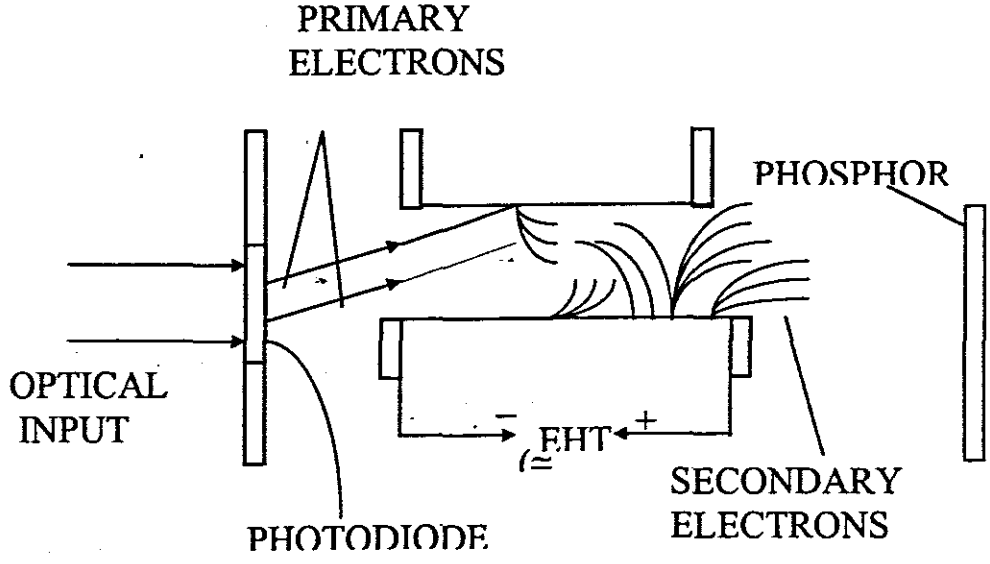

The schematic for a one channel in a microchannel plate is shown on figure 2.5.1. The microchannel plate is the recent development of the photomultiplier. A slab of insulating material(≅ 500μm thick) contains a large number of small diameter(≅ 10μm) holes or channels within it. A high voltage(500 - 1000V) is applied between its two faces. Photons incident upon a photocathode material close to one of the surfaces

generate electrons which enter the holes and then produce cascades of secondary electrons as they bounce along the holes triggered on by the potential difference.

The number of emerging electrons in the microchannel plate device can be directed on to a phosphor material to provide a considerably more intense version of the incoming photon stream. Photomultipliers can be used to intensity infrared images and thus they provide night vision via the infrared radiation emitted by objects, even at night, as a result of their temperature above zero.

2.6 The avalanche photodiode (APD)

A good compromise between the photodiode and photmultiplier is the avalanche photodiode. The pin junction photodiode is operated with a very high reverse bias voltage($\cong$ 200V). When an electron-hole pair is created by the incoming photon, the resulting charge carriers can aquire sufficient energy from the field across the junction to create further electron-hole pairs themselves, leading to an avalanche multiplication process similar to that in the photomultiplier.

An increase in sensitivity can be achieved at the expense of a higher operating voltage. Since the multiplication process is electrically noisy, the noise level of the photodection is increased. If each photogenerated charge carrier produced a constant number of secondary carriers, the noise present would be

$$\Delta i_s = M(2ei_p \Delta f)^{1/2}$$

Where M is the multiplication factor, e the electronic charge, i_p the photogenerated current and f is the bandwidth. The final detected current is obtained from

$$i_D = Mi_p$$

Hence

$$\Delta i_s = (2eMi_D \Delta f)^{1/2}$$

However there is excess noise associated with the multiplication process. The noise actually observed is expressed as follows

$$\Delta i_s = F^{1/2}(2eMi_D\Delta f)^{1/2}$$

Where F is the excess noise factor. Typical values of F lies in the range 2 - 20.

PHOTON COUNTING

A valuable technique for improving the detection signal-to-noise ratio(SNR) when the signal level is very low is known as photon counting. The arrival of a single photon at the detector will give rise to a pulse current whose height lies within in a known narrow range.

The randomly generated thermal noise(i_d) is distributed over a much larger range. The detector's output is fed into a **pulse-height discriminator.** The pulse-height discriminator rejects pulses which lie outside a preset range.

The pulses within the range are passed on to a pulse counter that counts the pulses arriving at the preset time. The number of pulses arriving at the pulse counter at any given time is proportional to the optical power. Since the pulse from the photodetector which receives a single photon is very small, therefore a large intrinsic sensitivity is required. The photomultipliers or avalanche photodiodes are often used in photon counting.

To improve the signal noise-to-ratio further, the input light is chopped. This allows the photon counting system to compare the light-on count rate with the light-off rate. This process also removes the random signals that happen to lie within the preset range. The improvements in the signal-to-noise ratio are typically by a factor of 2 or 3 (3 - 5dB). Figure 1 illustrates the discriminatory feature of photon counting.

Figure 1

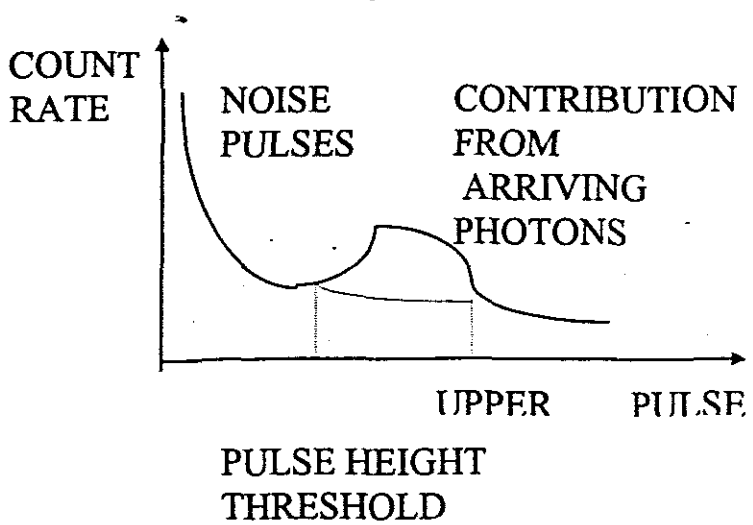

APPENDIX 3

AN ASSESSMENT OF OPTICAL WAVEGUIDE THEORY

INTRODUCTION

Optical waves can be considered as guided when they are constrained to lie within a channel between two other media, the refractive index of the channel material being slightly higher than those of the other media, so that the light can bounce along the channel by means of total internal reflection(TIRs) at the boundaries between the media.

In order to progress down the guide indefinitely, the waves from the successive boundaries must interfere constructively, forming essentially a *continuous and a stable interference pattern down the guiding channel.* If the wave is not fully constructive, the wave will eventually self-destruct, owing to the out-of-phase cancellations.

Wave propagation in a planar waveguide

Figure 1.1

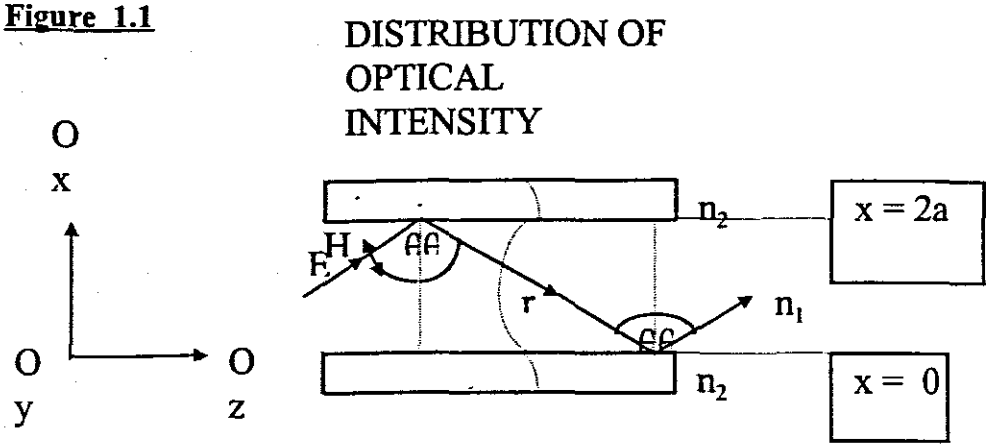

Figure 1.1 above shows the optical slab waveguide. The guiding channel consits here of a slab of material of refractive index n_1 surrounded by

two outer slabs, each of refractive index n_2. The resultant electric field for light which is linearly polarized in a direction pependicular to the plane of incidence(transverse electronic(TE) mode) is given by the sum of the upwards and downwards rays.

$$E_T = E_i + E_r$$

Where

$$E_i = E_0 \exp(i\omega t - ikn_1 x \cos\upsilon - ikn_1 z \sin\upsilon \text{ and}$$

and

$$E_r = E_0 \exp(i\omega t + ikn_1 x \cos\upsilon - ikn_1 z \sin\upsilon + i1/2\delta)$$

$$E_T = 2E_0 \exp(i\omega t + ikn_1 x \cos\upsilon + 1/2\delta s)\exp(i\omega t - ikn1z\sin\upsilon + i1/2\delta s$$

Since

$$\cos^2(1/2\delta s) = \cos^2(kn_1 2a\cos\upsilon + 1/2\delta s)$$

and

$$2akn_1\cos\upsilon + \delta s \approx m\pi$$

For free space propagation $k = (2\pi)/\lambda$.

Hence $\beta_1 = n_1 k$
$\beta_2 = n_2 k$

Along Oz : $\beta = n_1 k \sin\upsilon$
Along Oz : $q = n_1 k \cos\upsilon$

β is the effective wavenumber for the propagation down the guide.

$$E_T = 2E_0 \cos(qx + 1/2\delta s)\exp i(\omega t - \beta z + i1/2\delta s)$$

Phase velocity :

$$c_p = \frac{\omega}{\beta} \qquad \text{and} \qquad c_g = \frac{d\omega}{d\beta}$$

For the velocity with which the optical energy propagates down the guide.

For all real υ, $\beta \leq n_1 k$ and $\sin\upsilon \geq \frac{n_1}{n_2}$

For TIR condition, $\beta = n_1 k \sin\upsilon \geq n_2 k$

Therefore $n_1 k \geq \beta \geq n_2 k$ or $\beta_1 \geq \beta \geq \beta_2$

In other words, the wavenumber describing the propagation along the guide axis always lies between the guiding medium(β_1) and the other medium(β_2).

Since β varies with ω between these two limits,

$$k = \frac{\omega}{c_o}$$

Where c_o is the free space velocity. The expression for the phase changes which occur under TIR at the given angle can be written as follows

$$\tan 1/2\delta s = \frac{(n_1^2 \sin^2\upsilon - n_2^2)^2}{n_2^2 \cos\upsilon}$$

and the case where the electric field is perpendicular to the plane of incidence

$$\tan 1/2\delta p = \frac{n_1(n_1^2 \sin^2\upsilon - n_2^2)^2}{n_2^2 \cos\upsilon}$$

For the case where it lies in the plane of incidence

$$\tan 1/2\delta p = \frac{n_1^2 p}{n_2^2 q} \tan 1/2\delta s$$

If $p^2 = \beta_2 - n_2^2 k^2 = k^2(n_1^2 \sin^2\upsilon - n_2^2)$, the transverse resonance can be represented as follows

$$\tan(aq - 1/2m\pi) = \frac{p}{q}(E_\perp)$$

and the perpendicular polarisation as

$$\tan(aq - 1/2m\pi) = \frac{n_1^2 p}{n_2^2 q}(E_{||})$$

$E_{\perp}$ is the transverse electric(TE) and the $E_{||}$ is the transverse magnetic (TM).

The solution for this equations can be separated into odd and even types according to whether m is odd or even. For m odd we have

$$\tan(aq - 1/2m_{odd}\pi) = \cot aq$$

and for m even

$$\tan(aq - 1/2m_{even}\pi) = \tan aq$$

Taking m to be even

$$aq \tan aq = ap(E_{\perp})$$

From definition of p and q

$$a^2p^2 + a^2q^2 = a^2k^2(n_1^2 - n_2^2)$$

Taking rectangular axes ap and aq, this relation between p and q translates into a circle of radius ak(n12 - n22)1/2. See figure 1.2 below

Figure 1.2

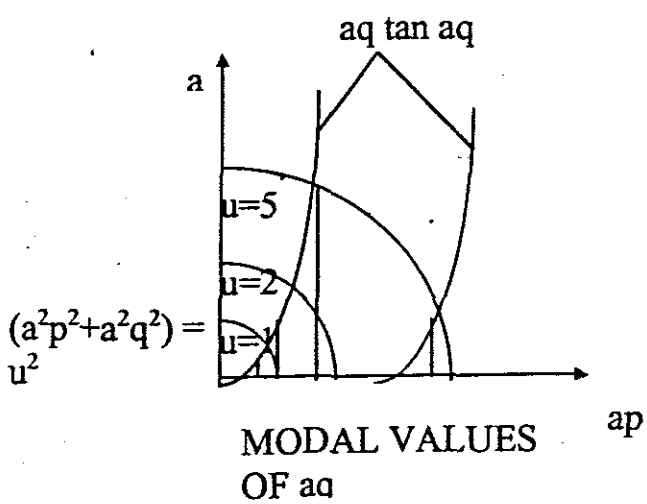

Figure is the graphical solution of the modal equation equation for the slab waveguide

APPENDIX 4

AN ASSESSMENT OF SPECIFICATIONS USED IN DESIGNING WITH OPTICAL FIBRES

Guiding properties of a glass fibre

There are certain guiding properties in the manufacturing of optic-fibre. The speed of propagation of a light ray depends upon the density of the medium in which it travels. The more dense the medium the slower it travels. Thus when a light ray moves from a medium of high density to a medium of low density, refraction occurs, whereby the wave moves faster and bends, as shown in "a" below.

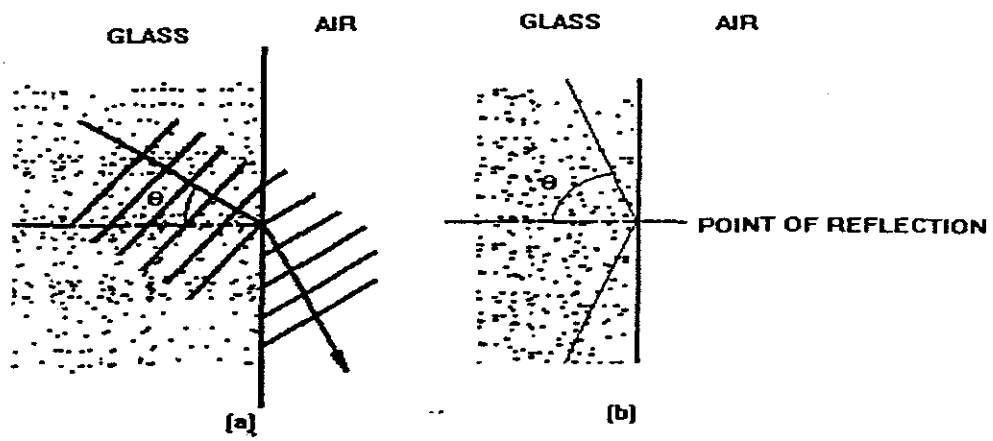

As the angle of refraction is increased, a point is reached where the light is no longer refracted, as indicated in "b" above, and total internal reflection takes place. Under these conditions the light ray does not leave the glass medium, and so this principle of total internal reflection accounts for the fact that a light ray can be propagated down a glass fibre. This principle is illustrated below.

The effect of surface imperfections

Surface imperfections on the glass would lead to undesirable losses that have to be overcome if a light ray has to be propagated along a fibre for an appreciable distance. These losses are overcome by surrounding the glass fibre with a cladding layer so that any imperfections lie on the cladding layer. The effect and solution is shown on the following diagrams.

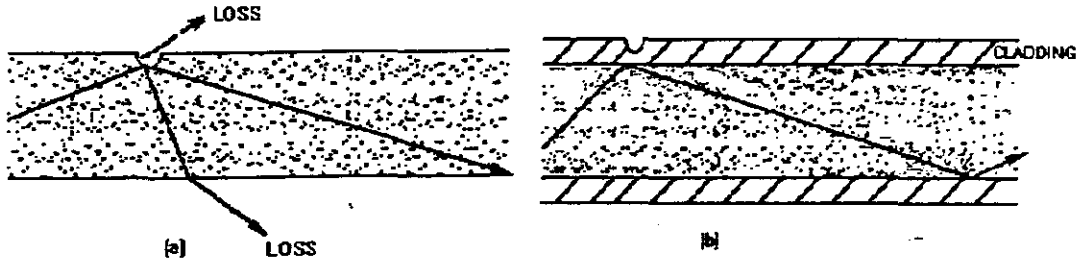

Numerical Aperture

If total internal reflection is to take place, then the rays launched into the fibre must fall within a certain angle. This angle is referred to as the Acceptance Angle q A, and from it can be formed the Acceptance Cone. The light collecting ability of the fibre is expressed in terms of its Numerical Aperture NA, where :

$$NA = \sin q\, A$$

Thus the magnitude of the NA is dependant upon the acceptance angle, that is the greater q A the greater the NA and consequently the light collecting ability of the fibre. The figure below shows the acceptance cone.

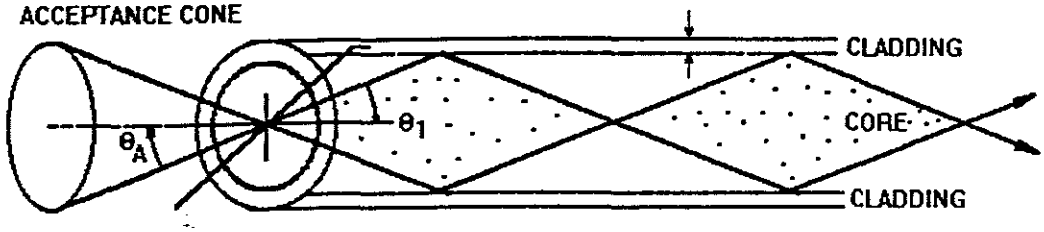

Dispersion

Rays launched at different angles within the acceptance cone will all be propagated along the fibre, but will follow different path lengths as shown below.

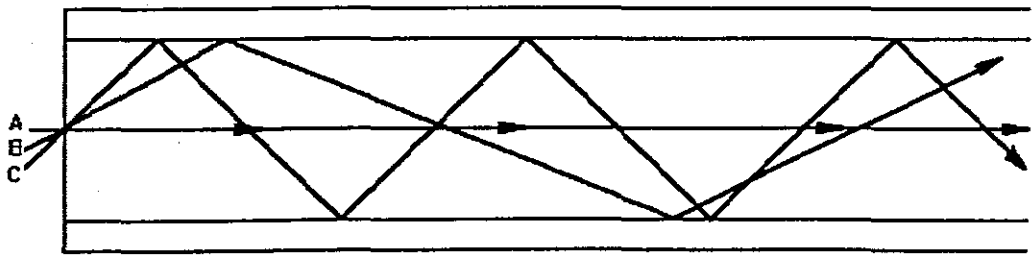

At the receive end, these rays arrive at different times and this lead to distortion of the transmitted pulses known as Dispersion, as shown below.

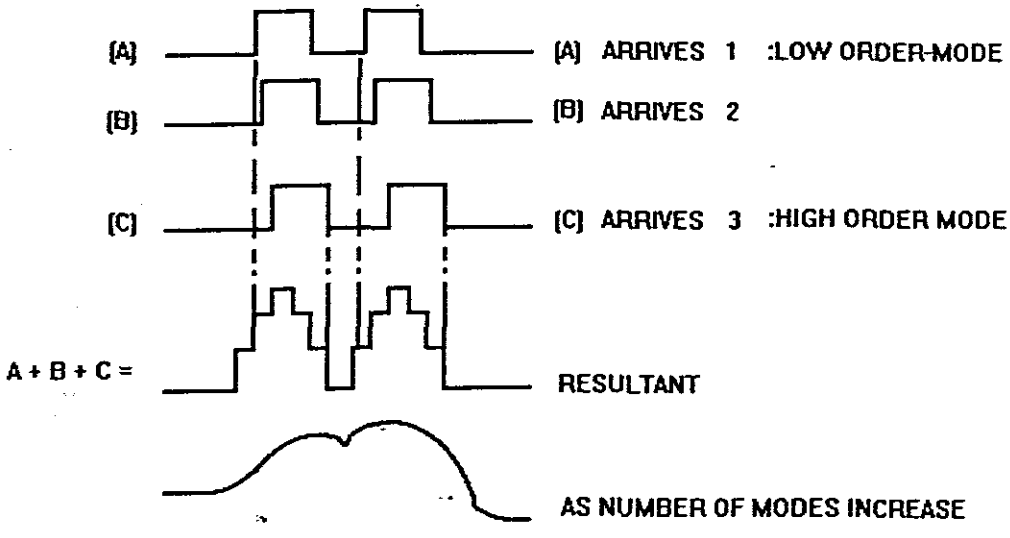

Each path that is followed is known as the Mode of Propagation. The number of modes that an optical fibre can support is given by :

$$M = 0.5 \{ \pi d.NA / l \}^2$$

where d is the diameter of the core. Thus for a given NA and light wavelength the number M decreases as the diameter of the core is reduced. When the core diameter approaches the light wavelength, only a single mode will propagate.

Optical fibres can be classified as either single-mode or multi mode.

Multi Mode Propagation

There are two types of multi mode, Stepped index fibre and the Graded index fibre.

Stepped Index Fibre

This type of fibre consist of a glass core with a diameter in the region of 75 mm, that has a uniform refractive index surrounded by a cladding of glass having a slightly lower refractive index, giving an entire optic-fibre diameter of 100 mm. This large diameter lead to a high dispersion, leading to bandwidth reduction of approximately 30 ns/km. It's figure is shown below.

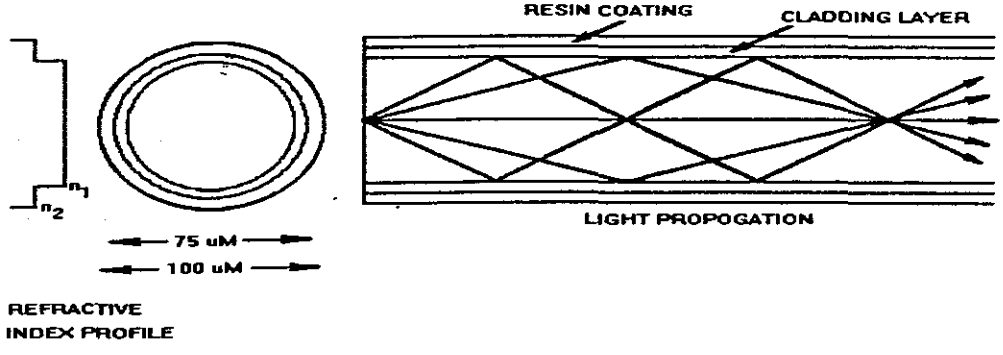

Rays launched into the fibre can follow a number of different paths, where each path is known as a mode of propagation. This type of transmission is referred to as Multi mode Propagation, and has a serious drawback in that dispersion of light takes place. This means that if pulses of light are propagated along such a cable they will tend to spread, and can even start running into one another. This makes detection of the presence or absence of light at the receive side very difficult and puts limit on the signalling rate. The effect on the light pulses is similar to that exerted on electrical pulses when they are passed through a bandwidth limiting filter and gives rise to a concept of fibre bandwidth. Fibre bandwidth is given by:

$$\textit{Fibre bandwidth} = \frac{0.44}{\textit{Dispersion}}.$$

From the fiber bandwidth formula, it is seen that in order to increase fiber bandwidth, dispersion must be reduced to a minimum. Since dispersion occurs as a result of the fact that a number of path lengths, or modes of propagation exists, it is obvious that by reducing the number of modes N, the bandwidth can be increased. One solution to this problem is to use graded index fibre.

Graded Index Fibre

This type of fibre consist of a glass core with a diameter of about 125 mm in which the refractive index gets progressively lower as one proceeds from the centre of the core outwards. In this fibre light rays are propagated by refraction so that they bent in sinusoidlike curves about the fibre axis. Dispersion is reduced in this type due to the fact that propagation through the glass of lower refractive index is faster than that through glass with a higher refractive index. Consequently those rays away from the core travel faster than those in the core and this tends all rays to reach the same point at the same time, thus compensating for the differences in path lengths. For graded index fibre, dispersion can be as low as 0.5 ns/km, corresponding to a fibre bandwidth of 16 Hz. It's figure is illustrated below.

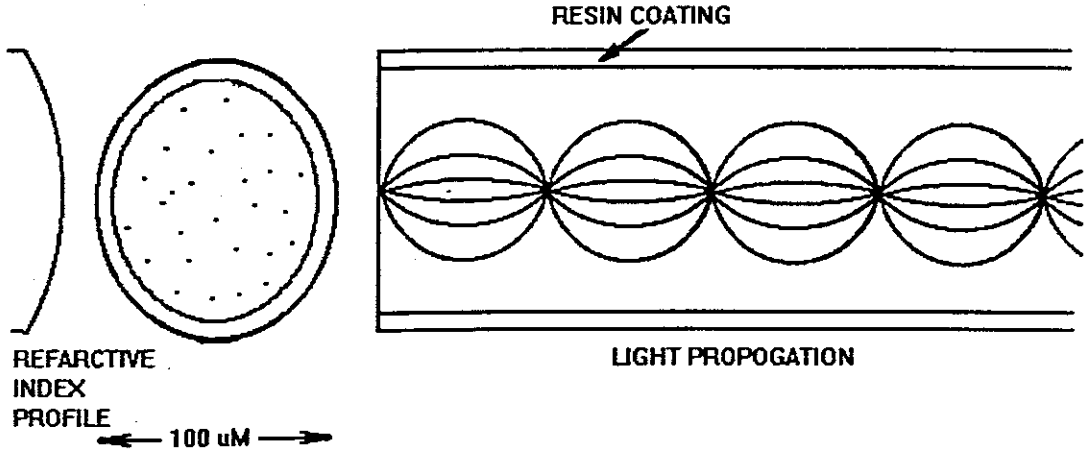

In both types the fibres are given a further coating of resin that preserves the inherent tensile strength of the glass by preventing micro-cracks from developing on the surface of the fibre while at the same time absorbing any light that may be emitted from the surface.

To manufacture fibres, gas mixtures are passed through a silica tube that is rotated while a hot flame traverses the outside walls. The temperature is sufficiently high enough to result in glass being deposited on the inside of the tube. To produce a stepped index fibre only one gas mixture is used. By varying the gas mixture the refractive index of the glass can be changed with each pass of the flame to produce a graded index fibre. When sufficient glass has been deposited on the silica tube, the original flame is replaced by one that is sufficiently hot to cause the tube to collapse into a solid rod. From this rod, termed a Preform, the fibre is drawn.
As was suggested earlier, another solution is to reduce the number of modes of propagation. This can be achieved by reducing the core diameter, thus when

the core diameter is nearly the same as the wavelength of the light to be propagated, single mode propagation becomes a reality.

Single Mode Propagation

Single mode fibres offer the potential of extremely wide bandwidths and low losses. To achieve propagation in one mode, however, the fibre core diameter must be no more than 5 mm. Together with the cladding the diameter adds up to 100 mm. It's figure is shown below.

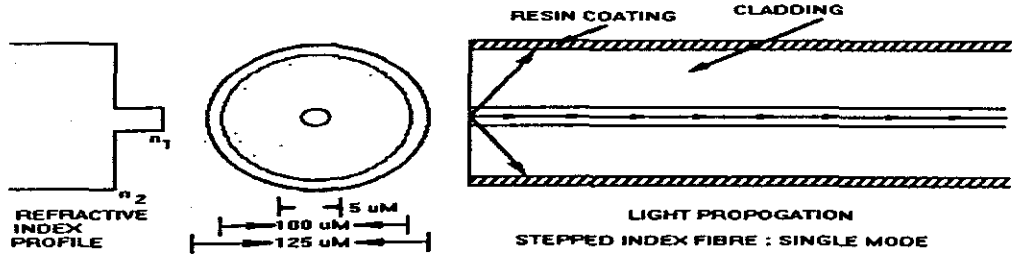

Dispersion of a single-mode fibre is the sum of two separate types of dispersion, namely material dispersion due to the refractive index of glass, and hence speed of light, varying with wavelength, and waveguide dispersion due to the distribution of light varying with wavelength. These two types of dispersion are in the infrared wavelength range opposite in sign, and with the simple single mode fibre waveguide structure, the two elements of dispersion add to zero at 1300 nm as shown in the following figure number 1.

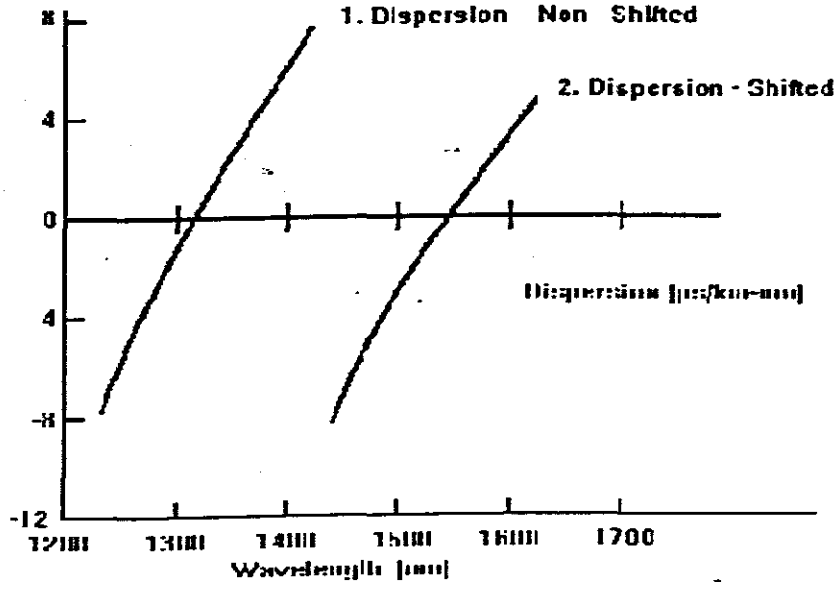

Fibres with different variations of refractive index with radius have different waveguide dispersion. Designers can take advantage of this fact to develop dispersion shifted fibres, where the dispersion curve looks like that of conventional fibres, but the zero point is shifted to 1550 nm as shown on the previous figure number 2.

Attenuation in optic-fibres

Signals travelling along an optical fibre also suffer a loss in amplitude. Rays launched from the light source falling outside the numerical aperture will be lost. This tends to attenuate the light signal, reducing the strength of the signal. So it is essential that the dimensions of the light source must be such that all light radiated from it must fall within the NA of the fibre to reduce attenuation.

Another possibility is the dispersion flattened fibre, in which the waveguide dispersion is tailored so that total dispersion is low between 1300 and 1500, as shown below.

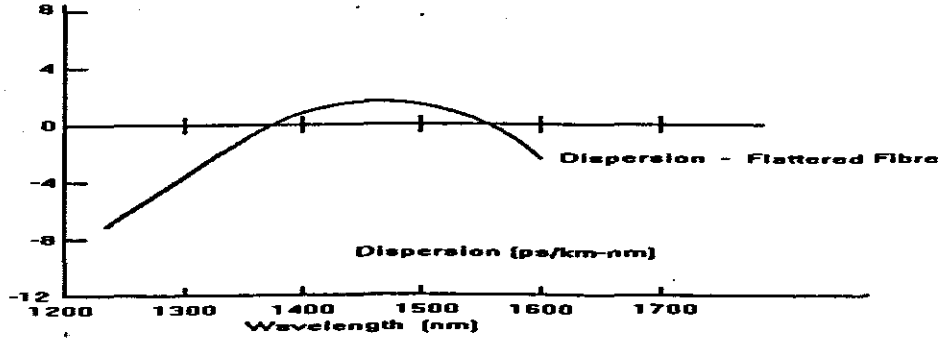

The first dispersion shifted fibre to reach the market is the segmented core design. It's waveguide structure shown in the below figure, differs from that of the current single-mode in two ways. The refractive index of the inner core changes gradually with distance from the fibre axis instead of abruptly. In addition there is an annular outer core, having a refractive index level between the inner core centre and the cladding.

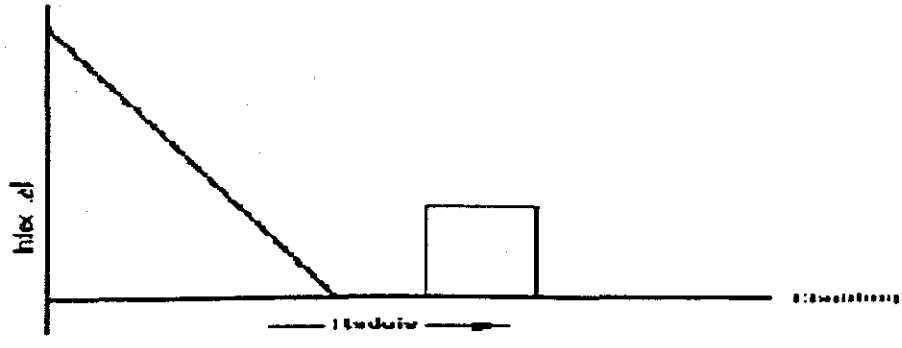

The segmented core design, can be used for dispersion flattened fibres if the inner core is made with a step index profile. This makes waveguide dispersion more closely approximate the inverse material dispersion, giving a total dispersion curve shown in the previous second figure. As can be seen, dispersion flattening is not perfect, but does provide two zero-dispersion wavelengths and as low dispersion region between them.

A major advantage of the segmented core design is low losses at 1550 nm. Losses as low as 0,17 dB/km, with a medium loss of 0,21 dB/km have been measured. The segmented core also offers an effective spot size of 10 μm, large enough to avoid excess splice losses. A more subtle advantage of the segmented core design is its inherently high uniform waveguide dispersion, which allows material dispersion to be offset without having to resort to small fibre cores. Thus segmented core fibres have a longer cut-off wavelength, that is the wavelength below which the fibre will transmit only one mode of light. One problem with short cut-off wavelengths is that they make fibres subject to increased microbending losses, which can cause excess cable losses.

Another issue is the zero dispersion wavelength. Many fibres with short cut-off wavelengths have significant variation in zero dispersion wavelength. With these designs, minor fluctuation in core diameter can cause significant changes in zero dispersion wavelengths.

Signals travelling along an optical fibre also suffer a loss in amplitude. Rays launched from the light source falling outside the numerical aperture will be lost. This tends to attenuate the light signal, reducing the strength of the signal. So it is essential that the dimensions of the light source must be such that all light radiated from it must fall within the NA of the fibre to reduce attenuation.

Another source of attenuation is caused by the scattering due to metal ions, such as iron and copper, and by absorption due to water in the OH radial form, producing absorption peaks at 720, 820, 945 and 1400 mm. Peaks in attenuation / wavelength characteristics for a graded index and the single mode fibre are shown in the figures respectively on the following page.

Fibre attenuation depends strongly on wavelength and is usually given in decibels per kilometre at a specific wavelength. Raleigh scattering is due to inhomogenities in the glass. This effect is inversely proportional to the fourth power of the wavelength and the loss.

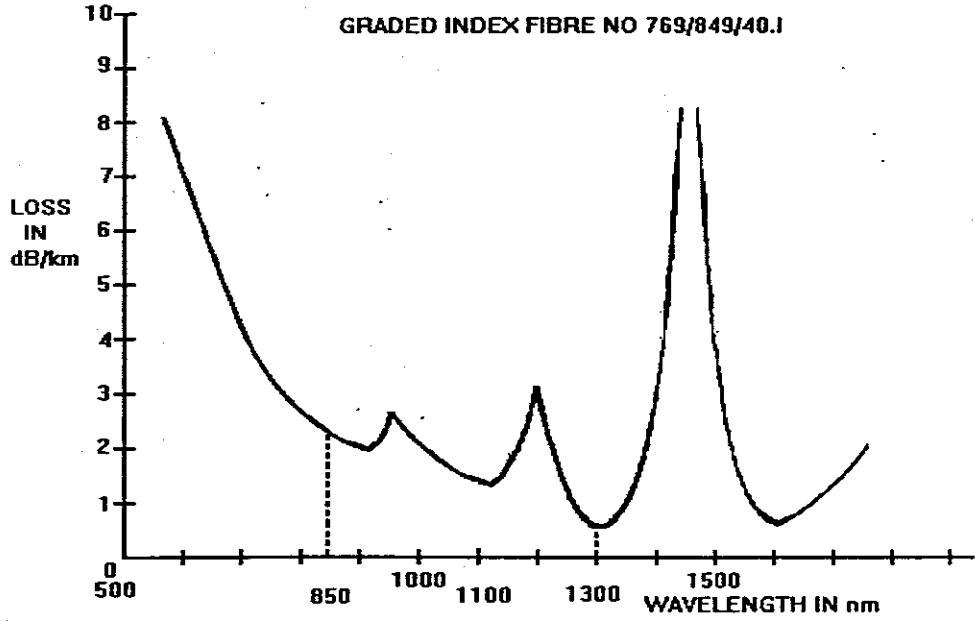
GRADED INDEX FIBRE NO 769/849/40.I
LOSS IN dB/km
10
9
8
7
6
5
4
3
2
1
0
500
850
1000
1100
1300
1500
WAVELENGTH IN nm

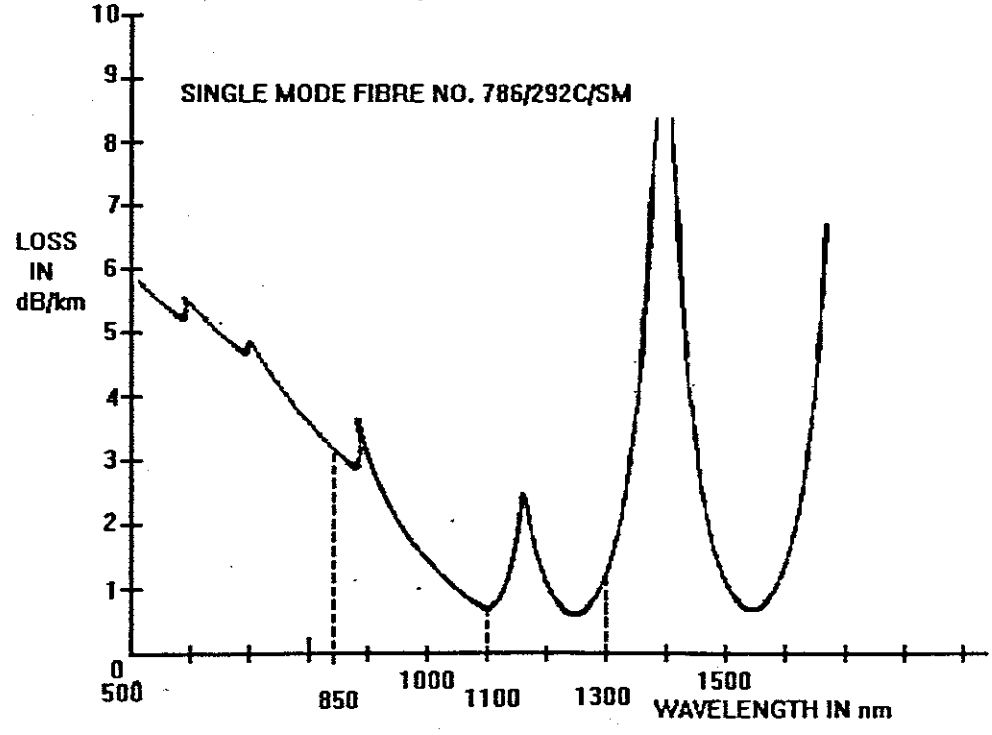
SINGLE MODE FIBRE NO. 786/292C/SM
LOSS IN dB/km
10
9
8
7
6
5
4
3
2
1
0
500
850
1000
1100
1300
1500
WAVELENGTH IN nm

APPENDIX 5

Assessment and comparison of Opto – Electronic Sources such as LEDs & Laser Diodes

Light Emitting Diode lightwave sources

Introduction

LED's are semiconductor light sources which emit light in the visible and near IR portion of the spectrum. Since they emit at wavelengths which provide a close match to the peak spectral response of silicon photodetectors, both GaAs and GaAlAs LEDs are often used with PIN and APD photodetectors.

What is an LED?

LEDs are solid state p-n junction devices which emit lightwaves when forward biased. Unlike incandescent lamps which emit light over a very broad range of wavelengths, LEDs emit light over such a narrow bandwidth that they appear to be emitting a single "color". Their small size, long operating lifetimes, low power consumption, compatibility with solid state drive circuitry and relatively low cost, make LEDs the preferred light source in many applications.

LEDs are made from a wide range of semiconductor materials. The emitted peak wavelength depends on the semiconductor material chosen and how it is processed. LEDs can be made which emit in the visible or near infrared part of the spectrum.

LED Type	Color	λp
SiC	Blue	500 nm
GaP	Green	569 nm
GaAsP/GaP	Yellow	585 nm
GaAsP/GaP	Orange	635 nm
GaAsP/GaAs	Red	655 nm
AlGaAs	Red	660 nm
GaP/GaP	Red	697 nm
GaAlAs	Infrared	820 nm

GaAlAs	Infrared 880 nm
GaAs	Infrared 940 nm
GaAlAsinP Alloys	Infrared 1300 - 1500 nm

The P-N junction is formed by doping one region of the material with donor atoms and the adjacent region with acceptor atoms. Like all P-N junction devices, LEDs exhibit the familiar diode current-voltage characteristics. LEDs emit light only when they are biased in the forward direction. Under forward biased conditions carriers are given enough energy to overcome the potential barrier existing at the junction. After crossing the junction these carriers will recombine. A percentage of the carriers will recombine by a radiative process in which the hole-electron recombination energy is released as a photon of light. The remaining carriers recombine by a nonradiative process and give up their energy in the form of heat. The amount of light generated, or power output of the LED, varies almost linearly with forward current. Doubling the forward current approximately doubles the power output.

Physically, most LED chips resemble a cube with a metallized bottom surface and a top metal contact. Some visible LED devices are planar processed with buried junctions. The majority of high efficiency LED chips have P-N junctions which extend out to the four sides of the chip. Since injected carrier recombination takes place within a few diffusion lengths of the junction, the light produced by the LED is generated in this region. Once generated, the light travels out in all directions. Thus, light is not only emitted from the top surface of the chip but also from the sides. As the light travels through the chip some is reabsorbed. Light that strikes the LED chip surface at an angle greater than the critical angle of the dielectric interface is internally reflected. Only that light that exits the LED chip is useful. The packaging used to house

the LED chip serves three functions; to protect the chip and its lead wire(s) from hostile environments, to increase the percentage of photons that can escape from the chip to the outside world and to "focus" the light through the use of incorporated lenses and reflectors.

"N" on"P" 880 nm GaA 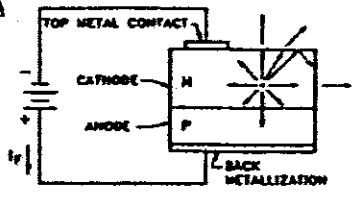

(LED)

Characteristics of LEDs

Measurement of Power Output

It is standard industry practice to characterize the output of a LEDs in terms of power output. Since the amount of light of a LED generates depends on the value of the forward drive current (I_F), the power output is always stated for a given value of current. Also, the ambient temperature must be specified inasmuch as the radiant power decreases with increasing temperature, typically -0.9%/°C.

Two methods are used to measure light power output.

Total Power (P_O)

This method involves collecting and measuring the total amount of light emitted from the LED regardless of the direction. This measurements is usually done by using an integrating sphere or by placing a very large area

detector directly in front of the LED so that all light emitted in the forward direction is collected. The total output power is measured in units of watts.

The total power method ignores the effect of the beam pattern produced by the LED package. It cannot predict how much light will strike an object positioned some distance in front of the LED. This information is vital for design calculations in many applications. However, total output power measurement is repeatable and quite useful when trying to compare the relative performance of devices in the same type of package.

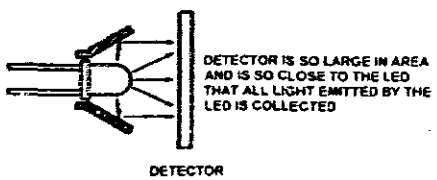

Measuring Total Power - All Light Is Collected

On Axis Power (P_A)

This method characterizes the LED in terms of axial intensity. Many practical applications require knowledge of what percentage of IR power emitted is incident upon a detector located at some distance in front of the LED. In order to achieve repeatable and meaningful measurement of this parameter it is necessary that the distance from the LED to the detector and the active area of the detector be specified. This is because the radiation pattern observed for many LEDs is dependent on the distance from the LED.

For many of emitters, Optoelectronics states a minimum irradiance (E_e), which is the average power in milliwatts per square centimeter (mW/cm^2) incident onto a surface of diameter (D) at a distance (d). The irradiance will in general not be uniform over this whole surface, and may be more or less intense on the

optical axis. Irradiance at other distances may be determined from the graphs showing irradiance versus distance.

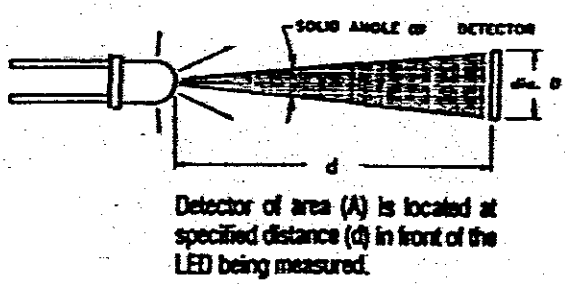

Measuring On-Axis Power

The on-axis power can also be stated as a radiant intensity (I_e) which is the average power per unit of solid angle expressed in units of milliwatts per steradian (mW/sr). To calculate the irradiance at any distance the following formula is applicable.

$$E_e = I_e/d^2 (mW/cm^2)$$

where:

I_e = radiant intensity (mW/cm^2)

d = distance (cm)

However, it should be noted that the LED cannot be treated as a point source when the spacing between the LED and receiver is small, less than ten times the LED package diameter. Attempts to use the inverse square law can lead to serious errors when the detector is close to the LED. Actual measurements should be used in this situation.

For LEDs of any particular package type there is a direct relationship between all three methods used for specifying power output. However, imperfect physical packages and optical aberrations prevent perfect correlation.

Efficiency vs Drive Current

As mentioned in the definition of LED's once injected carriers cross the junction they can recombine by a radiative process which produces light or by a nonradiative process which produces heat. The ratio between these two processes is dependent on the current density (Amps/cm^2 of junction area).

At low current densities (.1A/cm^2) the nonradiative processes dominate and very little light is generated. As the current density is increased the radiative mechanisms increase in efficiency so that a larger and larger percentage of the forward current will contribute to the generation of light. At sufficient current densities, the percentage of forward current which produces light is almost a constant. For an LED of "average" junction area (0.014" x 0.014") this region of linear operation is in the range of approximately 2 mA to 100 mA. Also, at high forward drive currents the junction temperature of the chip increases due to significant power dissipation. This rise in temperature results in a decrease in the radiative recombination efficiency. As the current density is further increased, internal series resistance effects will also tend to reduce the light generating efficiency of the LED.

Light Output Degradation

In normal operation, the amount of light produced by an LED will gradually decrease with time. The rate of decrease depends on the temperature and the current density. LEDs driven at low forward currents at ambient room temperature will degrade more slowly than LEDs driven at higher forward drive currents and at elevated temperatures. Typical degradation data is presented in the data sheets.

Light output degradation is caused by stress placed on the LED chip, be it mechanical, thermal or electrical. Stress causes defects in the chip to propagate along the planes of the chip's crystalline structure, called dark line defects, increase the percentage of non-radiative recombinations. Forward biasing the LED provides energy which aids in the formation and propagation of these defects. The designer using LEDs must address the light output degradation with time characteristic by including adequate degradation margins in the design so that it will continue to function adequately to the end of the design life.

Peak Spectral Wavelength (λp)

LEDs are commonly considered to emit monochromatic light, or light of one color. In fact, they emit light over a narrow band of wavelengths, typically less than 100 nm. The wavelength at which the greatest amount of light is generated is called the peak wavelength, ?p. It is determined by the energy bandgap of the semiconductor material used and the type of dopants incorporated into the LED. The peak wavelength is a function of temperature. As the temperature increases, ?p shifts towards longer wavelengths (typically 0.2 nm/°C). At 25°C EG&G Optoelectronics' GaAs LEDs emit at a peak wavelength of 940 nm and the GAAlAs LEDs emit at 880 nm.

Forward Voltage (V_F)

The current-voltage characteristics of LEDs, like any other PN junction device, obeys the standard diode equation.

$$I_F = I_O [e^{qVF/nKT} - 1]$$

V_F is the voltage drop across the LED when it is forward biased at a specific current, I_F. It is important to note that V_F is a function of temperature,

decreasing as temperature increases. Plots of V_F vs I_F as a function of temperature are included in the data sheets.

Reverse Breakdown Voltage (V_{BR})

This is the maximum reverse voltage that can safely be applied across the LED before breakdown OCRs at the junction. The LED should never be exposed to V_{BR} even for a short period of time since permanent damage can occur.

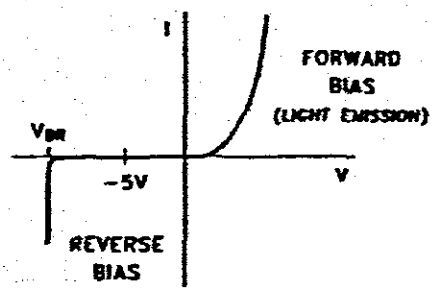

Power Dissipation

Current flow through an LED is accompanied by a voltage drop across the device. The power dissipated (power = current x voltage) causes a rise in the junction temperature of the LED. The effect of this temperature rise is a decrease in the light output of the LED (approximately -0.9%/°C). If the junction temperature becomes too high permanent damage to the LED will result. The maximum power dissipation rating of a semiconductor device defines that operating region where overheating can damage the device.

In any practical application, the maximum power dissipation depends on: ambient temperature, maximum (safe) junction temperature, the type of LED package, how the LED package is mounted and the exact electrical drive current parameters.

While the LED chip generates heat, its packaging serves to remove this heat out into the environment. The package's ability to dissipate heat depends not only on its design and construction but also varies from a maximum, if an efficient infinite heat sink is used, to a minimum, for the case where no heat sink is present. The thermal impedance rating of the package quantifies the package's ability to get rid of the heat generated by the LED chip under normal operation. Thermal impedance is defined as:

$$\theta_{JA} = (T_J - T_A)/P_D \text{ In } (°C/W)$$

where:

θ_{JA} = thermal impedance, junction to ambient

T_J = junction temperature

T_A = ambient temperature

P_D = power dissipation of the device

By definition θ_{JA} assumes that the device is not connected to an external heat sink and as such represents a worse case condition in as far as power dissipation is concerned. For plastic packages and non heat-suck hermetics:

$$\theta_{JA} \approx 400°C/W$$

Increasing the forward drive current will increase the amount of light generated by the LED. However, increasing the drive current also increases the power dissipation in the device. This raises the LED's junction temperature resulting in a decrease in the LED's efficiency. One way to overcome this performance limiting characteristic is to pulse the LED on and off rather than driving it with a dc current. Maximum light output is obtained because the average power dissipated is kept small. Above 100 mA of drive current it is advisable to limit

the maximum pulse width to a few hundred microseconds, and a 10% duty cycle.

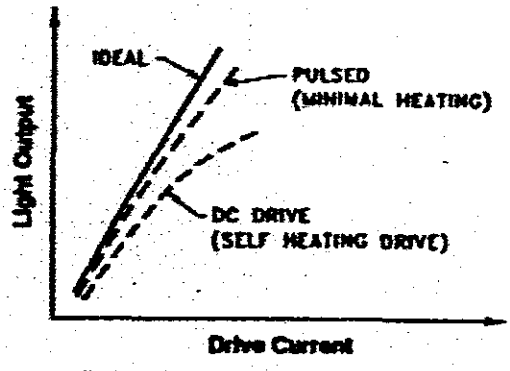

Laser diodes continue to find new product applications as the lasing wavelength is pushed lower into the visible spectrum. The latest generation of Visible Laser Diodes (VLD's) operate at or near 633nm; this wavelength being equivalent to a helium neon gas laser, is highly visible to the human eye. VLD's in the range from 633nm to 690nm are replacing the traditional HeNe laser in many commercial products for good reasons: lower cost, compact size, and superior long-term reliability. Another intrinsic benefit, laser diodes are generally better suited for battery operated devices and other low voltage applications.

While visible diodes are used extensively in commercial products, the near-infrared diodes are certainly not extinct. There are many applications still using lasers operating in the 780nm~850nm range as some machine vision systems and sensors are optimized for near-infrared light sources. The near-infrared diodes may not be considered as user-friendly as the VLD's; however, with the right tools, some of the inconveniences can be managed. In either case, visible or near-infrared.

Simpler Fabrication

There are no mirror facets and in some structures no striped geometry.

Cost

The simpler construction of LED leads to much reduced cost which is always likely to be maintained.

Reliability

The LED does not exhibit catastrophic degradation and has proved for less sensitive to gradual degradation and has proved for less sensitive to gradual degradation than the injection Laser. It is also immune to self pulsation and modal noise problems.

Simpler Drive

This is due to the general lower drive currents and reduced temperature dependence which makes temperature compensation circuits unnecessary.

Linearity

Ideally the LED has a linear light output against current characteristic unlike the injection laser. This can prove advantageous where analog modulation is concerned.

Generally a lower optical power coupled into a fiber(microwatts)

Relatively small modulation bandwith(less than750MHz)

Harmonic distortion

Efficiency

The absence of optical amplification through stimulated emission in the LED tends to limit the internal quantum efficiency(ratio of photons generated to inject electrons) of the device. Relience on spontanious emmision allows non radiative recombination to take place within the structure due to crystalline

imperfection and impurities giving at best an internal quantum efficiency of 50% for simple homojunction devices. Double hetrogenious structures have internal quantum efficiency of 0-80%.

Modulation Bandwith of LED is generally determined by 3 mechanisms.

The doping level in the active layer
The reduction in radiative lifetime due to the injected carries
The parasitic capacitance of the device.

Common Light Sources

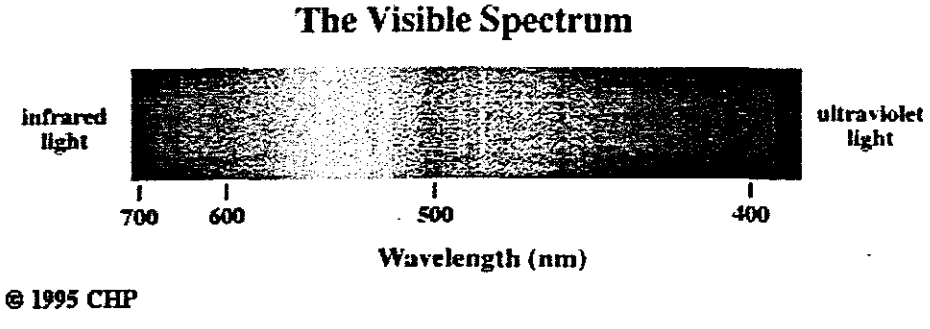

Incandescent lamps can be considered as black body radiators whose spectral output is dependent on their color temperature. The sun has approximately the same spectral radiation distribution as that of a black body @ 5900 K. However, as viewed from the surface of the earth, the sun's spectrum contains H_2O and CO_2 absorption bands.

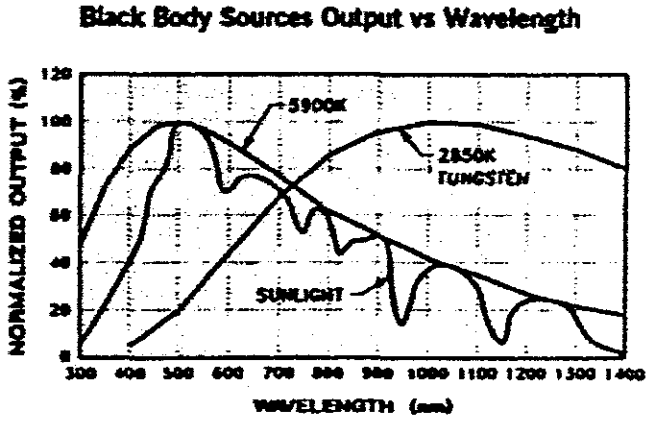

Fluorescent lamps exhibit a broad band spectral output with narrow peaks in certain parts of the spectrum. Shown below is a plot of the light output of a typical daylight type fluorescent tube.

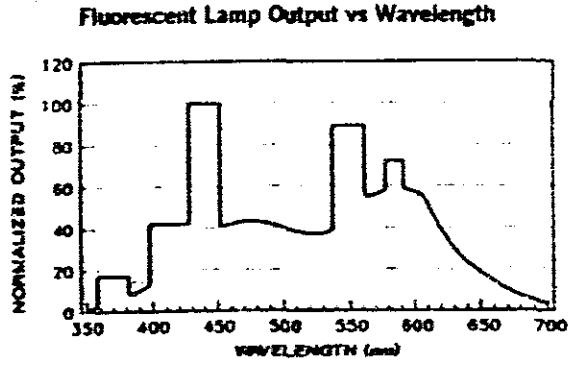

Due to their long operating lifetimes, small size, low power consumption and the fact that they generate little heat, LEDs are the light sources of choice in many applications. When biased in the forward direction LEDs emit light that is very narrow in spectral bandwidth (light of one color). The "color" depends on which semiconductor material was used for the LED.

LED Light Sources

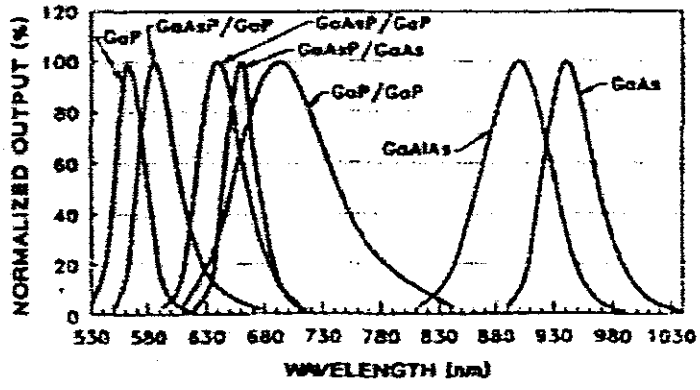

LED Type	Color	Wavelength
GaP	Green	569 nm
GaAsP/GaP	Yellow	585 nm
GaAsP/GaP	Orange	635 nm
GaAsP/GaAs	Red	655 nm
AlGaAs	Red	660 nm
GaP/GaP	Red	697 nm
GaAlAs	Infrared	880 nm
GaAs	Infrared	940 nm

The intensity of the light emitted by visible LEDs is often given in units of millicandela. Millicandela is a photometric unit of measure which assumes the human eye as the detector. For most detectors other than the human eye, the most convenient system for measurement is the radiometric system. Listed below is the typical power output of some LEDs measured at two different forward drive currents. Note that LEDs of a given type can show a 5:1 manufacturing spread in power outputs.

LED Type	Color	λp	Power Output	
			$I_f = 1$ mA	$I_f = 10$ mA
GaP	Green	569 nm	1.2 μW	24.1 μW
GaAsP/GaP	Yellow	585 nm	.3 μW	26.2 μW
GaAsP/GaP	Orange	635 nm	3.2 μW	101.9 μW
GaAsP/GaAs	Red	655 nm	6.2 μW	102.1 μW
AlGaAs	Red	660 nm	33.8 μW	445.1 μW
GaP/GaP	Red	697 nm	54.3 μW	296.2 μW
GaAlAs	Infrared	880 nm	76.8 μW	1512.3 μW
GaAs	Infrared	940 nm	35.5 μW	675.0 μW

Laser lightwave sources

Introduction

A laser is a coherent and highly directional radiation source. LASER stands for Light Amplification by Stimulated Emission of Radiation.

A laser consists of at least three components:

1. a gain medium that can amplify light that passes through it
2. an energy pump source to create a population inversion in the gain medium
3. two mirrors that form a resonator cavity

The gain medium can be solid, liquid, or gas and the pump source can be an electrical discharge, a flashlamp, or another laser. The specific components of a laser vary depending on the gain medium and whether the laser is operated continuously (cw) or pulsed. The following headings describe specific laser designs.

Gas Lasers

Gas lasers are typically excited by an electrical discharge.

Schematic of a cw gas laser

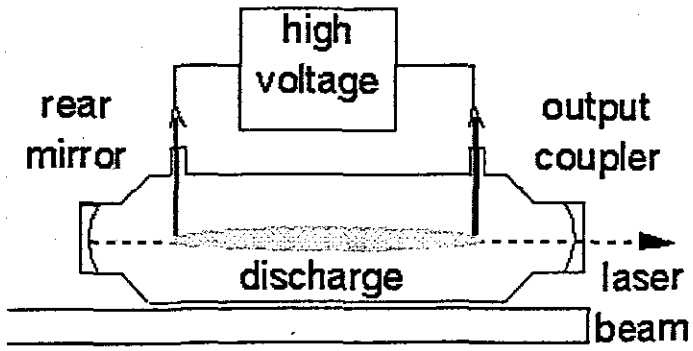

Some gas lasers and their dominant lasing wavelength(s):

- excimer : ArF^* - 248 nm, $XeCl^*$ - 308 nm (pulsed)
- nitrogen : 337 nm (pulsed)
- He-Ne : 632.8 nm (cw)
- Ar ion : 488, 541 nm (cw)
- CO2 : 10.6 μm (cw or pulsed)

Solid-State Lasers

The gain medium in a solid-state laser is an impurity center in a crystal or glass. Solid-state lasers made from semiconductors are described below. The first laser was a ruby crystal (Cr^{3+} in Al_2O_3) that lased at 694 nm when pumped by a flashlamp. The most commonly used solid-state laser is one with Nd^{3+} in a $Y_3Al_5O_8$ (YAG) or $YLiF_4$(YLF) crystal or in a glass. These Nd^{3+} lasers operate either pulsed or cw and lase at approximately 1064 nm. The high energies of pulsed Nd^{3+}:YAG lasers allow efficient frequency doubling (532 nm), tripling (355 nm), or quadrupling (266 nm), and the 532 nm and 355 nm beams are commonly used to pump tunable dye lasers.

Semiconductor Lasers

Semiconductor lasers are light-emitting diodes within a resonator cavity that is formed either on the surfaces of the diode or externally. An electric current passing through the diode produces light emission when electrons and holes recombine at the p-n junction. Because of the small size of the active medium, the laser output is very divergent and requires special optics to produce a good beam shape. These lasers are used in optical-fiber communications, CD players, and in high-resolution molecular spectroscopy in the near-infrared. Diode laser arrays can replace flashlamps to efficiently pump solid-state lasers. Diode lasers are tunable over a narrow range and different semiconductor materials are used to make lasers at 680, 800, 1300, and 1500 nm.

Schematic of a semiconductor diode laser

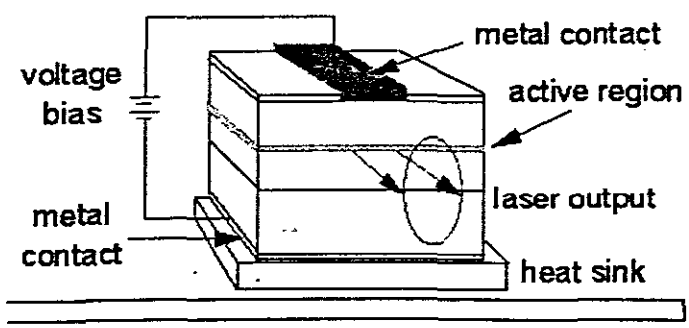

Dye Lasers

The gain medium in a dye laser is an organic dye molecule that is dissolved in a solvent. The dye and solvent are circulated through a cell or a jet, and the dye molecules are excited by flashlamps or other lasers. Pulsed dye lasers use a cell and cw dye lasers typically use a jet. The organic dye molecules have broad fluorescence bands and dye lasers are typically tunable over 30 to 80 nm. Dyes exist to cover the near-uv to near-infrared spectral region: 330 - 1020 nm.

Schematic of a pulsed dye laser

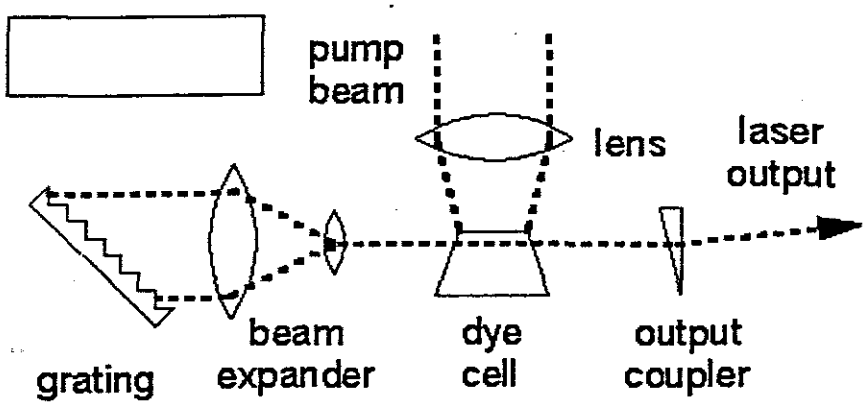

Essential Components of a Laser

Now we know atoms like to occupy the ground state. But as long as we are able to produce population inversion, there will be a possibility of laser action. However, in most cases, this is not good enough. Because the gain through a single pass is typically of the order of 1 to 10%. We need to create so-called a resonant cavity to sustain light amplification. We need both amplification through the laser medium and positive feedback to create multiple passes through the laser medium. Let's take a look at Figure 1. The cascading action runs along a direction defined by the cavity mirrors, M1 and M2. If light travels out of this direction, or 'walks-off', it will not be amplified further and

die off after a while. Typically, M1 is 100% reflective and M2 has a reflectivity of 40 to 90%.

. *Essential components of a laser.*

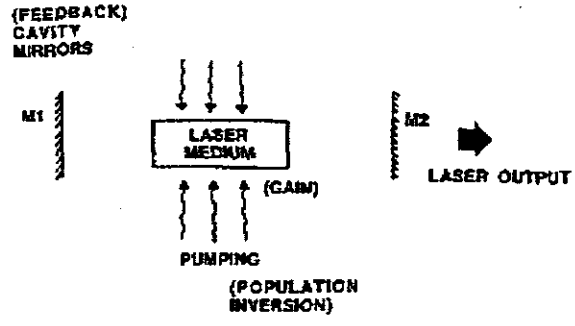

Hence, it is very surprisingly simple to build a laser. All you have to do is to obtain some medium that will provide the gain. The medium can be a gas, a liquid, a solid (crystal), or some free electrons. You pump it with energy to provide population inversion, and place the active medium between a couple of cavity mirrors. You then pray for laser light to be emitted. That's at least theoretically. *Figure 2* illustrates the configuration of a Nd:YAG laser pumped from one end with a series of diode lasers. In this design, we have to use highly specialised dielectric coatings, such as one that transmits the light emitted by the diode lasers (at 810 nm) but reflects the infrared light (at 1064 nm) produced by the Nd:YAG laser rod.

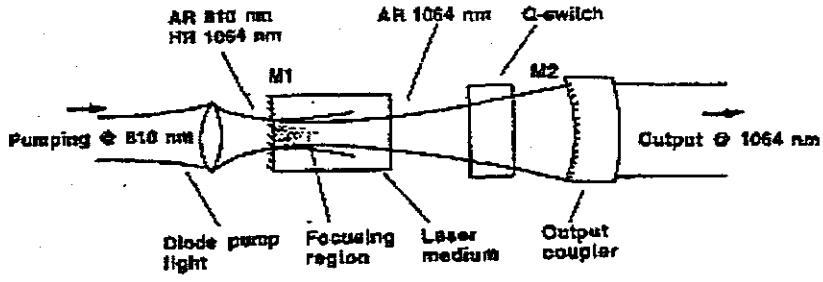

. *Configuration of an end-pumped Q-switched Nd:YAG laser*

Properties of Laser Light

It is ***coherent***. This is because of the properties central to stimulated emission, which is the physical process that renders laser light possible.

It is ***monochromatic***, since laser action can only occur between 2 energy levels. The energy of the emitted photon is therefore discrete as energy levels are quantized.

Laser light is highly ***directional***, because feedback along a direction defined by the end mirrors is necessary to sustain the laser action.

Also, laser light is very ***bright*** because the beam can be focused down to a very small spot.

In practice, these properties can only be achieved for lasers operating at very low overall efficiencies. The laser radiation commonly encountered in engineering applications, for example, is *quasi-monochromatic* (but the wavelengths are so close to one another that it cannot be detected by common detectors, e.g. the human eye), and has a certain amount of *beam divergence* (typically 1 degree).

A laser may be operated continuously (also called continuous-wave or *CW* operation), electrically pulsed, pulsed at high frequencies using a *Q-switch*, or pulsed with intracavity round-trip time intervals in the *mode-locking* manner. The shape of the laser beam may also be round and symmetrical (gaussian beam profile), or may be patterned in a structured manner. Figure 3 illustrates the formation and shapes of some low-order transverse electromagnetic ***(TEM)*** modes. So if you have a beam that provides a

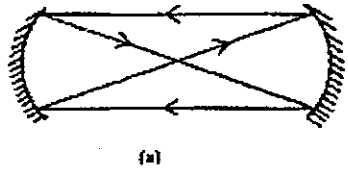

(a)

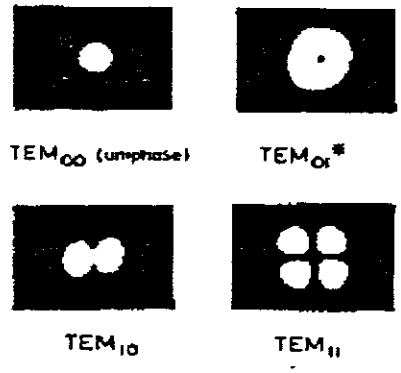

combination of all these transverse modes, you can imagine that the intensity of the focussed beam will not be uniform. These are some of the practical aspects of lasers.

Transverse modes. (a) Example of a nonaxial self-replicating ray that gives rise to transverse modes. (b) Some low-order TEM modes.

High radiance due to the amplifying effect of stimulated emission. Injection lasers will generally supply milli watts of optical output power.

Narrow line width of order of 1nm(10A) or less which is useful in minimizing the effects of material dispersion.

Modulation capabilities which at present extend up into the gigabit or giga hertz range and will undoubtedly be improved upon.

Classes of Lasers

Owing to the relative ease in making a laser, you may imagine that there are many different types of lasers that you can buy in the shops. This is hardly the case. Although there are literally hundreds of different types of lasers that have been invented in research laboratories all over the world over the past 33 years, not all of these inventions can survive the heats of the commercial world. Most lasers are delicate and expensive. The successful commercial lasers, those that can be applied to engineering, have to bear the costs of R & D in the different areas of optical engineering, electrical engineering, electronic engineering, mechanical engineering, and precision engineering. On the other hand, the more we are aware of the many potentials in the usage of lasers, the cheaper the lasers will eventually become. Lasers do obey the simple law of Supply and Demand.

The figure below shows the regions in the electromagnetic spectrum in which lasers operate. Basically, the laser media include ionic crystals, gases, liquid dyes, free electrons, and semiconductors. Most of these lasers operate at discrete frequencies, e.g. ruby at 694.3 nm, Nd:YAG at 1.064 microns, etc.

However, certain lasers could operate at a number of wavelengths, e.g. Ar+ (488 nm or 512 nm), HeNe (632.8 nm, 543.5 nm, 1.15 microns, 3.3 microns), or over a wide bandwidth as in dye lasers and some solid-state lasers. Frequency-selective optics, such as gratings, prisms, Fabry-Perot etalons, thin-film dielectric coatings, etc. would have to be inserted into the laser cavity to operate the laser at a particular wavelength.

Wavelength ranges for existing lasers.

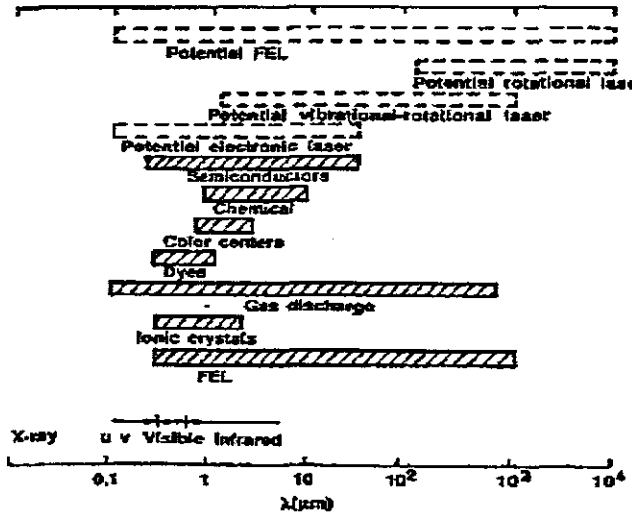

Just how big are lasers? A laser can be as small as a grain of rice, such as the edge-emitting diode laser, or even smaller, such as the surface-emitting diode laser. On the other hand, a laser can be as large as a football field used in inertial confinement fusion research.

The performance data of some of the lasers are summarized in **Table 1**. The dominant laser wavelength, mode of operation, average and/or peak powers, pulse durations, and slope efficiencies are tabulated.

Table 1: Performance characteristics of some common lasers

Laser	Mode of Operation	λ	Average power (W)	Peak power (kW)	Pulse duration	Slope efficiency (%)
Ruby	Q-switched	694.3nm	1	$10 - 10^4$	1ms - 10ns	< 0.1
Nd : YAG	CW	1064 nm	200			1-3
Nd : YAG	Pulsed	1064 nm	1000	10	1 - 5 ms	1-3
Nd : YAG	Q-switched	1064 nm	10	$2x10^4$	10 - 20 ns	1-3
He-Ne	CW	632.8nm	$10^{-3} - 10^{-2}$			< 0.1
Cu	Pulsed	510.5nm	40	100	20 - 40 ns	1-2
Ar^+	CW	514.5nm	10 - 150			< 0.1
He-Cd	CW	325 nm	0.1			
CO_2	CW	10.6 μm	$(1-50)x10^3$			10 - 20
CO_2(TEA)	Q-switched	10.6 μm	10^2	10^4	0.1-0.5 μs	10
N_2	Pulsed	337.1nm	0.1	10^3	10 ns	< 0.1
KrF	Pulsed	248 nm	500	$5x10^3$	10 ns	1
Rh6G	Pulsed	590 nm	100	100	10 μs	0.5
Rh6G	CW	590 nm	5			
HF	CW	2.6-3.3 μm	$10^4 - 10^6$			
HF	Pulsed	2.6-3.3 μm		10^3		
GaAs	CW	850 nm	1			40
FEL	CW	mm to blue	≤100			1 - 10

APPENDIX 6

CIRCUIT DIAGRAMS

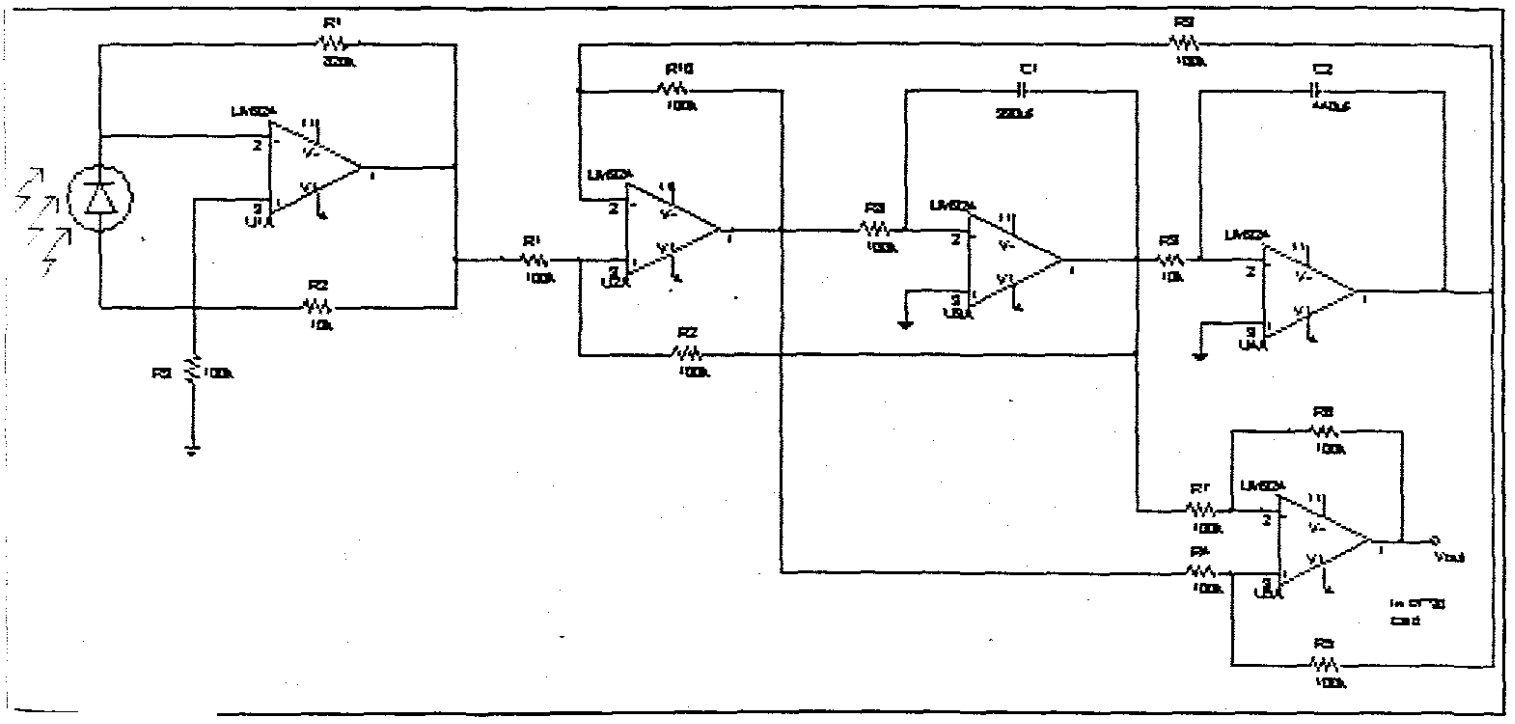

APPENDIX 7

LIST OF EQUATIONS

$$W_g^x(a,b) = {}^1/\sqrt{a} \int x(t) g_{a,b}(t)\,dt$$

$$g_{a,b}(t) = g^*((t-b)/a)$$

$$0 < C_g = \int \frac{|g(f)|}{f} df < \infty$$

$$\int \Vert g(t) \Vert \, dt < \infty$$

$$x(t) = \frac{1}{C_g} \iint \frac{W_g(a,b)}{\sqrt{a}} \left(\frac{g^*\left(\frac{t-b}{a}\right)}{a^2} \right) da\,db$$

$$\psi(t) = \exp(i2\pi f_o \Vert t \Vert) \exp\{-\Vert t \Vert^2/2\}$$

$$E = h f\backslash$$

$$E = hc/\lambda$$

$$\frac{dE_g}{d\lambda} = -hc\lambda^2$$

$$\frac{\Delta E_g}{\Delta \lambda} = -\frac{hc}{\lambda^2}$$

$$\Delta\lambda = \frac{\lambda^2 \Delta E_g}{hc}$$

$$\lambda = hc/E_g$$

$$E_r = [H_r]\, E_i$$

$$[H_r] = r_1[I] - t_1 t_1' r_2' [J_{21}] \{[I] - r_1' r_2' e^{j2\theta} [J_{12}][J_{21}]\}^{-1} [J_{12}] e^{j2\theta}$$

$[J_{12}] = [J_{21}] = [I]$

$$[H_r] = \frac{(1 - e^{2j\theta})\sqrt{R}}{1 - \mathrm{Re}^{2j\theta}},\ R = r^2 = (r')^2,$$

$$R_{11} = [H_r]^2 = \frac{4R\sin^2\theta}{(1-R)^2 + 4R\sin^2\theta}.$$

$E_r = kE_i(1+V\cos\theta)$

$$\theta = (4\pi nL)/\lambda$$

$$\theta = (4\pi fnL)/c \qquad \{c=f\lambda\}$$

$$\Delta\theta_s = \theta + \Delta\theta_p$$

$$[K]_{2x2} = t_c\begin{bmatrix}[K_{A1}] & [K_{A2}]\\ [K_{B1}] & [K_{B2}]\end{bmatrix},$$

$$[K_{A1}] = [K_{B2}]\ [K_{A2}] = [K_{B1}],$$

$$[K]_{2x2} = t_c\begin{bmatrix}[K_t] & [K_c]\\ [K_c] & [K_t]\end{bmatrix},$$

$$[K_t] = \sqrt{(1-k)}[I],\ [K_c] = j\sqrt{k}[I],$$

$$[K]_{2x2} = t_c\begin{bmatrix}\sqrt{(1-k)}[I] & j\sqrt{k}[I]\\ j\sqrt{k}[I] & \sqrt{(1-k)}[I]\end{bmatrix},$$

$$\begin{bmatrix}E_a'\\ E_b'\end{bmatrix} = \begin{bmatrix}[J_{AA}] & [J_{AB}]\\ [J_{BA}] & [J_{BBA}]\end{bmatrix}\begin{bmatrix}E_a\\ E_b\end{bmatrix},$$

$$[J_{AA}] = [K_t][H_r][K_t] + [K_t],$$

$$[J_{AB}] = [K_c][H_r][K_t] + [K_c],$$

$$[J_{BA}] = [K_t][H_r][K_c] + [K_t],$$

$$[J_{BB}] = [K_t][H_r][K_t] + [K_c],$$

$$[E_a'] = [J_{AA}]E_a + [J_{AB}]E_b,$$

$$[E_b'] = [J_{BA}]E_a + [J_{BB}]E_b,$$

$$T_{AA} = \frac{E_A^{*T}[J_{AA}]^{*T}[J_{AA}]E_A}{[E_A]^2},$$

$$T_{AB} = \frac{E_A^{*T}[J_{BA}]^{*T}[J_{BA}]E_A}{[E_A]^2},$$

$$E_1(\omega) = E_{in}S(\omega),$$

$$\frac{dE_{PR}}{df} = kR\frac{dE_{PI}}{df}(1+\cos\theta_s).$$

$$\frac{dE_{PR2}}{df} = kR_2\frac{dE_{PI2}}{df}(1+sos\theta),$$

$$E_{PI2} = \alpha E_{PI},$$

$$\frac{dE_{PR2}}{df} = k^2R_1R_2\alpha\frac{dE_{PI}}{df}(1+\cos\theta_s)(1+\cos\theta_0).$$

$$\int\cos\theta_0 df = 0, \quad \int\cos\theta_{ri} df = 0,$$

$$E_{PR} = k^2R_1R_2\alpha E_{PI}(1-\frac{1}{2}\cos\theta_P).$$

$$M(dx_m/dt) + C(x_m - x_s) = 0$$

$$-\omega^2 A_m\cos\omega t + \omega_0^2(A_m - A_s)\cos\omega t = 0$$

$$A_m = \left(\frac{1}{1-E^2}\right)A_s$$

$$E = \omega/\omega_0$$

$$l_o = sqrt(2)\ \pi na/N$$

$$p(x) = \lim_{\Delta x\to 0}\left(\frac{P(x+\Delta x) - P(x)}{\Delta x}\right)$$

$$P(x+\Delta x) - P(x) = \int_x^{x+\Delta x} p(x)dx$$

$$= (\Delta t_1 + \Delta t_2 + \Delta t_3)/T$$

$$= \frac{\sum_k \Delta t_k}{T}$$

$$x = \int_{\infty}^{\infty} x p(x) dx$$

$$\sigma^2 = \int_{\infty}^{\infty} (x - \bar{x})^2 \, p(x) dx$$

$$P(x) = 0.5 + erf\left(\frac{x - \bar{x}}{\sigma}\right)$$

$$R_{xy} = \sum_{n=0}^{N-K-1} (x(n) * y(n + k)$$

$$R_{xy} = 1/N \sum_{n=0}^{N-1} (x(n) * y(n + k)$$

$f(t) \leftrightarrow F(w)$

$g(t) \leftrightarrow G(w)$

$$\rho_{fg}(\tau) = \int_{-\infty}^{\infty} f(t)\, g(t + \tau) dt$$

$$R(\tau) = \lim_{T \to \infty} \frac{1}{T} \int_0^T x(t) x(t + \tau) dt$$

$$E_{PI} = kR_1R_2(1 + 0.5\cos(\theta)$$

$\varphi = q/M$

$\Delta L = qD/M$

$e_p = v_t \, Ln(i_p/I_d)$

$i_p = r\phi_e$

$e_p = kT/q(Ln(r\phi/I_d)$

$$y(n)=\sum_{k=0}^{M-1} c_k x(n-k)= x(n+N)$$

$$F(z)=\sum_{k=0}^{M-1} c_k\ z^{-k}$$

$$H(z)=\frac{\sum_{m=0}^{M-1}[c_m z^{-m}\prod_{r=0}^{m}(1-b_r)]}{1-\sum_{l=0}^{M-1} c_l b_l z^{-N-1}-\sum_{i=1}^{M-1}\{c_i z^{-N-i}\sum_{j=1}^{i}[b_{i-j}\prod_{k=1}^{j}(1-b_{i+1-k})]\}}$$

$$z=\frac{1+(T/2)s}{1-(T/2)s}$$

$$\Omega=\frac{2}{T}\tan(\omega/2)$$

$$H(s)=\prod_{i=1}^{q} K_i\frac{b_{2i}s^2+b_{1i}s+b_{0i}}{a_{2i}s^2+a_{1i}s+a_{0i}}$$

$$H(s)=K\frac{s^2+b_1 s+b_0}{s^2+a_1 s+a_0}$$

$$H(s)=K\frac{s+a}{s+b}$$

$$H(z)=\frac{c_0-c_0 b_0+(c_1-b_0 c_1-b_1 c_1+b_0 b_1 c_1)z^{-1}}{1-b_0 c_0 z^{-1}-(b_0 c_1-b_0 b_1 c_1+b_1 c_1)z^{-2}}$$

$$H(s)=\frac{(0.00695+0.54905s)(1+s)}{0.00695+0.5421s+3.45095s^2}$$

$$i_o=\frac{R_f}{R_1}i_p$$